Characterization and Design of a Stripper for a Continuous Direct Air Capture System

Nelson van de Poll

Characterization and Design of a Stripper for a Continuous Direct Air Capture System.

by

Nelson van de Poll

to obtain the degree of Master of Science

at the Delft University of Technology,

to be defended publicly on February 26, 2021 at 09:00 AM.

Student number:	4216059	
Project duration:	February 14, 2020 – February 26, 2021	
Thesis committee:	Prof. dr. ir. E. Goetheer,	TU Delft, supervisor
	Prof. dr. ir. W. De Jong,	TU Delft
	Prof. dr. ir. B. J. Boersma,	TU Delft
	Ir. M. Sinha,	Zero Emission Fuels

This thesis is confidential and cannot be made public until February 26, 2023

TU Delft

Abstract

Capturing CO_2 directly from the air has gained wide attention as it is one of the possible solutions to mitigate the risks of climate change. Zero Emission Fuels (ZEF) is a start-up in Delft that develops a small-scale plant to produce methanol from sunlight and air only. CO_2 and H_2O is captured from the air by a direct air capture unit that operates continuously by means of an absorption and stripping column. Liquid amines are investigated as chemical sorbent. In this work, the stripping column is characterized and optimized for the liquid amine tetraethylenepentamine (TEPA).

A vapor-liquid equilibrium based stage-by-stage stripper model was established using mass and energy balances for each stage individually. A number of input parameters was specified to understand the effect of those parameters on the performance of the stripping column. The parameters include; composition, temperature and mass flow rate of the feed, number of stages, H_2O reflux ratio, temperature of the reboiler and absolute pressure of the column. The mass balance was solved according to the Rachford-Rice equation while using bisection as numerical root finder.

To validate the stripper model, experiments were performed for varying configurations regarding the input parameters mentioned above. For this, a trayed stripping column with bubble caps, was build and adjusted according to the experimental plan. Furthermore, single stage kinetic experiments were performed at 115 °C and 950 mbar to find the limitations of the desorption process inside the column. Subsequently, the Damköhler number was estimated to understand the effects of reaction rate and diffusion during the process.

Sensitivity analyses were performed to find the effect of input parameters on the performance of the stripping column. The effect was measured in terms of; CO_2 concentration in the outlet stream, cyclic capacity of the liquid solvent, CO_2 and H_2O vapor ratio in the top stage of the column and energy demand per desorbed mol of CO_2. Based on the results, a tool to predict the performance of the stripper in an elementary way was produced.

Based on the kinetic experiments, it was found that a typical hold up time that is required for the system to reach equilibrium was measured at 600 s. This number was used to estimate the liquid hold up volume per stage in the final stripper design.

The experimental and model results were combined in a new stripper design considering the operating conditions stated by ZEF. The 5 stage column operates at 1000 mbar and a reboiler temperature of 120 °C. The feed was preheated up to 105 °C and the mass flow rate was determined at 0.31 g/s resulting in a hold up volume of 187 ml per stage. The cyclic capacity of the system equals 3.3 mol CO_2 per kg TEPA and the energy demand was found to be 279 kJ per mol CO_2.

In addition, a new design for ZEF's direct air capture system was presented where the absorption column is modelled as a black box. An heat exchanger was implemented to minimize the energy demand of the system, which resulted in a lowest energy demand of 2319 kWh per ton of CO_2. This is slightly higher than the DAC energy demand of companies like Climeworks, Carbon Engineering and Global Thermostat, but could potentially decrease when optimizing the system.

Acknowledgements

The establishment of this research is undeniably build on the help of people that I would like to thank.

Firstly, I would like to thank Earl Goetheer for taking the time to supervise me during this thesis project. During each of our meetings you provided me with new insights and directions. Your enthusiasm regarding direct air capture has truly inspired me.

A big thanks goes to Mrigank Sinha. Working together on almost a daily base has been a great pleasure. Evenings were never too late and mornings never too early to finish an experiment or debate on some new unexpected findings. Trying to push viscous TEPA through a thin hose is something that I will not forget anytime soon.

Next, I would like to thank Jan van Kranendonk who helped me greatly during the course of this research. Especially for helping me with the creation of the stripper model in Matlab, but also discussing results and understanding experimental phenomena. I'm still mesmerized by the knowledge you have on every subject that is required to develop a complex system like ZEF's methanol plant.

Ulrich Starke and Hessel Jongebreur. I would like to thank you both for making me part of the ZEF team. Also, your positive support and funny jokes have been very valuable to me during this project.

I would like to thank Michel, Jaap and Daniël for providing the chemical substances and mechanical components that were required to perform the stripping experiments.

I would also like to thank all the students that I worked together with at ZEF and making me feel at home while drinking coffee. Especially the members of the DAC team with whom I could brainstorm on possible experimental solutions and complain about the stickiness of TEPA with.

Finally, I would like to thank my family and friends for supporting me during this somewhat difficult pandemic period. My parents, Dan and Lies, for always supporting me unconditionally no matter what I decide to do. Without you, building this foundation for my future would not have been possible. Thanks to my brother and sister, Giel and Luna, for being close to me and providing emotional support when needed. Also a big thanks to my roommates; Jorn, Matthijs, Timothy and Wilco for supporting me while I was writing at home during lockdown and providing with help and necessary distraction in any kind of way. Also, thanks to my other friends who have always been there for me when it was needed. If you read this, I'm probably talking about you right now, so thanks!

Contents

List of Figures

List of Tables

Table 1: List of symbols used in this work including their description and units.

Symbol	Description	Units
J	Diffusion flux	$[mol/m^2 \cdot s]$
c	Molar concentration	$[mol/m^3]$
CC	Cyclic capacity	$[mol/kg]$
c_{gas}	Solubility of gas	$[mg/L]$
c_p	Specific heat	$[J/kg \cdot K]$
D	Diffusion coefficient	$[m^2/s]$
Da_{ll}	Damköhler number	$[-]$
k_B	Boltzmann constant	$[m^2 \cdot kg/s^2 \cdot K]$
μ	Dynamic viscosity	$[Pa \cdot s]$
η	Efficiency	$[-]$
r	Radius	$[m]$
r	Reaction rate	$[mol \cdot s/m^3]$
R	Universal gas constant	$[J/mol \cdot K]$
R	Reflux ratio	$[-]$
R_{top}	Vapor top ratio in column	$[-]$
K	K value	$[-]$
k	Reaction rate coefficient	$[s^{-1}]$
k_L	Mass transfer coefficient in liquid phase	$[m/s]$
h	Height	$[m]$
h	Molar enthalpy	$[J/mol]$
H	Henry constant	$[mol/m^3 \cdot Pa]$
H_{vap}	Heat of vaporization	$[kJ/mol]$
H_{lat}	Latent heat	$[kJ/mol]$
H_{abs}	Heat of absorption	$[kJ/mol]$
y	Vapor phase mole fraction	$[-]$
x	Liquid phase mole fraction	$[-]$
z	Feed mole fraction	$[-]$
E	Energy demand	$[mol/kg]$
E_a	Activation energy	$[J/mol]$
Ha	Hatta number	$[-]$
ρ	Density	$[kg/m^3]$
M	Molecular weight	$[g/mol]$
m	Mass	$[kg]$
$\dot{m}$	Mass flow rate	$[kg/s]$
Q	Heat	$[W]$
Q_{reb}	Reboiler duty	$[W]$
α	Relative volatility	$[-]$
γ	Activity coefficient	$[-]$
ϕ	Fugacity coefficient	$[-]$
β	Fraction that is vaporized	$[-]$
S	Stripping factor	$[-]$
T	Temperature	$[°C]$
t	Time	$[s]$
g	Gravitational constant	$[m^3/kg \cdot s^2]$

Table 2: Continuation of list of symbols used in this work including their description and units.

Symbol	Description	Units
A	Additional mass flow rate	$[mol/s]$
V	Volume	$[m^3]$
V	Vapor mass flow rate	$[mol/s]$
V_B	Boil up ratio	$[-]$
L	Liquid mass flow rate	$[mol/s]$
L	Diffusion length	$[m]$
L	Loading of mixture	$[mol/kg]$
F	Feed mass flow rate	$[mol/s]$
w	Mass fraction	$[wt\%]$
P_{abs}	Absolute pressure	$[mbar]$
P_i	Partial pressure of component i	$[mbar]$
N	Number of stages	$[-]$

Table 3: List of molecular structures used in this work including their description.

Molecular structure	Description
CaCO	Calcium Oxide
$CaCO_3$	Calcium Carbonate
$Ca(OH)_2$	Calcium Hydroxide
CH_3OH	Methanol
CO	Carbon Monoxide
CO_2	Carbon Dioxide
H_2	Hydrogen
HCO_3^-	Bicarbonate
H_2O	Water
K_2CO_3	Potassium Carbonate
KOH	Potassium Hydroxide
NaOH	Sodium Hydroxide
O_2	Oxygen
$R_1R_2NCOO^-$	Carbamate
R_1R_2NH	Secondary amine
$R_1R_2NH^+COO^-$	Zwitterion

Table 4: List of abbreviations used in this work including their description.

Abbreviation	Description
AEC	Alkaline Electrolysis Cell
ANN	Artificial Neural Network
CCS	Carbon Capture and Storage
CCU	Carbon Capture and Utilisation
COCO	Cape-open to Cape-open simulator
DAC	Direct Air Capture
DEEA	Diethanolamine
DS	Distillation
FM	Fluid Machinery
FTIR	Fourier-transform infrared spectroscopy
GC	Gas Chromatographer
HEX	Heat Exchanger
HT	High Temperature
LT	Low Temperature
MAPA	Monoamonium Phosphate
MDEA	Methyldiethanolamine
MEA	Mono-ethanolamine
MeOH	Methanol
MS	Methanol Synthesis
MSA	Moisture Swing Absorption
SIT	Specific Ion Interaction Theory
SR	Sum-Rates
TEPA	Tetraethylpentamine
TSA	Temperature Swing Absorption
VLE	Vapor-liquid equilibrium
ZEF	Zero Emission Fuels

Chapter 1

Introduction

This chapter gives an introduction to the topic of this research. First, global warming is explained and the start-up ZEF is introduced. Then, the aim of this thesis is established followed by the research objective and questions. Subsequent, the thesis approach is defined and a research methodology is initiated. To round off, the outline of this report is presented.

1.1 Global Warming

The global energy demand is increasing and with the increase of the world's population and the rise of lifestyle standards due to technological development, it will most probably continue to do so. As figure 1.1 visualizes clearly, fossil fuels still make up for the majority of the energy consumption. This leads to two serious problems: the available fossil fuel reserves are becoming depleted and the global emission of greenhouse gasses is increasing [18].

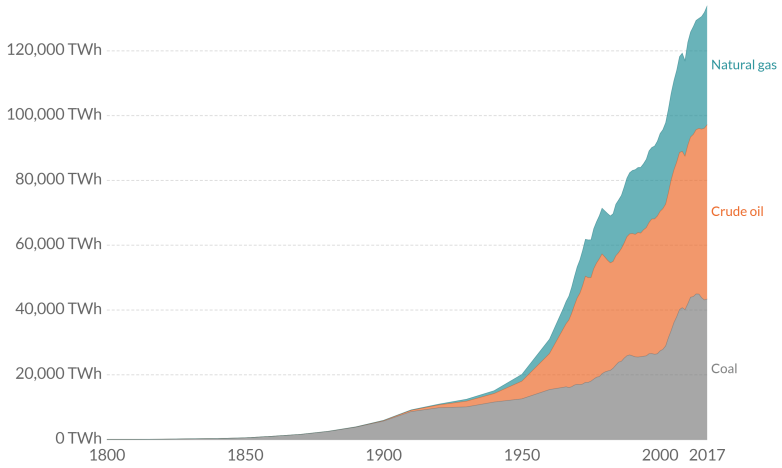

Figure 1.1: Global energy consumption in TWh per year [1].

The main component of these greenhouse gasses is CO_2 and the global concentrations of CO_2 in the atmosphere is presented in figure 1.2. One can see that the concentration has never been this high in the last 800.000 years.

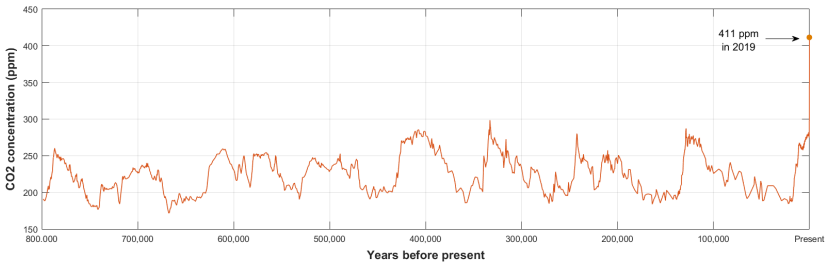

Figure 1.2: Global concentration of CO_2 in the atmosphere over the last 800.000 years [2] [3].

With the high concentration of greenhouse gasses in the atmosphere and the increase of greenhouse gas emissions, the global average temperature will also keep increasing steadily. Figure 1.3 presents the annual global average temperature relative to the average temperature between 1961 - 1990. The increase in temperature, also called global warming, is obvious and will remain increasing steadily if no drastic action is taken. To specify some clear goals, the Paris agreement was established in 2015 and signed by 189 parties [19]. To stay below a temperature increase of 1.5℃ in comparison to pre-industrial levels, a decrease of CO_2 emissions of 45% compared to 2010's emissions should be accomplished by 2030. Followed by a net zero emission in 2050 [19].

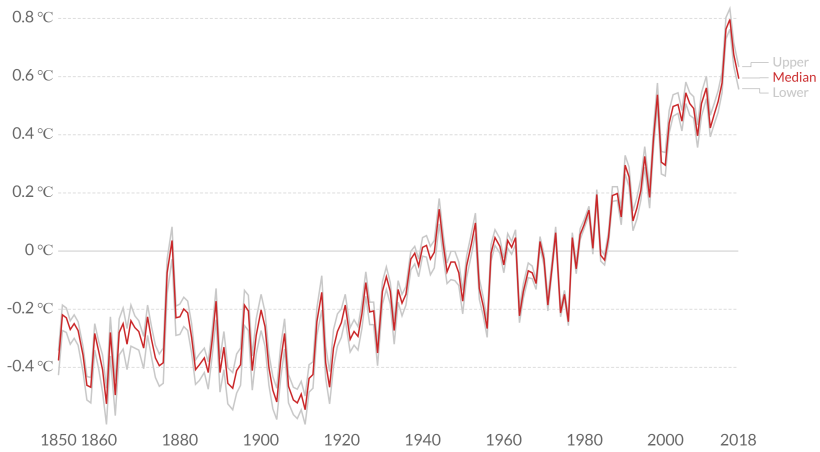

Figure 1.3: Annual global average temperature related to 1961 - 1990 [4].

Mitigation

As stated before, mitigation technologies are required to realize the Paris agreement goals. First of all, a switch from fossil fuel based energy to clean renewable energy is necessary. However, this should also come with development of energy efficient technologies to reduce the global energy demand and thus CO_2 emissions. Carbon capture and storage (CCS), is another way of minimizing the CO_2 emissions and is necessary to achieve the Paris agreement goals and stay below the 1.5℃ temperature increase [20]. Carbon capture and utilisation (CCU) is a rapidly developing technology where CO_2 is captured and used as feedstock for the carbon-based industry. Most research has been done on capture from large point sources such as flue gases and this technology is implemented in industry [21]. Nonetheless, to minimize the concentration of greenhouse gases, negative emissions are necessary

so CO_2 must be captured from the atmosphere. This technology is called direct air capture and this is where Zero Emission Fuels comes into play.

1.2 Zero Emission Fuels

Zero Emission Fuels (ZEF) is a start-up situated at the faculty of Energy & Process Technology at the Delft Technical University. It is focused on producing methanol from ambient air by making use of energy supplied by solar panels. Methanol produced in this way is also called carbon neutral methanol since it uses renewable energy as energy source [22].

Where a typical chemical factory has a significant size, ZEF is developing a zero-emission methanol micro-plant. An advantages of a small scale plant is that it is suitable for discontinuous operation, the size allows it to heat up and cool fast. Due to intermittent power supply from the solar panels, this is highly preferred. Also, ZEF is aiming on designing the micro-plant for mass manufacturing so that many micro-plants can be made for relatively low capital costs.

A single methanol micro-plant can be connected up to 3 solar panels, each producing an average of 300W electricity. This is enough energy for the micro-plant to operate. A schematic overview of the micro-plant is visualized in figure 1.4.

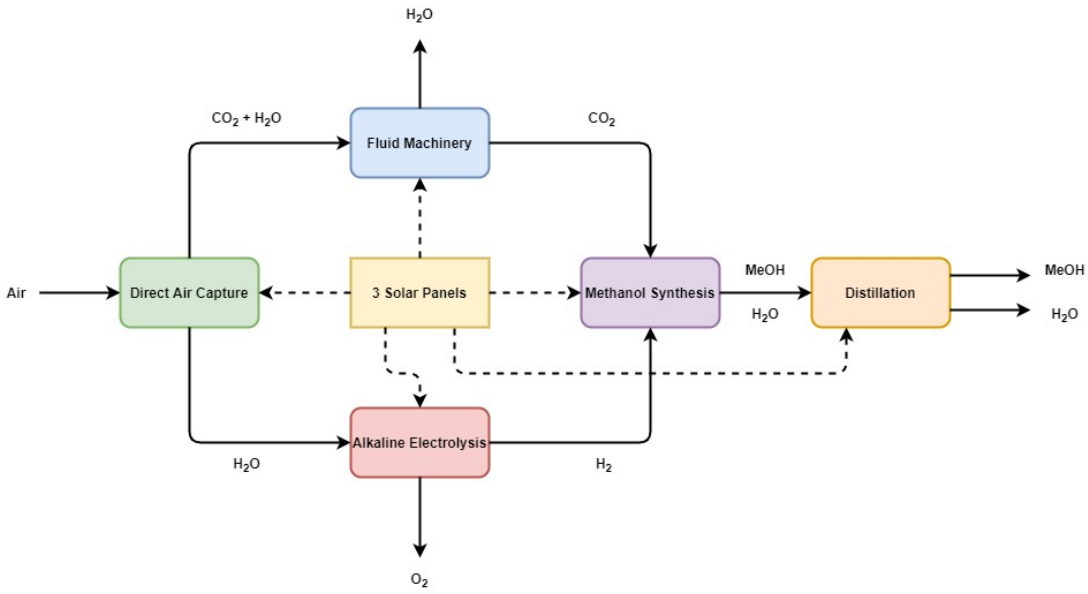

Figure 1.4: Schematic overview of the methanol micro-plant designed by ZEF.

As shown in figure 1.4, the micro-plant consists of five subsystems. Each subsystem will be briefly explained:

- In the **Direct Air Capture (DAC)** subsystem, H_2O and CO_2 are extracted from the air by a liquid in the absorption column. This liquid is transported into a stripping column where the H_2O and CO_2 are desorbed from the liquid at elevated temperatures. H_2O is then condensed and separated from the CO_2, but some H_2O remains in the vapor phase.

- The CO_2 and some H_2O in vapor phase are separated in the **Fluid Machinery (FM)** subsystem. The CO_2 enters a compressor where the pressure is brought up to 50 bar.

- The H_2O enters the **Alkaline Electrolysis Cell (AEC)** where it is split into H_2 and O_2. The O_2 is removed from the system into the atmosphere.

- The H_2 and pressurized CO_2 enter the **Methanol Synthesis (MS)** reactor where MeOH and H_2O are produced by a Lurgi methanol synthesis process.

- Finally, the MeOH and H_2O arrive at the **Distillation (DS)** subsystem where they are separated. The MeOH is collected and H_2O is fed back into the alkaline electrolysis cell.

The goal of a single micro-plant is to produce 217.5 kilograms of MeOH per year. Due to intermittent power supply from the solar panels, the system is able to run 8 hours per day when one assumes an average sunlight of 8 hours per day. This corresponds with the capture of 301.2 kg of CO_2 and 370.0 kg of H_2O by the DAC system, based on reaction 1.1.

$$CO_2 + 3\ H_2 \leftrightarrow CH_3OH + H_2O \tag{1.1}$$

As the production of a single methanol micro-plant is small compared to conventional chemical plants, scaling up by numbers results in high methanol production yields. For example, the micro-plants can be implemented in solar panel fields to establish solar methanol farms.

1.2.1 DAC Subsystem

ZEF has developed multiple direct air capture concepts. After multiple research and experimental phases, gaining more and more knowledge on DAC, it was decided to develop a continuous direct air capture concept. The DAC concept exists of two main parts, an absorption and a stripping column. In the absorption column, liquid polyamines flow down on a vertical surface where ambient air is blown over the liquid creating a counter current flow. In this way, H_2O and CO_2 are being absorbed by the liquid polyamine. In the stripping column, the loaded polyamine is heated so that the H_2O and CO_2 are desorbed. This all happens continuously. Figure 1.5 shows the current DAC setup that ZEF is using for research, which contains the absorption and stripping column at the right and left respectively. Literature and previous research at ZEF has proven that TEPA is one of the most favorable polyamines to use for this process in terms of CO_2 absorption kinetics, capacity and viscosity [11] [14] [23]. Life cycle analysis of the polyamine is also a topic of research for the DAC concept.

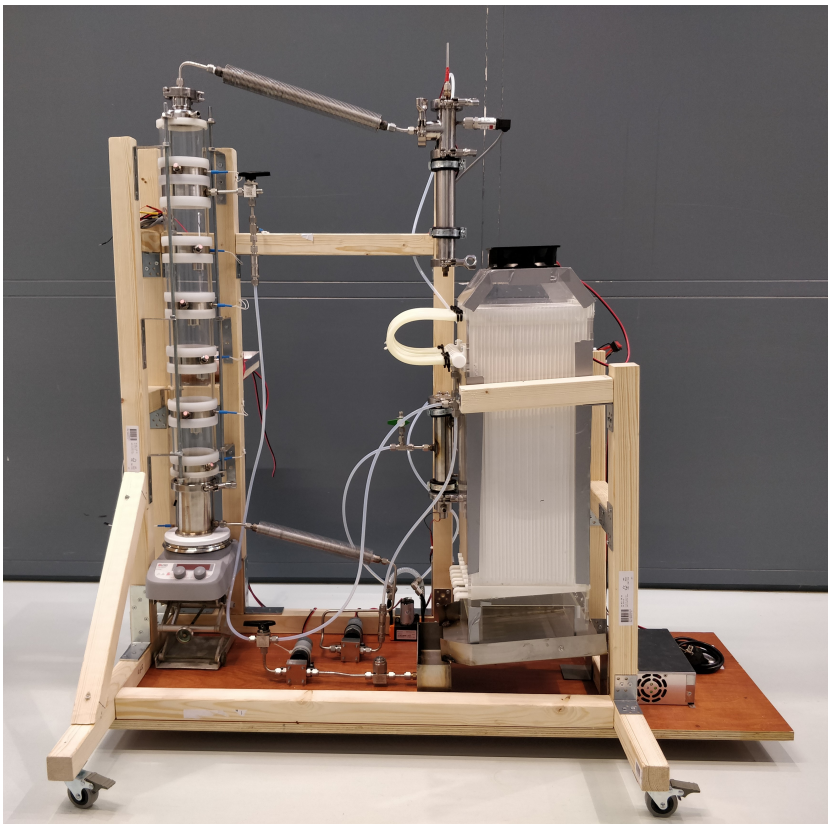

Figure 1.5: Direct Air Capture system designed and build by ZEF [5].

1.3 Aim of this Thesis

Stripping is a highly energy consuming process and accounts for the largest amount of the DAC subsystem's energy demand. Therefore, a better understanding of the process is essential to minimize the energy demand. This thesis investigates the desorption of CO_2 and H_2O from TEPA. At the moment, this is done by a state of the art multi-component stripping column which produces CO_2 and H_2O as product and the lean sorbent, TEPA-H_2O-CO_2 mixture, as bottoms. The multi-component stripping column is a rather complex system since it is dependent on numerous parameters. To get a better understanding of the desorption process it is important to understand the effects of these parameters on the performance of the multi-component stripping column. This will be done by performing experiments and establishing a stripper model which predicts the performance of the stripper for specified operating conditions. This model will also be used to design a stripper column to meet ZEF's requirements.

In conclusion, the aim of this thesis can be split into two separate objectives: understanding of the working principles of a stripper column where CO_2 and H_2O are desorbed from a TEPA-H_2O-CO_2 mixture and to design a stripper column that meets ZEF's requirements best.

1.4 Research Questions

The primary objective of this thesis is to characterize and design a stripper for a continuous direct air capture system. To break down the research objective into more specific subjects, research questions

are defined. Together they will contribute to fulfil the main research aim. The following research questions are formulated:

1. What are the main parameters influencing the stripper and how do they do so?

2. Which role plays kinetics during desorption inside the stripper?

3. How can the energy demand of the stripper be minimized? What factors influence it?

4. Which stripper design meets ZEF's requirements best?

1.5 Thesis Approach

It is important to define the scope of this research well since continuous direct air capture is a relatively novel research field. Therefore, to frame this thesis work precisely, one must presuppose the following:

- Any experiments presented in this work are performed with the ternary mixture of TEPA-H_2O-CO_2. This is due to choices made by ZEF and the availability of a VLE for this mixture. For this reason, no other mixtures are being experimented with in this research.

- This thesis focuses solely on desorption. Absorption and life cycle characteristics such as amine evaporation, degradation and corrosive behaviour are not being investigated. However, a basic knowledge of absorption is required since absorption and desorption are closely related to one another. Hence, absorption is explained in the literature research but no absorption experiments are performed.

- This research is based on desorption during steady state operation of the stripping column. Consequently, the transient behaviour of the stripper is left outside the scope of this research.

1.5.1 Methodology

To answer the first research question a model is made to predict the performance of the stripper for predetermined operating conditions. This model is based on literature review of applicable models for the vapor-liquid-equilibrium and vapor curve ZEF has at hand regarding the TEPA-H_2O-CO_2 mixture. Next, experiments are performed to validate the model for different operating conditions such as pressure, temperature, mass flow and mixture composition. More experiments are performed to get an understanding of the kinetics during desorption inside the stripper. Based on previous research and literature, an energy balance is implemented in the model to get an understanding of the energy usage for varying parameters. Finally, the model is used to find and propose a specific stripper design which meets ZEF's requirement. Likewise, a design is proposed to operate under the most efficient circumstances to obtain the optimal CO_2 production per energy usage. A schematic overview of the methodology is presented in figure 1.6.

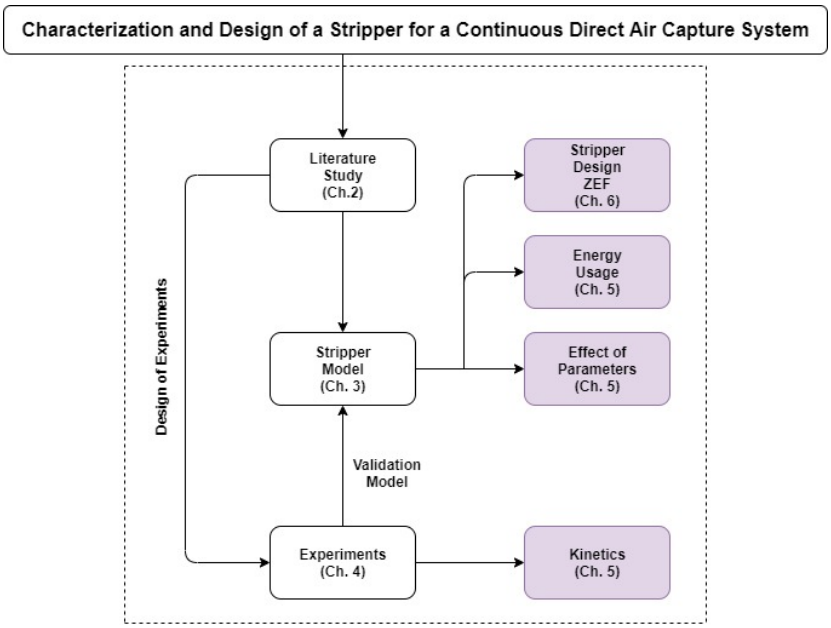

Figure 1.6: Schematic overview of the methodology of this thesis work.

1.6 Report Outline

The outline of this thesis follows the listed structure presented in table 1.1. Ch. 2 presents the theoretical background for subjects and concepts that are used in the following chapters. In Ch. 3, the stripper model is explained in detail in terms of assumptions and equations. The experimental equipment and procedures are described in Ch. 4. The results are listed and discussed in Ch. 5. A stripper design that meets ZEF's requirements is proposed in Ch. 6. Finally, conclusions and recommendations in terms of experiments, model and further research are given in Ch. 7.

Table 1.1: Report outline

Ch. 1	Introduction
Ch. 2	Background
Ch. 3	Model Description
Ch. 4	Experimental Equipment and Procedures
Ch. 5	Results and Discussion
Ch. 6	Proposed Stripper Design
Ch. 7	Conclusions and Recommendations

Chapter 2

Background

This chapter describes all the background information that is required to execute this study. An overview of CO_2 capture technologies is given. Next, the scope is narrowed down to liquid amine solvents for CO_2 capture and TEPA is being introduced. Afterwards, stripping is elaborated on in terms of stripping fundamentals and industrial stripping, followed by a detailed description of the energy usage in a stripper column. Also, the relevant vapor-liquid equilibrium and vapor curve are discussed. Then, a brief review of available stripper column solving methods is given and a decision on the most suitable method is made. Finally, a summarized conclusion is provided. An visual overview of this chapter is presented in figure 2.1

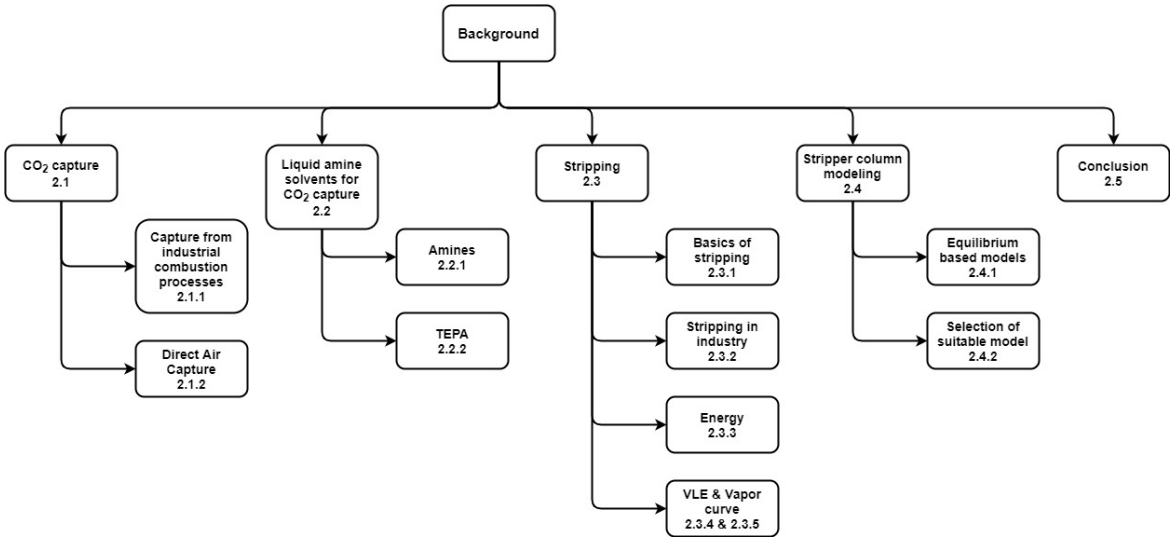

Figure 2.1: Visual overview of the background chapter outline.

2.1 CO_2 Capture

As explained in section 1.1, carbon dioxide has become the most crucial greenhouse gas that causes climate change. Since climate change is one of the main challenges humanity is facing nowadays, the field of CO_2 capture is growing rapidly [24]. Two main types of CO_2 capture technologies can be distinguished, CO_2 capture from industrial combustion processes and CO_2 capture from ambient air, also called direct air capture (DAC). Both technologies are discussed in the following sections.

2.1.1 CO_2 Capture from Industrial Combustion Processes

To capture CO_2 efficiently, it is most effective to capture CO_2 from large point sources of CO_2 [25]. These point sources include large fossil fuel or biomass energy plants, major CO_2 emitting industries and natural gas production [6]. Examples of CO_2 capture from industrial processes are briefly described and schematically presented in figure 2.2.

- **Post-combustion capture**: CO_2 is captured from the flue gases produced by the combustion process. This CO_2 capture technology can be easily adjusted and implemented into existing power plants [6] [24].
- **Pre-combustion capture**: The fuel is gasified and afterwards a water gas shift reaction occurs where CO and H_2O turn into H_2 and CO_2. The CO_2 is captured and the H_2 is combusted. Although the initial fuel conversion steps are more costly, it leads to higher CO_2 concentrations in the gas stream. Also the use of higher pressures simplifies the separation process [6] [26].
- **Oxyfuel combustion capture**: A continuous oxygen gas stream is added to the combustion process which produces CO_2 and H_2O that can be simply separated. However, the purification of the air for the continuous oxygen supply is a costly process [6] [26].

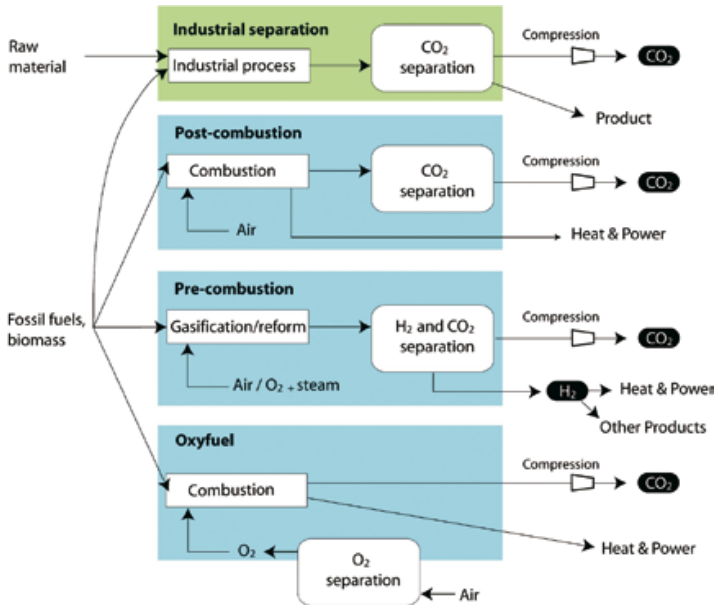

Figure 2.2: Schematic representation of industrial CO_2 capture systems, including post-combustion, pre-combustion and oxyfuel capture [6].

CO_2 capture from these industrial gas streams can be accomplished in multiple ways, for instance absorption, adsorption and membrane separation [27]. The most effective method depends on the CO_2 concentration, amount of available CO_2 and location of the source.

2.1.2 Direct Air Capture

To reduce the emissions of distributed CO_2 emitting sources such as transport and agriculture, direct air capture can have a significant impact since it extracts CO_2 from the ambient air [28]. DAC is a relatively novel technology and is therefore not widely implemented yet. The advantages of direct air capture compared to CO_2 from industrial combustion processes are the following:

- Firstly, DAC can be used to decrease the concentration of CO_2 in the atmosphere. In other words, it can result in negative CO_2 emissions. This is an essential part of the strategy to achieve the Paris agreement goals.

- Small scale CO_2 emission points from mobile applications such as ships or airplanes can not be minimized by conventional capture technologies [29] [18]. DAC can reduce the impact of these small scale emissions by capturing CO_2 from the air.
- Lower concentrations of contaminants like NO_x and SO_x in ambient air compared to flue gases, result in an increase in the life time of sorbents in a DAC system [18].
- Moreover, DAC can be part of the CCU technology, the captured CO_2 from the air is used as feedstock for production processes.

The major disadvantage of DAC is the small amount of CO_2 present in air compared to flue gases, 0.04% and 10% respectively [30] [31]. Consequently, the energy demand to extract CO_2 from air is higher than from flue gases. Figure 2.3 presents the minimal energy demand per captured mol CO_2, based on thermodynamics, for direct air capture compared to CO_2 capture from industrial combustion processes. It is clear that DAC requires 2 to 3 times more energy to capture CO_2 compared to capture from industrial processes.

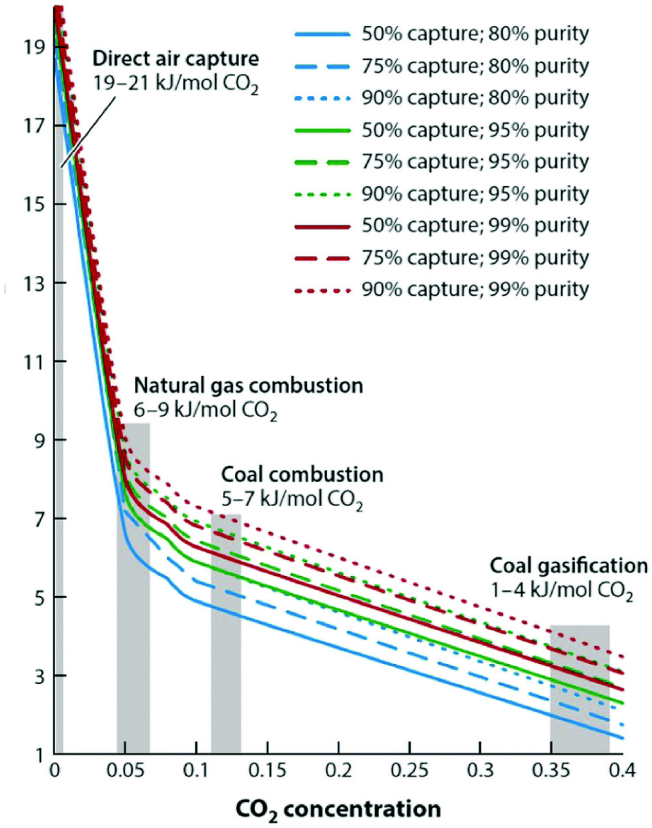

Figure 2.3: Overview of different CO_2 capture technologies and their energy demand per mole CO_2 [7].

Based on the type of sorbent, there can be two main DAC system categories classified, namely high temperature (HT) liquid solvent and low temperature (LT) solid sorbent systems, presented in figure 2.4 [8] [10] [32]. These systems will be explained in the following sections. Also, some technologies that are still in the research phase will be briefly mentioned.

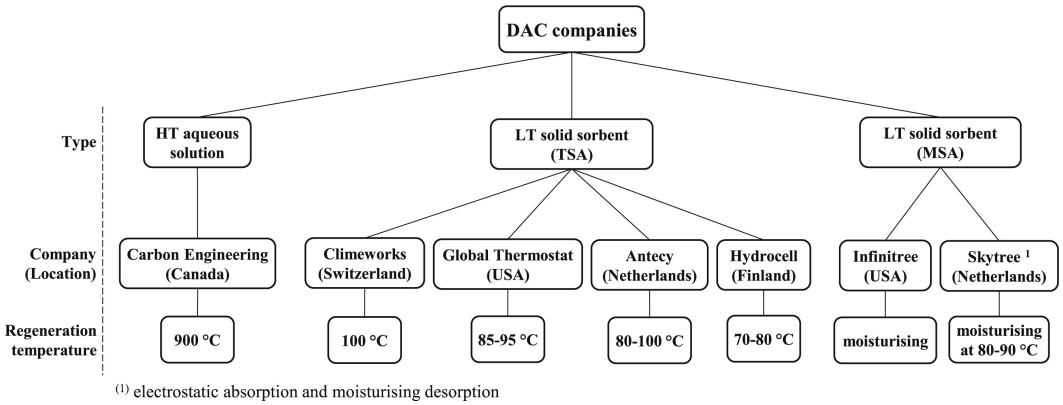

Figure 2.4: Overview of different DAC technologies and companies active in the specific field [8].

High temperature liquid solvent systems

Typical liquid solvents for this CO_2 capture technique are strong bases like potassium hydroxide (KOH), sodium hydroxide (NaOH) and calcium hydroxide ($Ca(OH)_2$). [10] [33] [34]. In the air contacter, the solutions are brought into contact with ambient air which facilitates the solution to absorb CO_2. To return the solution to its original state, without CO_2 absorbed, a regeneration process is required [32]. A design for a possible DAC system using KOH as solution is presented by Keith et al. [9], which consists of two cycles connected in a loop, figure 2.5. In the first cycle, CO_2 is captured by the present KOH solution and produces K_2CO_3. The rich solution is sent into a pellet reactor where it reacts with calcium hydroxide ($Ca(OH)_2$) which results in the recovery of KOH and the production of calcium carbonate ($CaCO_3$). The recovered KOH is send back into the air contacter to absorb new CO_2 whereas the $CaCO_3$ is brought into a calciner to release the absorbed CO_2. The byproduct of this reaction is a solid CaO which is reacted with H_2O in the slaker to produce calcium hydroxide which is transported to the pellet reactor [9].

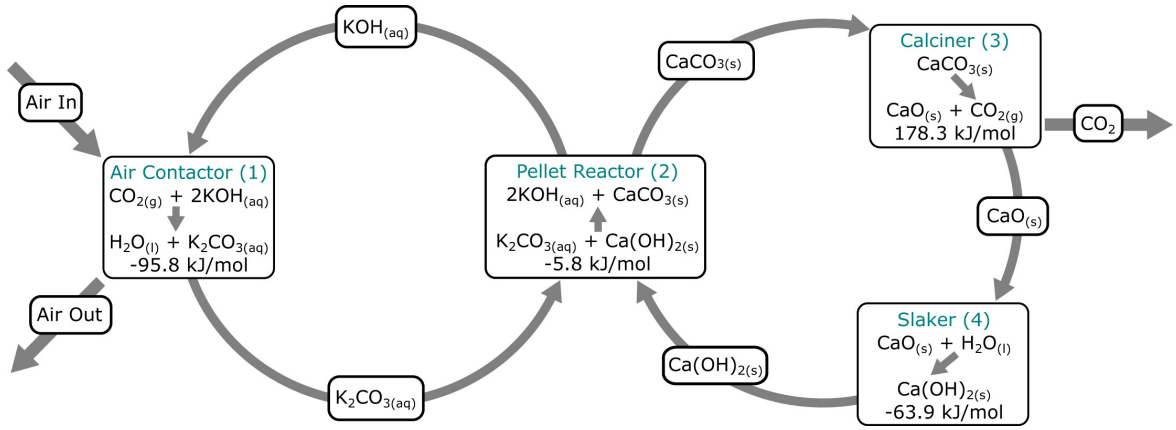

Figure 2.5: A possible high temperature liquid solvent DAC system that uses a KOH solution [9].

Advantages of liquid solvent systems are continuous operation of the system, cheap contactor design and long contactor lifetimes [9]. The main disadvantages are the high energy demand in the regeneration step of the process and stability of the liquid solvent [9].

An example of a company that uses a liquid solvent DAC system is **Carbon Engineering**. It uses a potassium hydroxide solution to capture CO_2 and operates according to the process described by figure 2.5. The typical regeneration temperature is around 900 $℃$. An energy supply of 1460 kWh heat and 366 kWh electricity is required per ton of CO_2 captured [9].

Low temperature solid sorbent systems

This system, similar to liquid solvent systems, consists of an adsorption and desorption process [10]. In the adsorption process, a solid structure made of a CO_2 adsorbing material gets in contact with air by making use of a fan. The CO_2 adsorbing material chemically bonds with the CO_2, it attaches to the surface of the sorbent. Depleted air gets blown out of the system. In the desorption process, the adsorbing material can be regenerated in various ways including pressure, temperature or humidity swing [32] [35]. This process is illustrated in figure 2.6.

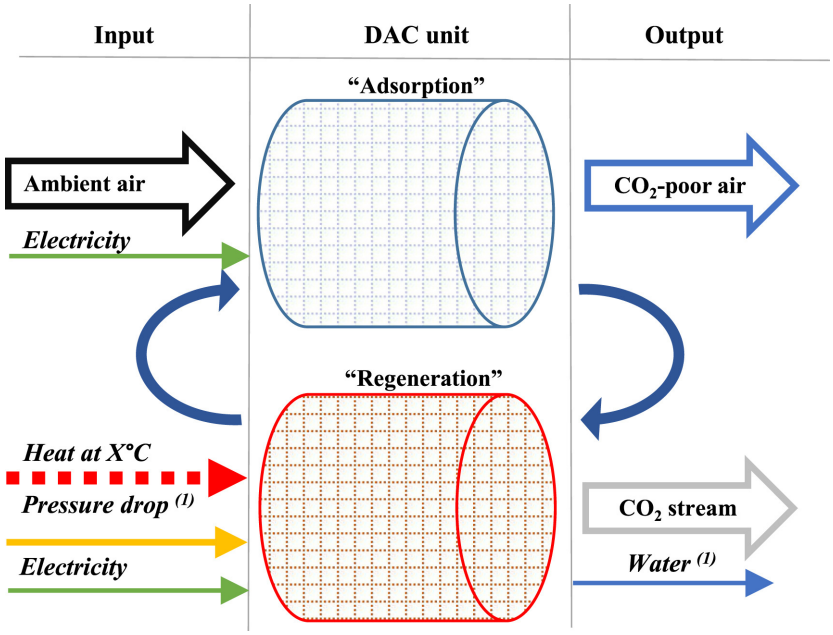

Figure 2.6: Schematic illustration of a low temperature solid sorbent DAC process [10].

Advantages of solid sorbent systems are the strong bonding with CO_2 at low partial pressures and the relatively low energy demand and operating costs compared to liquid solvent systems [9] [29]. Disadvantages are the potentially short lifetime of the sorbents due to degradation [8]. Furthermore, the design of the system is much more complex since both processes must occur in a single chamber [9]. As a consequence, the reciprocity between the adsorption and desorption process does not allow the system to have these processes operating continuously.

Examples of companies that use solid sorbent DAC systems are:

- **Climeworks** uses a cellulose fiber in combination with amines which works as a solid filter that bonds CO_2 chemically. To release the CO_2 from the solid sorbent, the pressure is reduced and the system is heated up to 100 $℃$ [8] [36]. Climeworks uses 200 - 300 kWh electricity and 1500 - 2000 kWh heat per ton of CO_2 captured [8].

- **Global Thermostat** uses amine polymer sorbents to capture the CO_2. The captured CO_2 is stripped off using low-temperature steam, between 85 and 100 $^{\circ}C$ [37]. Global thermostat requires 150 - 160 kWh electricity and 1190 - 1400 kWh heat per ton of CO_2 captured.

Other systems

Next to the two main system types of DAC, literature suggests new methods which are currently being investigated. An example is Ion-exchange resins that capture CO_2 by making use of quaternary amine functionality onto membranes [38]. The positive charge of the quaternary amine is balanced by free hydroxyl or carbonate counter-ions. When dry, they adsorb CO_2 and when wet, they release CO_2. Also, electro-swing reactive CO_2 capture is a newly investigated technique based on work of Voskian and Hatton [39].

As mentioned in section 1.2.1, ZEF has chosen for a liquid amine sorbent system as DAC technique. Liquid amine sorbents are commonly used to capture CO_2 from flue gases, however DAC applications that make use of this technique are not operational yet. Hence, Liquid amines are investigated to understand absorption and desorption fundamentals as well as complications that these liquid sorbents can cause in a DAC system.

2.2 Liquid Amine Sorbents for CO_2 Capture

2.2.1 Amines

Amines are chemical species in which an amino group is present. The amino group consists of a nitrogen atom, with zero, one or two hydrogen atoms connected to it. Next to the hydrogen atoms, the nitrogen atom is also connected to one, two or three organic substiluents. The amount of substiluents determines the type of amine, namely primary, secondary or tertiary amine [40]. The chemical structure of these amines is presented in figure 2.7.

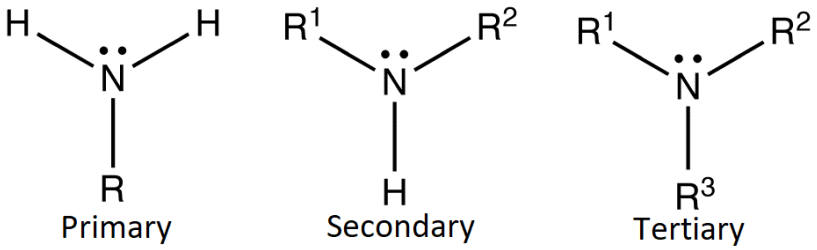

Figure 2.7: Simplified chemical structure of primary, secondary and tertiary amines.

Carbon capture by making use of liquid amines is one of the oldest and most promising ways to capture CO_2 and is already operating on a commercial scale for flue gas and natural gas capture applications [24] [25] [26]. A generic liquid amine-based CO_2 capture system consists of an absorption and desorption column. The aqueous amine solution is fed into the absorption column where it flows downwards. Air is blown from the bottom into the column and creates a counter current flow with the liquid amine. During this contact, CO_2 is absorbed into the solvent which becomes loaded with CO_2 and is referred to as rich amine or rich loaded amine. This rich amine is then fed into the stripping column where the reboiler, which is situated at the bottom, heats up the rich amine. Due to this heat, CO_2 starts to desorb from the amine. After desorption, the amine has become a lean amine since it

contains a lesser amount of CO_2. The lean amine leaves the stripping column and flows through an heat exchanger where it passes the rich amine that is in this way preheated. Eventually, the lean amine is fed back into the absorption column. The CO_2 in gas phase, which leaves the stripper at the top, is collected.

For a continuous process at equilibrium, the values of the rich and lean loaded amine remain constant. The amount of CO_2 that is being absorbed and later desorbed, which corresponds to subtracting the lean from the rich loading, is specified as the cyclic capacity. Since the rich and lean loading remain constant, the cyclic capacity also remains constant. The cyclic capacity determines, together with the mass flow rate, the production yield in a direct air capture system.

MEA and DEA are conventional amines that are generally used to capture CO_2. MEA is often used in literature as a benchmark to analyse the performance of unconventional amines [41].

Absorption in liquid amines

Absorption of CO_2 in liquid amines occurs typically between 40 - 50 ℃ in flue gas capture applications [42]. During absorption, 4 chronological steps can be distinguished [43]:

1. CO_2 diffuses from bulk gas to the gas-liquid amine interface.
2. CO_2 dissolves physically in the liquid amine.
3. CO_2 reacts with the liquid amine.
4. Reacted CO_2 diffuses through the liquid amine.

Step 1 and 2 can be described by Fick's law of diffusion and Henry's law, equations 2.1 and 2.2 respectively.

$$J = -D\frac{dc_a}{dz} \tag{2.1}$$

where J = diffusion flux, D = diffusivity and dc_a/dz = molar concentration gradient

$$H_{gas} = \frac{p_{gas}}{c_{gas}} \tag{2.2}$$

where H_{gas} = Henry constant, p_{gas} = partial pressure and c_{gas} = solubility of the gas.

In the third step, CO_2 reacts with the present amine. For primary and secondary amines, stable carbamates are formed during this reaction. The reaction starts with the formation of a zwitterion, an ion with both negative and positive charge, which is afterwards deprotonated so that it forms a carbamate, reactions 2.3 and 2.4. This carbamate is hydrolysed which results in the creation of a bicarbonate and the regeneration of the amine, reaction 2.5 [44] [45].

$$R_1R_2NH + CO_2 \leftrightarrow R_1R_2NH^+COO^- \tag{2.3}$$

$$R_1R_2NH + R_1R_2NH^+COO^- \leftrightarrow R_1R_2NH_2^+ + R_1R_2NCOO^- \tag{2.4}$$

$$R_1R_2NCOO^- + H_2O \leftrightarrow R_1R_2NH + HCO_3^- \tag{2.5}$$

The formation of a single carbamate species requires two amine molecules, which results in a maximum loading of 0.5 mol of CO_2 per mol amine at low pressures [34] [44]. Greater loadings can be realized when increasing the CO_2 partial pressure, leading to the formation of bicarbonate [34].

For tertiary amines, this reaction mechanism works differently since it follows a single chemical reaction when forming bicarbonates, equation 2.6 [46]. A proton is transferred to the present amine which allows bicarbonate to be formed.

$$R_1R_2R_3N + CO_2 + H_2O \leftrightarrow R_1R_2R_3NH^+ + HCO_3^- \tag{2.6}$$

This chemical reaction results in a theoretical maximum loading of 1 mol CO_2 per mol of amine. This is two times higher as that of primary and secondary amines. However, the reaction rate in tertiary amines is lower compared to primary and secondary amines [46].

In the last step, the diffusion of reacted CO_2 through the amine is described by the Stokes-Einstein equation, equation 2.7. This equation holds for liquids with a low Reynold's number [47].

$$D = \frac{k_B T}{6\pi\mu r} \tag{2.7}$$

where T = temperature of the fluid, k_B = Boltzmann constant, μ = dynamic viscosity of the fluid and r = radius of spherical particle.

The absorption of H_2O in amines follows almost the same steps, however it does not react with the amine. H_2O only dissolves and is therefore an example of physical absorption [14]. Due to this difference in absorption type, H_2O adds extra moles to the mixture when absorbed where CO_2 does not affect the amount of moles present.

Desorption in liquid amines

Desorption is the inverse process of absorption and therefore the desorbed species follow the inverse steps as explained during absorption. Since absorption is an exothermic reaction, desorption is endothermic; additional heat is required to remove the solute species by mass transfer from the solvent into the gas phase. Diffusion of the solutes is again described by Stokes and Einstein in equation 2.7. The reaction rate is described by the Arrhenius equation, equation 2.8, where it expresses the dependency on temperature.

$$k = A \cdot \exp\frac{-E_a}{RT} \tag{2.8}$$

where k = reaction rate constant, the frequency of collisions that results in a reaction, A = pre-exponential factor, a constant for each chemical reaction, E_a = activation energy for the reaction and R = universal gas constant. The reaction rate constant describes the kinetics of the reaction. Whether kinetics plays a limiting role in desorption of the solute can be expressed in multiple ways. The Hatta number, equation 2.9, is a dimensionless number that compares the reaction rate in a liquid film to the diffusion rate through the film. When the Hatta number is high, it is diffusion limited whereas the Hatta number is low, it is limited by reaction kinetics [48]. A typical Hatta number for desorption of CO_2 from an amine is in the range of 10 to 35 which means that the reaction kinetics are relatively fast [49].

$$Ha = \frac{1}{k_L}\sqrt{D_{CO_{2,am}} k_2 C_{amine}} \tag{2.9}$$

where $D_{CO_{2,am}}$ = CO_2 diffusivity in the amine solution, k_2 = second order reaction rate constant, C_{amine} = amine concentration and k_l = mass transfer coefficient in liquid phase [50] [51]. The second

Damköhler number, equation 2.10, is a dimensionless number which also relates the reaction rate to the diffusion rate [52].

$$Da_{II} = \frac{L^2 r}{DC} \tag{2.10}$$

where r = reaction rate, C = concentration of CO_2 in the amine , D = diffusion coefficient and L = length the CO_2 has to travel inside the amine.

Complications for liquid amines in DAC

As explained in section 2.1.2, the regeneration of liquid amine sorbents remains an important limitation of this CO_2 capture technology. Furthermore, the net cyclic capacity of liquid amines is relatively low. That is, the amount of CO_2 absorbed and later desorbed per mol amine is low and results in high energy demands of the DAC system. ZEF has found an amine with a specially high net cyclic capacity, namely tetra-ethylpentamine. This amine could be a possible solution for the energy demand problem and is elaborated on in the next sections.

2.2.2 Tetra-ethylenepentamine

Tetra-ethylenepentamine (TEPA) is an amine which has been thoroughly researched by ZEF and chosen as the most equipped amine to operate the direct air capture system with. TEPA has a relatively high absorption rate and equilibrium solubility of CO_2 compared to other amines [11] [14]. Figure 2.8 presents the simplified chemical structure of TEPA, which shows clearly that TEPA holds both primary and secondary amino groups.

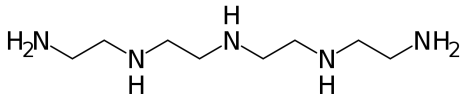

Figure 2.8: Simplified chemical structure of Tetra-ethylenepentamine.

Some general properties of TEPA are displayed in table 2.1. Note that the boiling point of TEPA is much higher than the desorption temperature of H_2O and CO_2. Ovaa et al. [14] found that the density of TEPA changes when H_2O is being absorbed, however the variation is very small.

Table 2.1: General properties of TEPA.

Property	TEPA
Molecular weight $[g/mol]$	189.31 [53] [54]
Density $[g/cm^3]$	0.99 (at 20℃) [53] [54]
Boiling point $[℃]$	375 [55]

The viscosity of TEPA is highly dependent on temperature and loading of CO_2 and H_2O [11]. Figure 2.9 shows that loading TEPA with CO_2 and H_2O increases the viscosity significantly. An increase in temperature results in a decrease of the viscosity.

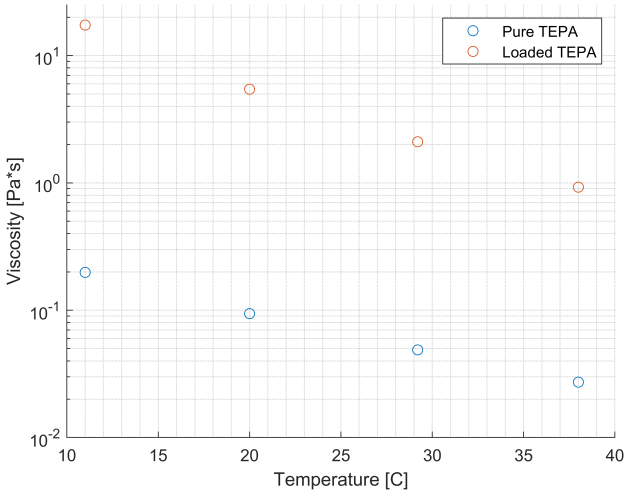

Figure 2.9: Temperature dependency of the viscosity for pure TEPA and a TEPA, 30 wt% H_2O and 9.5 wt% CO_2 mixture [11].

Absorption in TEPA

Since TEPA holds primary and secondary amino groups, it absorbs CO_2 following reactions 2.3, 2.4 and 2.5. Sinha et al. [11] performed experiments to understand the effect of H_2O on the absorption of CO_2 in TEPA. The results are shown in figure 2.10. It was found that the presence of H_2O highly influences the absorption rate of TEPA, the more H_2O is present, the higher the absorption rate becomes. This proves that a significant amount of H_2O is required in the ternary mixture to realize high loadings.

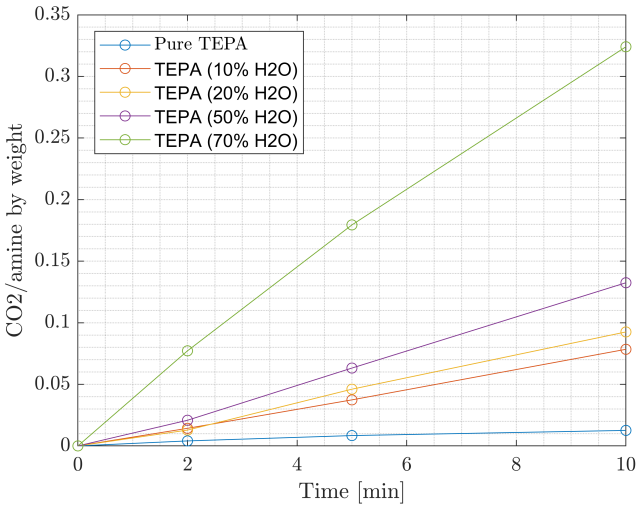

Figure 2.10: Data loading experiment TEPA with varying H_2O wt% [11].

Desorption in TEPA

After absorption, desorption is required to regain the lean ternary mixture of TEPA-H_2O-CO_2 and produce CO_2 and H_2O streams. Desorption of H_2O and CO_2 from TEPA occurs typically at temperatures between 80 and 140 °C [42] [56] [57]. Ovaa et al. performed various batch experiments on the net cyclic capacity of CO_2 from a rich TEPA-H_2O-CO_2 mixture [14]. The rich mixture contains 4.35 wt% CO_2, which corresponds to 1.24 mol CO_2/kg TEPA, and 30 wt% H_2O. It was found that an increase in temperature and a decrease in pressure results in a higher net cyclic capacity of CO_2. One must notice that the experiments are performed at nearly vacuum, desorption at higher pressures are still to be investigated. The same experiments showed that all the H_2O is evaporated at the end of the experiment [14]. Note that these experiments took nearly 1000 minutes which explains the complete desorption of H_2O at these low pressures. Nonetheless, it was concluded that an increase in temperature and decrease in pressure enhances the desorption of H_2O from TEPA [14].

Another experiment, displayed in table 2.2, shows that the desorption rate of CO_2 decreases when the loading of the sample decreases [14]. This continues until equilibrium is reached, at this point no CO_2 is desorbed from the mixture and the total CO_2 output remains constant. This occurred in the experiment at 26000 s.

Table 2.2: Experimental data of CO_2 desorption at 50 mbar and 120 °C [14].

Time $[s]$	Output $[mol\ CO_2/kg\ TEPA]$	Output $[\%]$
1670	0.19	20
3600	0.47	50
7400	0.76	80
12600	0.90	95
26000	0.94	100

ZEF uses a stripping column to regenerate the TEPA and produce CO_2 and H_2O product streams. The high viscosity of loaded TEPA can cause difficulties when desorbing inside a stripping column. Also, the high energy demand of the regeneration process is still a limitation for ZEF's direct air capture system. To tackle these complications, one must first get a deeper understanding in the working principles of a stripping column. Consequently, stripping is explained in the following section.

2.3 Stripping

This section explains the principles of stripping and applications of strippers in industry are illustrated. Also, the energy demand of strippers is investigated and equilibrium phenomena are described.

2.3.1 Basics of Stripping

In stripping, a feed mixture of a sorbent and a solute, the solute is a species that is absorbed into the sorbent, is fed into the top of the stripping column where the solute is desorbed from the sorbent. The heat that is required to desorb the solute is supplied by the reboiler which is situated at the bottom of the stripping column. For plant-size stripping columns, the reboiler is mostly an external heat exchanger in the form of a kettle-type or vertical thermosyphon-type reboiler [58]. For smaller stripping columns, the reboiler is often located in the bottom of the column to avoid piping. The desorbed solute

rises through the column and creates a counter current flow with the liquid feed mixture flowing downwards. Because of the facilitated contact between the desorbed solute and the liquid feed mixture, a temperature gradient appears in the column. The top of the column is consequently the coldest. The desorbed solute will leave the stripping column in gas phase at the top as top product. Due to the conditions, there will always be some residual solute left in the solvent, which leaves the column at the bottom, also called bottom product. The top of the column consists of a reflux condenser and reflux drum. Here, the evaporated solute condenses and is partly fed back into the column. The reflux ratio is determined as the amount of condensed vapor fed back over the amount discarded from the column, equation 2.11. In the reboiler, the bottoms is partly evaporated and fed back into the column. The amount fed back into the column over the bottoms that is discarded from the system is defined as the boilup ratio, equation 2.12. The reflux and reboiler are generally used to purify the top and bottom product [58]. A design trade-off is normally made between the number of stages and the reflux ratio [58]. A general schematic for a stripping column with reflux and reboiler is shown in figure 2.11.

$$R = \frac{L}{D} \tag{2.11}$$

$$V_B = \frac{V}{B} \tag{2.12}$$

where L = condensed vapor fed back into the column, D = top product discarded from the system, V = liquid fed back into the column and B = bottom product discarded from the system.

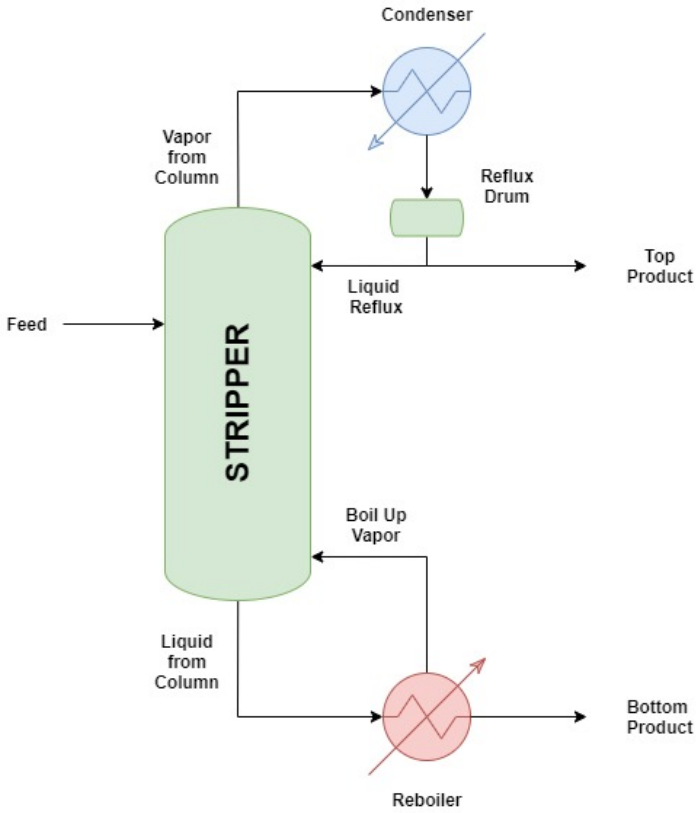

Figure 2.11: General schematics of a stripping column with reflux and reboiler

Multi-component stripping

The working principle of multi-component desorption in a stripping column is in essence the same as normal stripping, however the number of solutes has increased. Note that it is important for the sorbent to have a significant higher boiling temperature than the temperature where desorption of the solutes occurs at. The desorbed solutes arrive in gas phase at the top of the stripper and are ideally separated from each other. A condenser is frequently implemented so that one of the solutes condenses whereas the other solute remains in vapor phase. The solutes should contain a large enough boiling point temperature difference so that high purified product streams can be realised [58].

2.3.2 Stripping in Industry

There is a wide variety of stripping techniques used in industry [58]. Stripping is mainly conducted in trayed and packed columns:

- A **trayed column** is a vertical pressure vessel in which a vapor and liquid gets in contact on a series of trays or stages. Liquid accumulates on each stage and flows over an outlet weir into a downcomer where gravity pulls the liquid to the stage below. Gas flows up through openings in each stage and bubbles through the liquid film present in that stage. Commonly used stage openings are perforation, valve cap and bubble cap openings [58]. Ideally, no vapor bubbles are flowing down with the liquid (occlusion) or liquid droplets are carried up by the vapor (entrainment). Also, there is no weeping of liquid through the vapor openings. Each stage represents an equilibrium between the present liquid and vapor in that stage, also called vapor-liquid equilibrium, which will be further explained in section 2.3.4.
- A **packed column** is a vertical pressure vessel which contains one or multiple sections of packing material. The liquid flows over the packing material surface downwards and the vapor flows upward through the wetted packing where it contacts the liquid. Commercial packing materials are split in two categories: random and structured packings. Random packings are tiny objects with a high surface area and are poured randomly in the column. Structured packings are mostly sheets of metal or plastic that are perforated, embossed or surface roughened and stacked in the column. Structured packings are substantially more expensive than random packings, though they hold a higher efficiency and capacity [58].

Other stripping techniques are spray towers, bubble columns and centrifugal contactors [58].

Configurations of stripping columns differ widely within industrial applications. Interheated stripping columns use multiple heating elements positioned at different heights within the column. This contributes often to a lower energy demand and lower lean loadings leaving the column [59]. Other stripping configurations include flashing feed, multipressure with split feed, internal exchange and matrix columns. These configurations offer mostly a higher energy efficiency for different sorbents or operating conditions [60].

For design or analysis of a stripper column one should consider a number of important factors [58]:

- Feed mixture, in terms of flow rate, composition, temperature and pressure.
- Operating pressure and temperature of the column.
- Type of stripping equipment.
- Number of stages or height of packing.

- Desired recovery of one or multiple solutes.
- Heat effects and need for extra heating or cooling.
- Necessity of implementation of a reboiler and reflux.
- General dimensions of the column, such as height and diameter.

Amine Stripping in Industry

As discussed in section 2.2.1, aqueous amines are used as liquid sorbents in carbon capture systems. This section presents some examples of industrial applications of amine strippers. Cousins et al. [61] analyzed a CO_2 capture plant located at the Tarong Power Station in Queensland, Australia. Calvert et al. [62] investigated a Thermoflow 29 ProMax 5.0 carbon capture process. Both capture processes used monoethanolamine (MEA) as liquid sorbent and a stripper to regenerate the solvent. An overview of the operating characteristics of these strippers is presented in table 2.3.

Table 2.3: Operating characteristics of the strippers investigated by Calvert et al. and Cousins et al.

Research	Calvert et al. [62]	Cousins et al. [61]
Sorbent	MEA 35 wt%	MEA 30 wt%
Abs. Pressure $[bar]$	2.2	1.8
Temperature $[℃]$	125	120
Rich loading $[mol\ CO_2/kg\ amine]$	7.37	8.02
Lean loading $[mol\ CO_2/kg\ amine]$	4.09	2.95
Reboiler duty $[MJ/kg\ CO_2]$	3.95	3.5

Table 2.4 shows an overview of the reboiler duties (i.e. energy consumption) in stripping columns for common amine sorbents. These duties are based on pilot plant or lab-scale plant results, but give a fair idea of the reboiler duties in industry [6]. It can be concluded that the reboiler duties presented in table 2.3 match the data in table 2.4 accurately. Moreover, amine blends seem to have a lower energy consumption than single conventional amine sorbents.

Table 2.4: Reboiler duties for various amine solvents in CO_2 capture plants.

Sorbent	Reboiler duty $[MJ/kg\ CO_2]$
30 wt% MEA	3.6 - 4.0 [63]
40 wt% MEA	3.1 - 3.3 [64]
MEA + MDEA	2.0 - 3.7 [65]
DEEA + MAPA	2.1 - 2.4 [66]

The high energy demand of a stripping column is caused by different energy phenomena that take place inside the column. Section 2.3.3 will identify the relevant phenomena and discuss their effect on the total energy demand of the stripper.

2.3.3 Energy

For a liquid amine stripping column, it was found that the energy demand to facilitate desorption is based on four energy principles, namely sensible heat, heat of desorption, heat of vaporization and

reflux [12] [14]. These phenomena are explained in this section and related coefficients for TEPA, H_2O and CO_2 are presented.

Sensible heat

The sensible heat represents the amount of heat that is needed to heat the ternary mixture from absorption to desorption temperature. This can be calculated according to equation 2.13.

$$Q_{sens} = \dot{m} \cdot c_p(T_{des} - T_{abs}) \tag{2.13}$$

where Q_{sens} = sensible heat, $\dot{m}$ = mass flow rate, c_p = specific heat and T_{des} and T_{abs} are the desorption and absorption temperature respectively. When one assumes the mixture to be incompressible, the specific heat is dependent on temperature only [67]. Table 2.5 shows an overview of the average specific heat of the ternary mixture components TEPA, H_2O and CO_2.

Table 2.5: Average specific heat of TEPA, H_2O and CO_2 in the liquid and vapor phase [15][16][17].

Constant	Description	TEPA	H_2O	CO_2	Units
$c_{p_{liq}}$	Specific heat liquid phase	460	75	160	$[J/mol\ K]$
		2430	4167	3636	$[J/kg\ K]$
$c_{p_{vap}}$	Specific heat vapor phase	0	33.5	37	$[J/mol\ K]$
		0	1861	841	$[J/kg\ K]$

Heat of desorption

The heat of absorption (ΔH_{abs}) is defined as the enthalpy associated with the absorption of a molecule in a sorbent. Absorption of CO_2 is exothermic, it releases energy. In contrary, desorption of these components is endothermic, it requires energy to break the chemical bonds and disassociate the molecules from the sorbent. Since absorption and desorption are inverse reactions of one another, the heat associated with it corresponds. The heat of desorption of CO_2 is a function of loading (CO_2/TEPA) and temperature [68] [69]. Dowling et al. [12] estimated the heat of absorption of CO_2 in TEPA for different loadings and temperatures, shown in figure 2.12a, 2.12b and 2.12c, using the Clausius-Clapeyron equation.

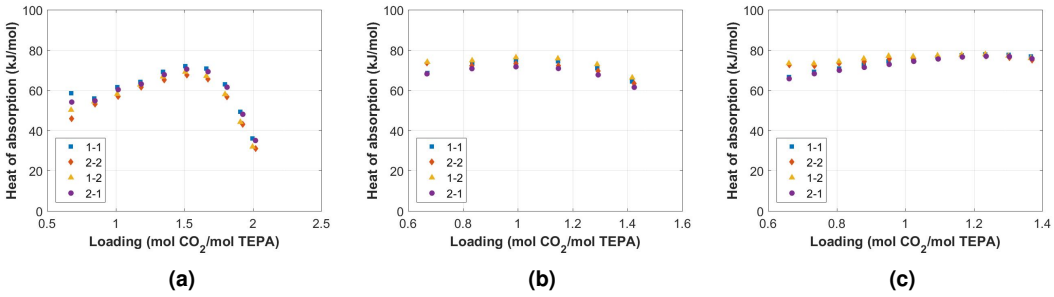

Figure 2.12: Heat of absorption calculated using the Clausius Clapeyron equation and the CO_2 absorption isotherms. The numbers in the legend refer to the different combinations of duplo measurements used for the calculations. (a) 30 $wt\%$ TEPA at 313.15 K and 353.15 K (b) 30 $wt\%$ TEPA at 353.15 K and 393.15 K (c) 70 $wt\%$ TEPA at 353.15 K and 393.15 K [12].

An approximation of the heat of desorption is made by looking at the values with higher loadings. For 30 $wt\%$ TEPA this is approximately between 70 and 75 kJ/mol. For 70 $wt\%$ the value lies between 75 and 80 kJ/mol [12]. This correlates with values found for conventional amines such as MEA (70 kJ/mol) [70].

Heat of vaporization

Sinha et al. [11] estimated the heat of vaporization of H_2O in TEPA for different H_2O-TEPA ratios. Since the heat of vaporization is higher than the latent heat of H_2O, this implies that heat of mixing, forming and breaking of hydrogen bonds also adds up to the heat of vaporization of H_2O [11]. The latent heat and average heat of vaporization of H_2O are shown in figure 2.6.

Table 2.6: Average heat of vaporization and latent heat of water.

	Description	H_2O	Units
H_{vap}	Heat of vaporization	60.3 [11]	$[kJ/mol\ H_2O]$
H_{lat}	Latent heat	40.8 [71]	$[kJ/mol\ H_2O]$

Reflux

Reflux can play an important role in the energy demand of the stripping column. Two types of refluxes can be distinguished, internal and external reflux. Internal reflux describes the liquid transport of a condensed vapor from a stage to the stage underneath. This phenomenon does not add up to the energy demand of the system since the heat remains within the system. However, external reflux adds up to the energy demand of the system. Evaporated H_2O which leaves the stripping column at the top is condensed in a cooler and collected in a flash tank. Some of the collected H_2O can be returned to the column, the amount is determined by the reflux ratio. The returned H_2O is cooled down and requires sensible heat and possibly heat of vaporization when again present in the stripping column. To conclude, a higher reflux ratio intensifies the energy demand of the stripping column.

The following section will present more insights on the coexistence of TEPA, H_2O and CO_2 by proposing and investigating vapor-liquid equilibria and vapor curves for the present components.

2.3.4 Vapor-Liquid Equilibrium

Vapor-Liquid Equilibrium Fundamentals

The state of coexistence of a gas and liquid phase, for a particular species, is defined as a vapor-liquid equilibrium, also known by its abbreviation VLE. For a mixture, this means that a liquid mixture, at a certain temperature T and pressure P, is in equilibrium with a vapor mixture with the same T and P [72] [73]. For this reason, a VLE describes the relation between temperature, pressure and composition of both, liquid and gas, phases. This implies that for a given P and T of a mixture, the composition of the liquid and gas can be calculated. For a stripper, the VLE behaviour of the mixture that needs to be separated is of great importance since it gives an accurate indication of the separation that is going to occur at a certain temperature and pressure [58] [74]. The equilibrium between gas and liquid phase for a particular species is described by Raoult's law:

$$y_i P = x_i P_{\text{vpi}} \tag{2.14}$$

Where y_i = vapor phase mole fraction, P = absolute pressure, x_i = liquid phase mole fraction and P_{vpi} = the saturation vapor pressure for species i. The derivation of Raoult's law for vapor-liquid equilibrium is in detailed explained in appendix A.1.

In literature, one finds a large amount of equilibrium data for binary systems. For multi-component systems on the other hand, much less data is available due to the long duration it takes to measure a decent data set. Also the visualization of multi-component vapor-liquid equilibrium data in graphs or tables is difficult. For this reason K values are introduced [58]. The K value of a specific species i expresses the tendency of the species to vaporize. The K value is defined as:

$$K_i = \frac{y_i}{x_i} \tag{2.15}$$

where y_i is the composition of the vapour phase that is in equilibrium with the composition of the liquid phase, x_i. K values are functions of temperature, pressure and composition. The relative volatility, $\alpha_{i,j}$, is a related concept which describes the feasibility of separation of components i and j in stripping and is defined by:

$$\alpha_{i,j} = \frac{K_i}{K_j} \tag{2.16}$$

In an ideal system, the liquid phase behaves according to Raoult's Law and the vapour phase according to the ideal gas law. For a certain system, the K value is given by:

$$K_i = \frac{y_i}{x_i} = \frac{p_i^0}{P} \tag{2.17}$$

where p_i^0 = the vapor pressure of a pure component i, which is temperature dependent, and P = the pressure of the total system. For a non-ideal system, the K value is also depending on the composition of the mixture:

$$K_i = \frac{\gamma_i^L}{\phi_i^V}\frac{p_i^0}{P} \tag{2.18}$$

Where ϕ_i^V = the vapor fugacity coefficient and γ_i^L = the liquid phase activity coefficient [58].

VLE for TEPA, H2O and CO2 mixture

Dowling et al. [12] build a specific ion interaction theory (SIT) model based on experiments performed on vapor-liquid equilibria between TEPA, H_2O and CO_2 for different temperatures and loadings [12]. This model works with the activity coefficient theory and uses the extended Debye-Hückel law. The activity coefficient equation has an extra linear term added, equation 2.19. This term accounts for the concentration dependent short-range interactions [75] [76].

$$log\gamma_i = -\frac{z_i^2 A\sqrt{I}}{1 + 1.5\rho^{-1/2}\sqrt{I}} + \sum c_j \epsilon_{ij} \tag{2.19}$$

Figure 2.13 displays the experimental points of the VLE experiments versus the SIT model prediction for the ternary mixture of TEPA, H_2O and CO_2. The model predicts the partial pressure of CO_2 accurately between a concentration of 30 and 70 $wt\%$ TEPA and a temperature between 313.15 and 393.15 K. Extrapolation outside these ranges is much less reliable [12]. Also, in the low loading range the model is less accurate since the absolute pressure was close to the accuracy of the pressure sensor [12].

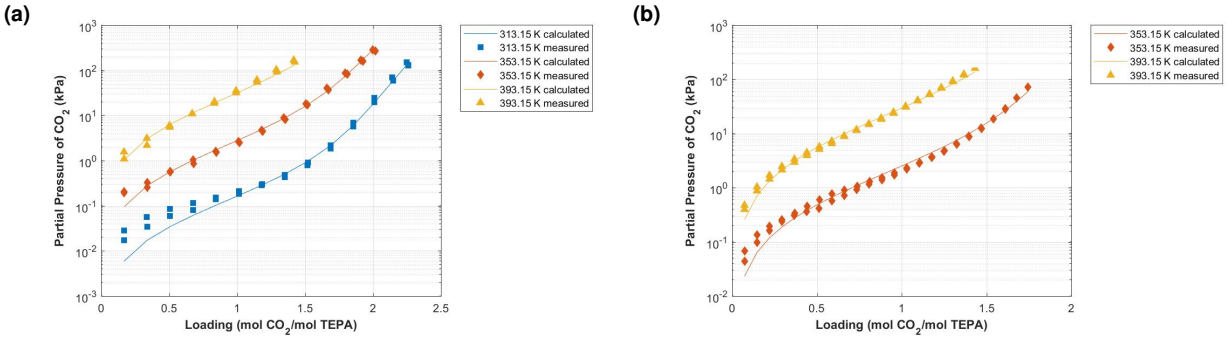

Figure 2.13: Experimental VLE data of the equilibrium CO_2 absorption in an aqueous solution of (a) 30 $wt\%$ TEPA at 313.15, 353.15 and 393.15 K and (b) 70 $wt\%$ TEPA at 353.15 and 393.15 K versus the ternary TEPA-H_2O-CO_2 model prediction [12].

Figure 2.14 represents the SIT model predictions for different isotherms. Note that this graph corresponds to 70 $wt\%$ TEPA and should be seen as an intersection of the total SIT model. The expression of loading in moles of CO_2 per kg TEPA is a standardized expression within ZEF. Further mentioning of loading in this work will be consistently expressed in moles of CO_2 per kg TEPA.

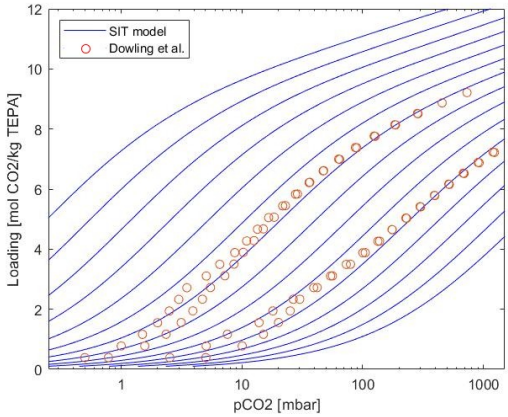

Figure 2.14: Experimental VLE data of 70 $wt\%$ TEPA versus SIT model with varying isotherms for loading $[mol\ CO_2/kg\ TEPA]$.

2.3.5 Vapor Curve

In the same research, experiments were performed to understand the equilibrium of a binary TEPA-H_2O mixture for different concentrations and temperatures [12]. According to the experimental data, a binary model was created based on the modified Raoult's law, Clausius-Clapeyron equation and Wilson's equation. The performed experiments and creation of the binary model are briefly explained in appendix A.2. The results of the performed experiments and binary model are shown in figure 2.15.

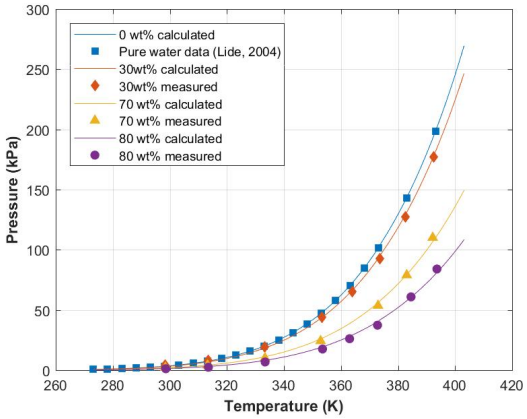

Figure 2.15: The equilibrium pressure of binary mixtures of TEPA and H_2O with 30, 70 and 80 $wt\%$ TEPA and pure water as a function of temperature versus the binary model based on Wilson's activity coefficients [12].

Note that the absence of CO_2 might influence the behaviour of the vapor curve greatly. This is something that still has to be investigated.

To conclude this chapter, different stripper models are proposed in the following section to be able to predict the performance of a stripping column for varying stripping conditions and configurations.

2.4 Modeling of a Stripping Column

To understand the effect of parameters on the stripper performance and to provide a new stripper design for ZEF it is crucial to first build a multi-component and multistage stripper model. A wide range of modeling methods is presented in literature. Seader and Henley [58] split these models into two fundamentally different categories: equilibrium and non-equilibrium based modeling methods. It is assumed that the stripping column operates at equilibrium. Section 5.1 will present the validation of this assumption. Hence, equilibrium based methods will be considered in the following sections and some examples are given. An overview of the methods is given in figure 2.16. Finally, the most suitable modeling method for the available TEPA-H_2O-CO_2 mixture data will be chosen.

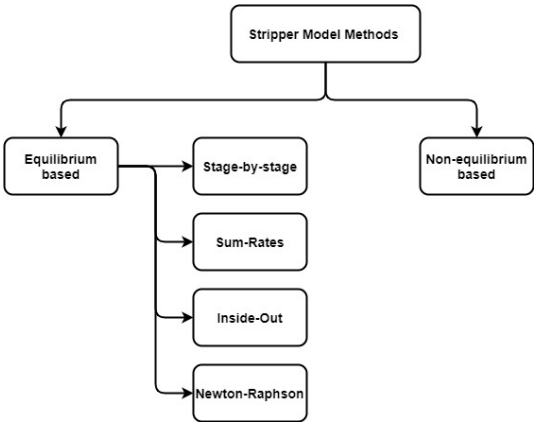

Figure 2.16: Schematic overview of stripper modeling methods.

2.4.1 Equilibrium Based Models

As the title suggests, equilibrium based models are build on the assumption of equilibrium between the liquid and gas phase in a generic stage. To remain in equilibrium, the temperature and absolute pressure in this stage are assumed constant. This equilibrium is described by the equilibrium equations, also known as the MESH equations, and includes component mass balances, total mass balance, phase equilibria relations and energy balances. A multistage stripper model consists of multiple interconnected generic stages. Stage-by-stage, Sum-Rates, Newton-Raphson and Inside-Out methods are equilibrium based model solving methods and will be further investigated in this section. The Boiling-Point method is generally restricted to narrow-boiling feed mixtures and thus more suitable for distillation than stripping [58]. The Boiling-Point method will consequently not be further investigated.

As mentioned above, modeling of a steady-state stripping column is generally done by making use of the mass and energy balances. These balances are mathematically explained in the MESH equations which stands for:

- Mass balance equations
- Phase equilibrium equations
- Mole fractions summation
- Energy balance equations

These equations can be performed separately for each stage of the column since it is assumed that vapor and liquid present in each stage are in phase equilibrium. Figure 2.17 shows an overview of the input and output streams in a generic stage j, with temperature T and absolute pressure P of the stripping column.

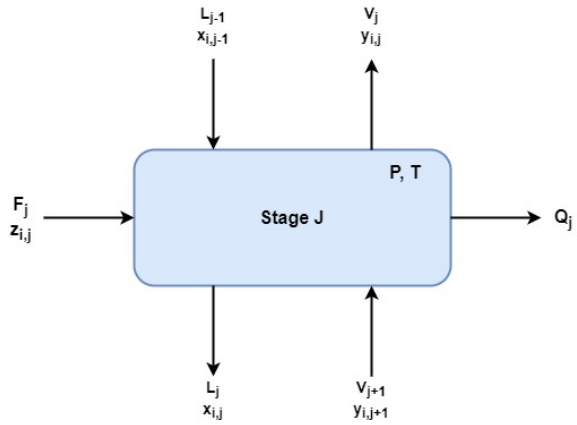

Figure 2.17: Schematic overview of input and output streams in a generic stage j

Where F_j is the flow rate of the feed stream into stage j, with molar fraction $z_{i,j}$ for component i, Q_j is the heat load leaving stage j (for conventional reasons it is assumed that heat is leaving the stage), L_j is the liquid flow rate from stage j into stage $j+1$, with molar fraction $y_{i,j}$ for component i. V_j is the vapor flow rate from stage j into stage $j-1$, with molar fraction $x_{i,j}$ for component i. The same applies for L_{j-1} and V_{j+1}, with $x_{i,j-1}$ and $y_{i,j+1}$ respectively. With these notations defined,

The MESH equations can be given:

$$F_j z_{i,j} + L_{j-1} x_{i,j-1} + V_{j+1} y_{i,j+1} - L_j x_{i,j} - V_j y_{i,j} = 0 \tag{2.20}$$

$$y_{i,j} - K_{i,j} x_{i,j} = 0 \tag{2.21}$$

$$\sum_{i=1}^{C} y_{i,j} = 1 \tag{2.22}$$

$$\sum_{i=1}^{C} x_{i,j} = 1 \tag{2.23}$$

$$F_j h_{F_j} + L_{j-1} h L_{j-1} + V_{j+1} h V_{j+1} - L_j h_{L_j} - V_j h_{V_j} = 0 \tag{2.24}$$

where C = number of components in mixture and h = molar enthalpy. Equation 2.20 represents the component mass balance, equation 2.21 presents the phase equilibrium equation, equations 2.22 and 2.23 give the mole fractions summation equations and equation 2.24 represents the energy balance. Equations 2.22 and 2.23 can be replaced by a total mass balance, equation 2.25 [58].

$$F_j + L_{j-1} + V_{j+1} - L_j - V_j = 0 \tag{2.25}$$

The MESH equations form the base of every equilibrium based stripper model solving method.

Stage-by-stage method

The stage-by-stage method is the simplest and oldest equilibrium based solving method [58]. Lewis-Matheson, 1932 [77], and Thiele-Geddes, 1933 [78], published papers on a stage-by-stage, equation-by-equation calculation procedure based on equation 2.20 and 2.24 for solving simple fractionators with one feed and two products [58]. This procedure only holds for ideal mixtures. They simplified generic stage j to a single stage flash vessel, shown in figure 2.18.

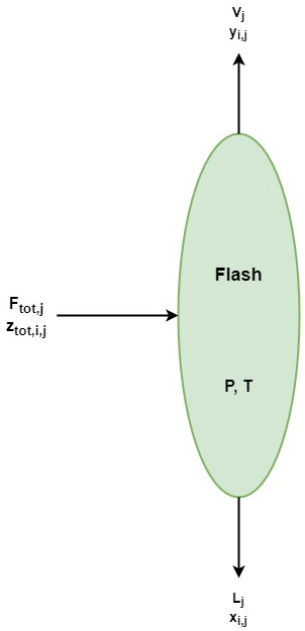

Figure 2.18: Schematic overview of input and output streams in a single stage flash vessel

where:

$$F_{tot,j} = F_j + L_{j-1} + V_{j+1} \tag{2.26}$$

$$z_{tot,i,j} = z_{i,j} + x_{i,j-1} + y_{i,j+1} \tag{2.27}$$

To solve the single stage flash, one must provide as inputs: T_j, P_j, $F_{tot,j}$ and $z_{tot,i,j}$. For a multi-stage stripper, N and initial guesses for L_{j-1} and V_{j+1} in equation 2.26 are required as well.

Sum-Rates method

SR method is generally used for absorption and stripping problems that involve wide-boiling feed mixtures. An important assumption in this method is that this mixture behaves as an ideal mixture [58]. Burningham and Otto [79] published an algorithm for the SR method. The following parameters should be specified: F_j, $z_{i,j}$, feed conditions (T_{F_j} and P_{F_j}), P_j, Q_j and N. Where N = number of stages. By initializing tear variables T_j and V_j, xi, j, L_j, new V_j, yi, j and new T_j can be computed. The tear variables are updated and new results are computed. This continues until the error τ is smaller than 0.01 N. This is also explained by the sum-rates equation:

$$L_j^{(k+1)} = L_j^{(k)} \sum_{i=1}^{C} x_{i,j} \tag{2.28}$$

where k = iteration number and L_j is obtained from V_j in equation 2.25.

Newton-Raphson method

Where the before mentioned modeling methods work only for ideal mixtures, Newton-Raphson is especially equipped for non-ideal mixtures [58]. Naphtali and Sandholm [80] introduced component flow rates, $v_{i,j}$ and $l_{i,j}$, according to the following equations:

$$V_j = \sum_{i=1}^{C} v_{i,j} \tag{2.29}$$

$$L_j = \sum_{i=1}^{C} l_{i,j} \tag{2.30}$$

where equations 2.31 and 2.32 present the mole-fraction definitions.

$$y_{i,j} = \frac{v_{i,j}}{V_j} \tag{2.31}$$

$$x_{i,j} = \frac{l_{i,j}}{L_j} \tag{2.32}$$

Equations 2.29 and 2.32 are substituted in equations 2.20, 2.21 and 2.24 to replace V_j, L_j, $y_{i,j}$ and $x_{i,j}$ with the component mass flows. If N, F_j, $z_{i,j}$, T_{F_j}, P_{F_j}, P_j and Q_j are specified, $v_{i,j}$, $l_{i,j}$ and T_j can be calculated [80].

Inside-Out method

Boston and Sullivan [81], presented in 1974 a double looped algorithm for multi-component separation operations. Just like Newton-Raphson, this method is well equipped for non-ideal mixtures. The iteration variables in the inner loop are linked to the stripping factor $S_{i,j}$:

$$S_{i,j} = K_{i,j} \frac{V_j}{L_j} \tag{2.33}$$

The outer loop is build on complex thermodynamic models, based on $P - v - T$ equations of state or liquid phase activity coefficients, and approximate thermodynamic models, based on K values. Before the loop calculations can start, one must provide good estimates of $x_{i,j}$, $y_{i,j}$, T_j, V_j and L_j for all the stages [81]. Convergence of this method can encounter problems when poor initial estimates are used [58].

2.4.2 Selection of Suitable Modeling Method

The stripper modeling method chosen for this work must fulfill certain requirements. Simplicity of the method is important since a rather complex method will make it drastically more difficult to build a flexible model. As explained in section 2.3.4, the SIT model lacks some accuracy in certain ranges of the VLE. The accuracy of the stripper modeling method is therefore not the main priority since errors are present in the data already. Based on this requirement, the stage-by-stage modeling method is chosen as the most suitable modeling method since it is relatively simple compared to the other modeling methods.

2.5 Conclusion

According to previous research at ZEF and literature the following conclusions can be formulated which are needed to specify the next steps that should be taken to continue with this research.

- Based on literature, a list of parameters that influence the performance of a stripper column is stated in section 2.3.1. To understand the influence of these parameters, more specifically on desorption of a TEPA-H_2O-CO_2 mixture, a number of experiments with varying parameter settings will be performed. Ovaa et al. [14] described the effect of temperature and low pressures on desorption of H_2O and CO_2 from TEPA. The experimental range of these parameters will be extended to obtain a better understanding.
- To obtain deeper insights in the effects of stripping parameters and in order to save time, an equilibrium based stripping model will be made to model different stripper configurations and process conditions for a TEPA-H_2O-CO_2 mixture. Multiple experiments must be performed to validate the model.
- It was found that the energy demand of a stripping column consists of sensible heat, heat of desorption, heat of vaporization and the reflux.
- Sinha et al. [11] pointed out that H_2O has a positive effect on the absorption of CO_2 in TEPA. The effect of H_2O on the desorption of CO_2 from TEPA will be investigated in this research.
- Literature also described the effect of diffusion and reaction kinetics in general amine stripping columns. It can be concluded that reaction kinetics are often high so diffusion plays a limiting

role. Experiments will be performed to identify the role of reaction kinetics in a TEPA-H_2O-CO_2 stripping column.

To proceed with this research, it is time to bring all the knowledge obtained in this chapter together in a stripping model. This model is thrown light upon in the next chapter.

Chapter 3

Model Description

This chapter describes the working principles of the stripping model. A stage-by-stage approach is chosen, elaborated on in section 2.4. Figure 3.1 presents a visual interpretation of the stripping model flowchart. Each of the model components will be individually described in this chapter.

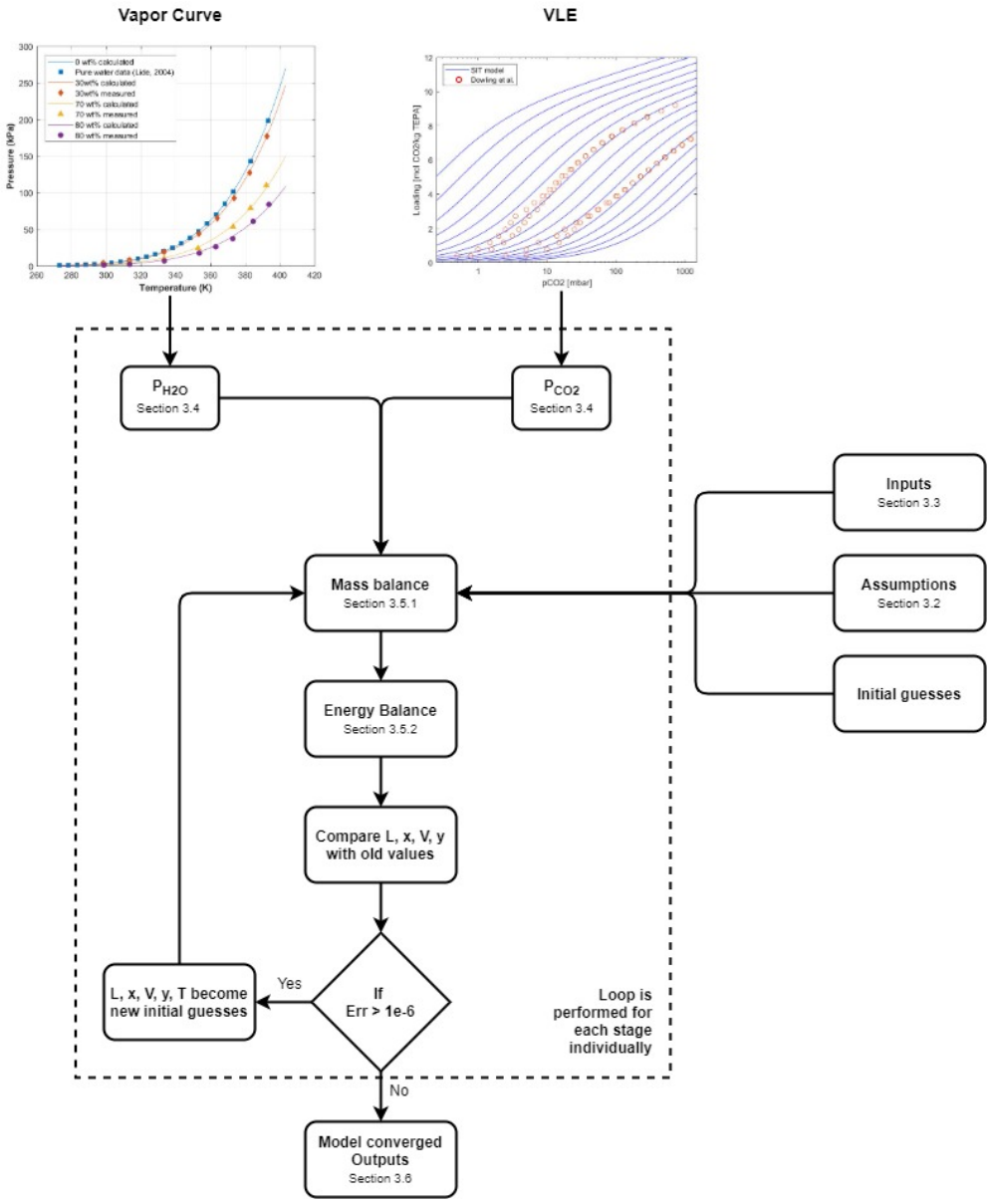

Figure 3.1: Flow chart of the complete stripping model solving methodology.

3.1 Basic Principles Model

As explained in section 2.4, the stage-by-stage approach solves the model for each stage individually inside the dashed rectangle, figure 3.1. To start of, the model requires certain inputs and initial guesses. These are used to find the corresponding P_{H_2O} and P_{CO_2} from the Vapor Curve and VLE. Rachford-Rice, a mass balance methodology, and an energy balance solve for the stage specific unknowns. These unknowns are then compared to the initial values. When the error is small enough, the model is converged and presents the final outputs. It is an iterative process which means that when the error is large, the calculated unknowns are used as new initial guesses and the loop starts over again. Bisection, a numerical root-finder, is chosen as the model solver.

3.2 Assumptions

In order to proceed with the model description, assumptions must be addressed. These assumptions are listed below:

- **The stripping column is operating at equilibrium.** The VLE and vapor curve assume equilibrium in each stage, so a prediction made by the model is only valid for equilibrium operation of the system.
- **Heat losses are assumed to be negligible in the stripping model.** This is to predict a best case scenario in terms of energy demand.
- **TEPA is assumed to not evaporate over time.** Due to the high boiling point of TEPA only a negligible amount will be present in the vapor phase. Consequently, the absolute pressure inside the column consists of only P_{H_2O} and P_{CO_2}.
- The vapor curve proposed in section 2.3.5 is not based on the presence of CO_2 in the liquid phase. **Therefore, it is assumed that the present CO_2 in the liquid phase has no effect on the vapor curve.** This is a somewhat ambiguous assumption, however the effect of CO_2 on the vapor curve was proven to be relatively small [12].
- **The specific heat of the present components are average values and assumed to be constant.** The specific heat is based on the weight fraction of components in the specific vapor or liquid phase. This deviates slightly from reality but still gives a fair indication of the specific heat of the present mixtures.
- **Also the heat of absorption is an average value and assumed to be constant.** It is normally depending on temperature and CO_2 loading, however the variation almost stabilizes when the temperature exceeds 80℃, section 2.3.3. Since the stripping column operates at high temperatures, a constant heat of absorption is a valid assumption. The constants are listed in table 3.1 and are taken from section 2.3.3.

Table 3.1: Overview of constants for stripping model.

Constant	Description	TEPA	H_2O	CO_2	Units
$c_{p_{liq}}$	Specific heat liquid phase	460	75	160	$[J/molK]$
$c_{p_{vap}}$	Specific heat vapor phase	0	33.5	37	$[J/molK]$
H_{abs}	Heat of absorption	0	60.3	75	$[kJ/mol]$

3.3 Model Inputs

To run the stripping model, a number of inputs are required. These are listed in table 3.2.

Table 3.2: Overview of inputs for stripping model.

Input	Description	Units
N	Number of stages	$[-]$
R	Reflux ratio	$[-]$
T_{reb}	Reboiler temperature	$[°C]$
T_{feed}	Feed temperature	$[°C]$
P	Column pressure	$[mbar]$
F_{rich}	Feed mass flow	$[mol/s]$
w_{TEPA}	Mass fraction TEPA	$[wt\%]$
L	Loading of feed	$[mol\, CO_2/kg\, TEPA]$

Where R is defined as reflux stream divided by the product stream and w_{TEPA} is the mass fraction of TEPA per TEPA + H_2O.

3.4 VLE and Vapor Curve

The SIT VLE model, proposed in section 2.3.4, is used to generate the data set for the ternary TEPA-H_2O-CO_2 mixture. The disadvantage of this model is the long running time that the model requires to create this data set, which will directly influence the running time of the stripping model. As a solution, an artificial neural network (ANN) was trained on the data set produced by the SIT model. The ANN reduces the running time of the VLE model to seconds. A comparison of the SIT and ANN model is visualized in figure 3.2, from which can be concluded that both models are almost identical. Note that this visualization is only a intersection of both three-dimensional models at a TEPA mass fraction of 70 wt%. Nonetheless, it is fair to assume that both models are almost identical due to the amount of data points that are used to train the ANN. A certain modification of the vapor curve is not obligatory since the Wilson solving method has a very low running time which makes it applicable as input for the stripping model.

For specified input parameters, functions are created to obtain the relevant data points from the VLE and vapor curve. These functions, equation 3.1 and 3.2, find the corresponding P_{CO_2} and P_{H_2O} for a certain temperature and composition.

$$P_{CO_2} = f(T, L, w) \tag{3.1}$$

$$P_{H_2O} = f(T, x) \tag{3.2}$$

Where x = the composition vector of the liquid mixture.

The assumptions and inputs are used as starting point for the model solving strategy of a single stage, which is explained in the following section.

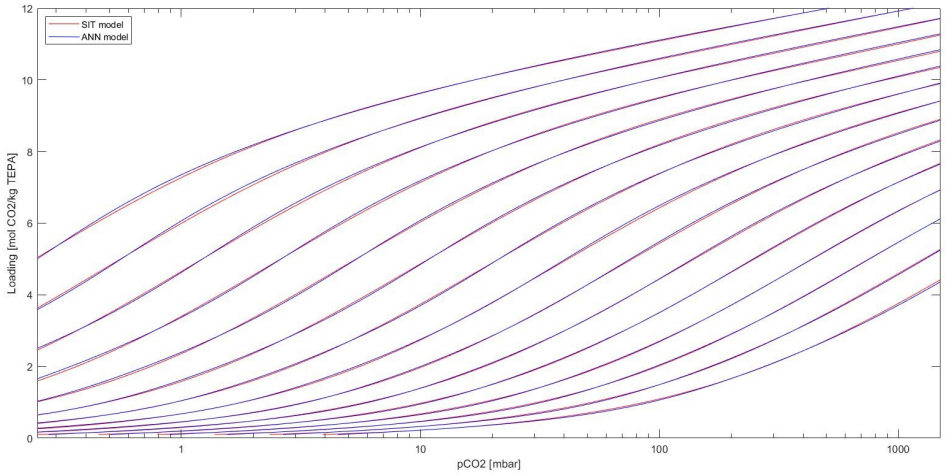

Figure 3.2: Comparison of the SIT and ANN model for a chosen TEPA mass fraction of 70 wt%.

3.5 Single Stage Model

The modeling and solving strategy of a generic single stage is the core of the complete stripping model. As introduced in section 2.4, a generic single stage of the stripping model can be simplified to a flash tank, shown in figure 3.3. To do so, the mass flows into the single stage are summed into feed mass flow F_i, equation 3.3. The feed mass flow holds a composition, $z_{i,j}$, defined by equation 3.4.

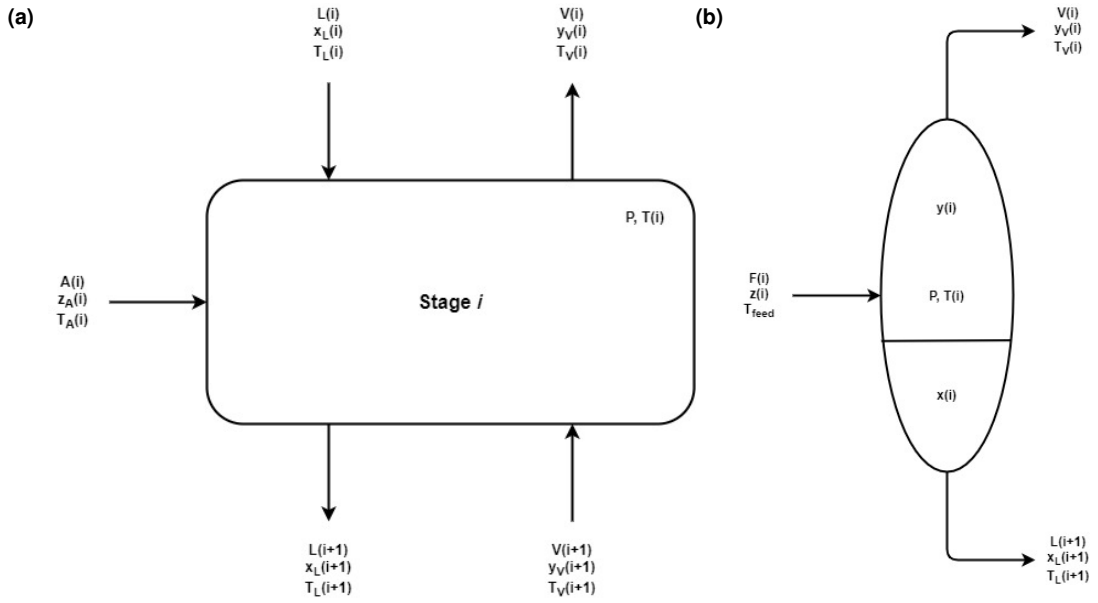

Figure 3.3: Simplification of a single stage i to a flash tank i at P and $T(i)$ including the relevant mass flows, compositions and temperatures with (a) single stage i and (b) flash tank i.

$$F_i = A_i + L_i + V_{i+1} \tag{3.3}$$

$$z_{i,j} = \frac{A_i z_{A_{i,j}} + L_i x_{i,j} + V_{i+1} y_{i+1,j}}{F_i} \tag{3.4}$$

Where F_i = total feed mass flow into the flash tank, A_i = additional mass flow into single stage i, $z_{i,j}$ = composition of the total feed mass flow and $z_{A_{i,j}}$ = composition of the additional mass flow into single stage i. A mass and energy balance are established to solve for the flash tank i specific unknowns.

3.5.1 Mass Balance

The mass balance for flash tank i is shown in terms of total and component specific mass flows in and out of the flash tank, equation 3.5 and 3.6 respectively.

$$F_i - L_{i+1} - V_i = 0 \tag{3.5}$$

$$F_i z_{i,j} - L_{i+1} x_{i+1,j} - V_i y_{i,j} = 0 \tag{3.6}$$

To solve the mass balances for the flash tank i, a trial-and-error iterative solution is required. The calculation to find this iterative solution includes solving the Rachford-Rice equation [82] [83]:

$$x_{i,j} = \frac{z_{i.j}}{1 + \beta(K_j - 1)} \tag{3.7}$$

Where β = fraction of the feed that is vaporized, lays between 0 and 1 and K_j = equilibrium constant for component j, equation 2.15. A double looped bisection solver is used to solve the Rachford-Rice equation for β and K_j. This numerical root-finding method is relatively slow but has the main advantage that it is guaranteed to converge [84]. The flow chart of the solving methodology of the Rachford-Rice equation is shown in figure 3.4.

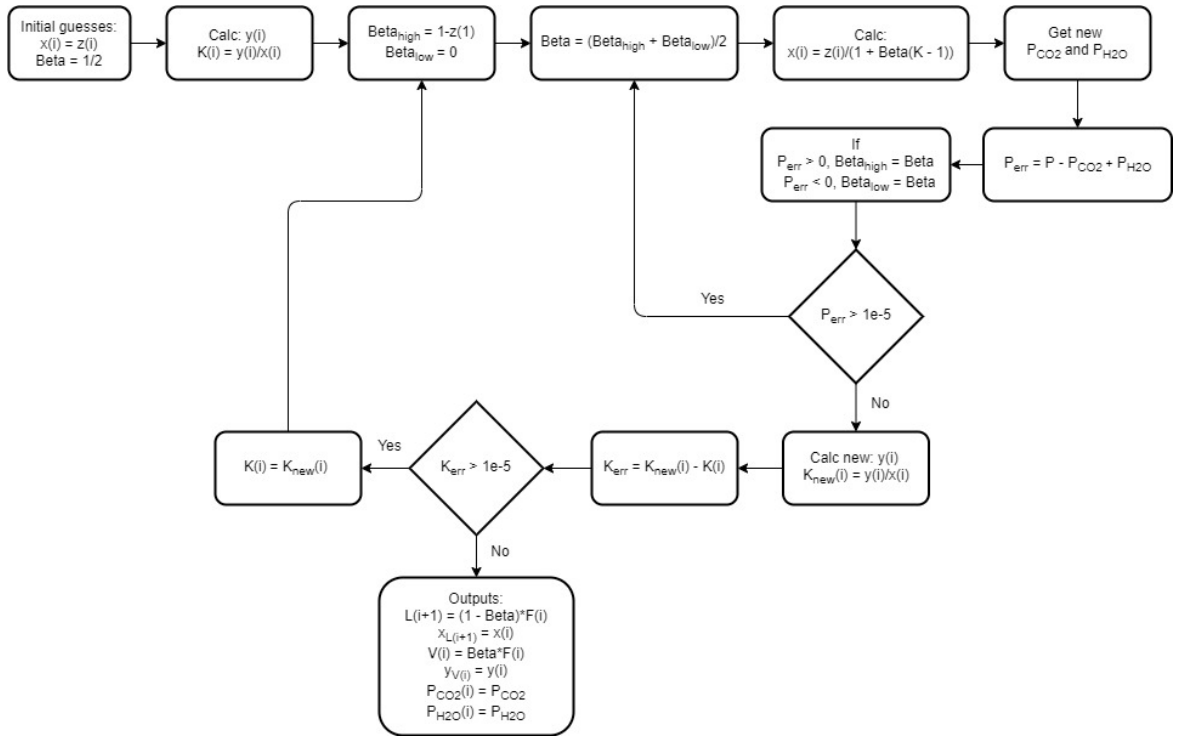

Figure 3.4: Flow chart of the Rachford-Rice solving methodology with a double bisection numerical root-finder for a flash stage i.

The composition vector of the vapor mixture y_i is determined by the partial pressures of H_2O and CO_2 and defined as:

$$y_i = [0 \quad \frac{p_{H_2O}}{p_{H_2O} + p_{CO_2}} \quad \frac{p_{CO_2}}{p_{H_2O} + p_{CO_2}}] \tag{3.8}$$

3.5.2 Energy Balance

The energy balance of a single stage i consists of energy terms depending on sensible heat and heat of absorption or desorption of the mass flows travelling in and out of the stage. Due to the assumption of zero heat loss, the energy balance is an ideal case and therefore represents the best case scenario in terms of energy demand. The proposed energy balance for single stage i is given in equation 3.9.

$$Q_{tot_i} = Q_{L_i} + Q_{V_i} + Q_{A_i} + Q_{abs_i} \tag{3.9}$$

Where Q_{tot_i} = total amount of heat entering the stage, Q_{L_i} = sensible heat brought into the stage by the liquid, Q_{V_i} = sensible heat brought into the stage by the vapor, Q_{A_i} = sensible heat brought into the stage by the additional feed and Q_{abs_i} = heat of absorption that is required to absorb the difference in gas flow rate through the stage. Each of these components is then calculated by equation 3.10 to 3.13.

$$Q_{L_i} = \sum_{j=1}^{C} L_i x_{i,j} c_{p,liq} (T_{L_i} - T_i) \tag{3.10}$$

$$Q_{V_i} = \sum_{j=1}^{C} V_{i+1} y_{i+1,j} c_{p,vap} (T_{V_{i+1}} - T_i) \tag{3.11}$$

$$Q_{A_i} = \sum_{j=1}^{C} A_i z_{A_{i,j}} c_{p,liq} (T_{A_i} - T_i) \tag{3.12}$$

$$Q_{abs_i} = \sum_{j=1}^{C} (V_{i+1} y_{i+1,j} - V_i y_{i,j}) H_{abs} \tag{3.13}$$

Where $c_{p,liq}$ = heat capacity of the components in the liquid phase, $c_{p,vap}$ = heat capacity of the components in the vapor phase and H_{abs} = heat of absorption of the components. Note that when the amount of vapor escaping the stage is larger than the amount entering, the contribution of H_{abs} becomes negative. In other words, the effect of desorption is larger than absorption so energy is required.

Next to calculating the energy phenomena inside the stage, the total energy entering the stage is also used to update the stage specific temperature. For that, one needs to find the average heat capacity of the liquid and vapor mixture present in the stage, which is multiplied with the total mass flow entering the stage. This multiplication should equal the liquid and vapor mass flows leaving the stage multiplied with the corresponding heat capacity, equation 3.14. According to the general sensible heat equation, the temperature difference can be calculated following equation 3.15. The found temperature difference is subsequently used to update the initial temperature of the single stage i, equation 3.16. The step size is strongly decreased to prevent overshooting during the iterative process.

$$F_i c_p = \sum_{j=1}^{C} L_{i+1} x_{i+1,j} c_{p_{liq}} + \sum_{j=1}^{C} V_i y_{i,j} c_{p_{vap}} \tag{3.14}$$

$$dT_i = \frac{Q_{tot_i}}{F_i c_p} \tag{3.15}$$

$$T_{new_i} = T_i + \frac{dT_i}{500} \tag{3.16}$$

Where c_p = average specific heat of stage i, T_i = temperature inside stage i, dT_i = calculated temperature difference and T_{new_i} = updated temperature inside stage i. The flow chart of the energy balance solving methodology including temperature update is visually presented in figure 3.5.

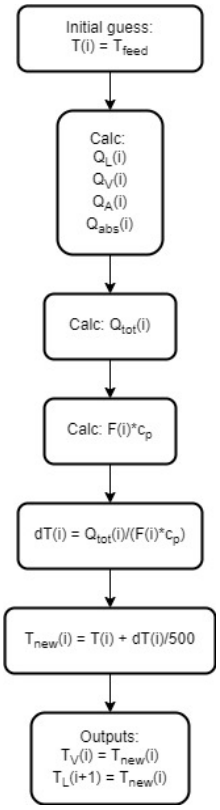

Figure 3.5: Flow chart of the energy balance solving methodology for a flash stage.

After establishing and solving the mass and energy balance, multiple stages are interconnected to simulate a multi-stage stripping column.

3.6 Multi-stage Model

The mass flow streams, compositions and temperatures in a multi-stage stripping model are presented in figure 3.6. It is clear that the column consists of N single stages as described in section 3.5, where stage N is the reboiler. The vapor stream from the bottom into the reboiler is zero since no vapor enters the system, $V_{n+1} = 0$. The liquid stream into the top stage, which is the reflux, is a function of the vapor stream leaving the system, equation 3.17, and is assumed to be pure H_2O.

$$L_1 = V_1 y_{1,2} \frac{R}{1+R} \tag{3.17}$$

Where L_1 = reflux stream, V_1 = vapor stream leaving the system, $y_{1,2}$ = H_2O mol fraction of vapor stream V_1 and R = reflux ratio.

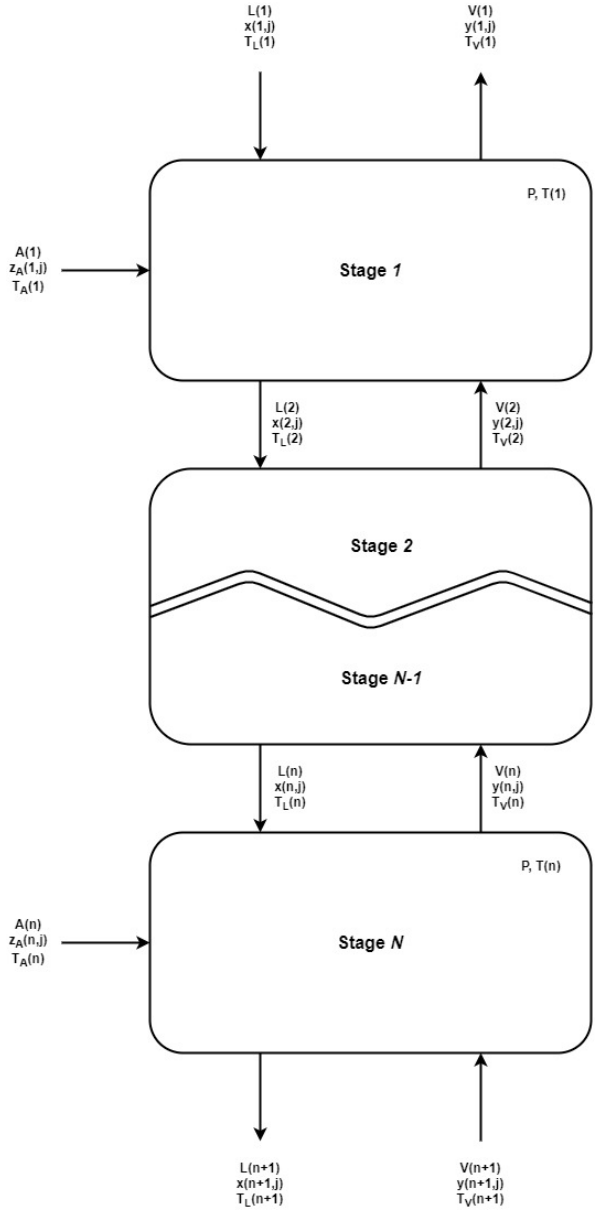

Figure 3.6: Overview of mass flow streams, compositions and temperatures in a stripping model with N stages.

As the temperature inside the reboiler is set as an input of the model, T_n remains constant. To maintain this constant temperature, heat must be supplied to cover the heat that is required due to sensible heat and heat of desorption. According to this theory, the reboiler duty is calculated via equation 3.18.

$$Q_{reb} = -Q_{tot_n} \tag{3.18}$$

When the mass flows and temperatures of all the stages are stabilized according to figure 3.1, the

model presents outputs for each stage as well as for the total stripping column. The outputs are listed in table 3.3 and 3.4.

Table 3.3: Overview of outputs for stripping model per stage.

Output	Description	Units
T	Stage temperature	$[°C]$
A	Feed stream into stage	$[mol/s]$ (per component)
V_{in}	Vapor flow in	$[mol/s]$ (per component)
V_{out}	Vapor flow out	$[mol/s]$ (per component)
L_{in}	Liquid flow in	$[mol/s]$ (per component)
L_{out}	Liquid flow out	$[mol/s]$ (per component)
w_{TEPA}	Mass fraction TEPA	$[wt\%]$
L	Loading of mixture	$[mol\ CO_2/kg\ TEPA]$
P_{CO_2}	Partial pressure CO_2	$[mbar]$
P_{H_2O}	Partial pressure H_2O	$[mbar]$

Table 3.4: Overview of outputs for total stripping model.

Output	Description	Units
Q_{reb}	Reboiler duty	$[W]$
E	Energy usage	$[kJ/mol\ CO_2]$
R_{top}	Vapor top ratio in column	$[-]$ $(H_2O : CO_2)$
CC	Cyclic capacity	$[mol\ CO_2/kg\ TEPA]$

Chapter 4

Experimental Equipment and Procedures

In this chapter, the experiments performed with different configurations of the stripper setup are described. First, the procedure of loading a lean master batch is explained in detail. Then, measurement methods of the present mixture components are discussed. Furthermore, the performed experiments are described in terms of; setup description, assumptions, experimental method and procedure. This is done for a 7 stage, single stage and a 3 stage stripper setup. Finally, the experiments and stripper model are validated and a list of experimental observations is provided.

4.1 Master Batch Preparation Methodology

A master batch with high concentrations of H_2O and CO_2 is required to perform desorption experiments. To conduct multiple experiments under changing conditions it is of great importance to maintain a constant H_2O and CO_2 concentration in the rich master batches, this makes comparing the different experiments possible. Prior to loading with CO_2, the master batch is well mixed with a predetermined amount of H_2O. The methodology of loading is described in section 4.1.1 and 4.1.2.

4.1.1 Loading Setup

The aim of this setup is to artificially load CO_2 in a TEPA-H_2O master batch mixture. The amount of H_2O is predetermined and CO_2 is loaded up to the high loading region of TEPA. Figure 4.1 shows a schematic overview of the setup that is used to load CO_2 into the aqueous TEPA solution. It consists of a pressurized CO_2 tank, 500 ml gas wash bottle, bottle head with disc filter, mass flow controller and a lab heater with magnetic stirrer. The CO_2 gas flows from the pressurized tank into the gas wash bottle and bubbles through the aqueous TEPA solution. Some of the CO_2 is absorbed and the non-absorbed CO_2 leaves the bottle at the top. The lab heater with magnetic stirrer is used to enhance mixing of the aqueous TEPA solution. The mass flow controller is used to keep the CO_2 mass flow coming out of the tank low. This serves two purposes. Firstly, the solution starts frothing when CO_2 bubbles flow through it. A high mass flow increases the froth layer drastically and can cause overflow of the froth from the gas wash bottle. Secondly, a high mass flow results in big CO_2 gas bubbles which decreases the volume-surface area ratio and so the efficiency of the used CO_2 gas. Consequently, the mass flow of the CO_2 gas was chosen to be 15 l/hr.

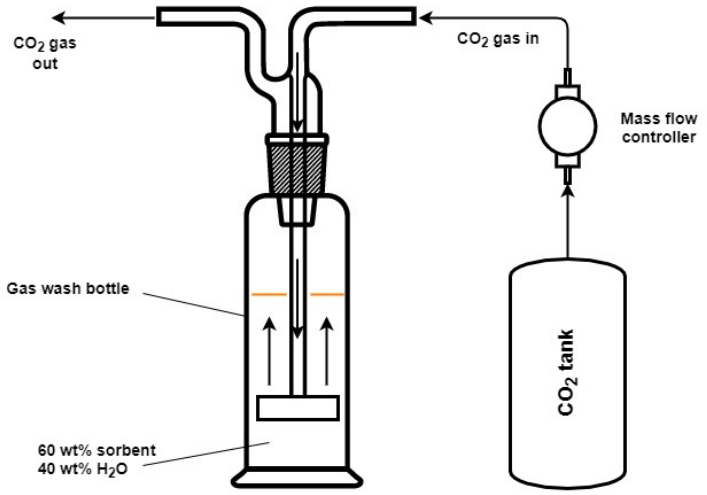

Figure 4.1: Schematic overview setup to load CO_2 into the sorbent.

4.1.2 Loading Procedure

The following steps must be performed to load a lean TEPA master batch with H_2O and CO_2.

1. Fill the gas wash bottle with 250 ml TEPA.
2. Add a predetermined amount of H_2O so that the mass fraction of H_2O arrives at 40 $wt\%$. After loading with CO_2, this will bring the final mass fraction of H_2O between 30 and 35 $wt\%$.
3. Mix the lean TEPA and H_2O mixture well by hand such that the H_2O is absorbed by the lean sorbent. The mixture warms up due to the heat of absorption of H_2O.
4. Place a magnetic stirrer inside the bottle.
5. Close the bottle with the wash bottle head and attach the head to the CO_2 tank.
6. Place the bottle on the lab heater and start stirring with 600 rpm and heat it to 35 $^{\circ}C$, this will both improve mixing and therefore absorption of the CO_2.
7. Start opening the mass flow meter of the CO_2 tank slowly until bubbles appear in the mixture. Make sure the mass flow of the CO_2 gas is at 15 l/hr.
8. Let the CO_2 gas bubble through the mixture for 30 minutes.
9. Close the CO_2 gas bottle and stop the lab heater.
10. Repeat this procedure several times until the master batch bottle is completely filled.
11. Mix the master batch by hand so that a homogeneous concentration of H_2O and CO_2 throughout the mixture is ensured.
12. Analyze the CO_2 and H_2O concentrations in the master batch.

4.2 Stripping Experiments

In this section the performed stripping experiments are described. First the stripping setup is explained in detail followed by the experimental methodology. An experimental plan is proposed and the analysis of the acquired data is elaborated on. Then, the assumptions are listed and the experiments are validated in terms of mass balances. The aim of these experiments is to understand the stripper performance for various operational conditions and setup configurations. Finally, experimental observations are listed and the stripper model is validated.

4.2.1 Stripping Setup

A process flow diagram of the stripping setup is shown in figure 4.2. The setup consists of a stripping column, with variable number of stages, where the reboiler is heated and mixed by a IKA C-MAG HS 7 lab heater and magnetic stirrer. A rich feed enters the column at the top and a lean solvent mixture leaves the column at the bottom where it is collected in a tank. The top of the stripper column is connected to a flash tank where the top products are collected and partially refluxed into the column. The vapor that is present in the flash tank is pumped through a mass flow meter to measure the produced vapor product. This vapor is finally released into the ambient air. A more elaborated description of the setup is provided in appendix B.1.

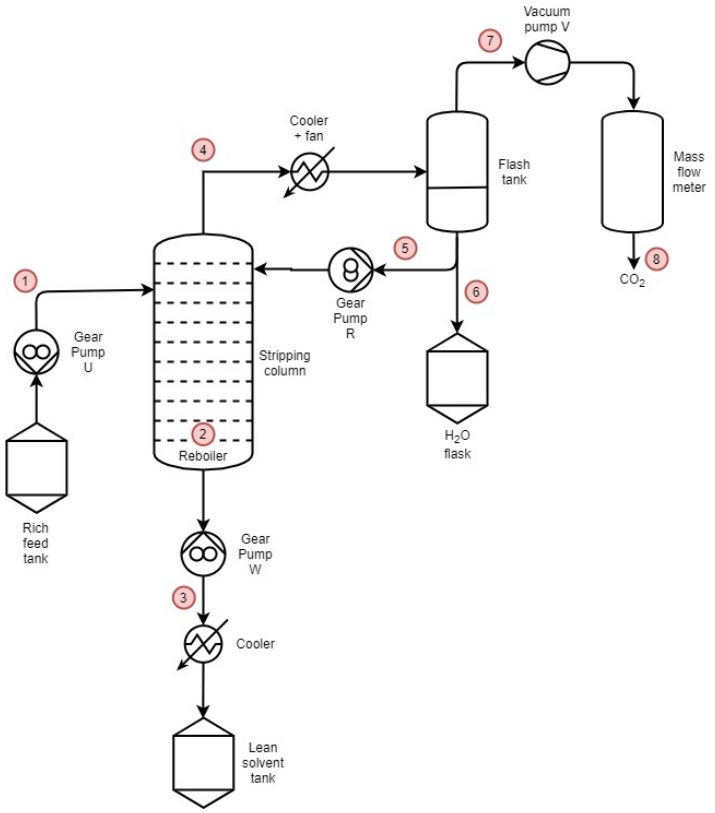

Figure 4.2: Process flow diagram of the experimental stripping setup.

In figure 4.2, the flow streams through the system are numbered. Each flow stream is individually described underneath:

1. Rich loaded feed is transported by gear pump U through a flexible hose. The feed passes a check valve that maintains the pressure inside the stripping column, a filter that filters any solid particles inside the feed and a temperature sensor that measures the feed temperature. The feed hose can be connected to different stages of the stripping column, which makes the feed inlet point variable.
2. The sorbent mixture that arrives at the bottom of the stripping column is heated by the reboiler. Part of it is evaporated and travels to the stage situated above the reboiler in the vapor phase.
3. Part of the sorbent mixture leaves the stripping column at the bottom where it is sucked out by gear pump W. It again passes a check valve to maintain the column pressure. Also, it travels through a finned cooling tube to where the temperature is passively brought down. At last, it arrives in a storage tank where the cooled sorbent mixture is kept and later analyzed.
4. Evaporated CO_2 and H_2O will leave the column at the top where it travels through a finned cooler which is actively cooled by a fan. Here, the H_2O will condense whereas the CO_2 remains in the vapor phase. Both product components are collected in the flash tank.
5. Part of the liquid H_2O that arrives in the flash tank is fed back into the top of the column by gear pump R.
6. The other part of the liquid H_2O is transported from the flash tank into a flask where it will be later analyzed. The connection to the flask is sealed such that the pressure inside the column remains constant.
7. Due to evaporation of CO_2 and H_2O inside the stripping column, the pressure inside the column rises. When the pressure exceeds the set experimental pressure, vacuum pump V sucks the CO_2 from the flash tank inside the mass flow meter. The vacuum pump functions as a check valve such that no CO_2 can flow back into the system.
8. When the pressure inside the mass flow meter arrives above 1.5 bar, the solenoid valve opens and the CO_2 that causes the over pressure escapes into the ambient air. A syringe can be connected to the solenoid valve to capture the CO_2 for analytical purposes.

The experimental setup is controlled by an Arduino nano for which a code was written in C++ programming language. With this code, the parameters presented in table 4.1 can be controlled. The temperature inside the reboiler is manually set and PID controlled by the IKA C-MAG HS 7 lab heater.

Table 4.1: Experimental parameters controlled by the Arduino.

Experimental parameter	Units
Duty cycle of gear pump U, W and R	$[\%]$
Opening time solenoid valve	$[ms]$
Opening pressure solenoid valve	$[bar]$
Sucking time vacuum pump V	$[ms]$
Experimental pressure	$[bar]$

4.2.2 Experimental Plan

The main goal of the performed experiments is to understand the effect of parameters on the performance of the stripping column. A list of the selected parameters that effect the performance of the

stripping column is given in table 4.2 with corresponding units.

Table 4.2: Experimental parameters.

Experimental parameter	Units
CO_2 loading feed	$[mol/kg]$
TEPA mass fraction feed	$[wt\%]$
Pressure	$[mbar]$
Reboiler temperature	$[°C]$
Feed temperature	$[°C]$
Number of stages	$[-]$
Reflux	$[-]$
Feed mass flow	$[mol/s]$

Next to getting insights in the effect of the parameters, the goal of the experiments is to validate the model presented in chapter 3. To be able to validate the model, experiments that correlate with varying model inputs are required. As the model predicts the effect of the parameters, these experiments are combined and presented underneath:

Table 4.3: Experimental plan to validate the stripping model.

Experiment	# stages	CO_2	TEPA	P_{exp}	T_{reb}	T_{feed}	Reflux
	$[-]$	$[mol/kg]$	$[wt\%]$	$[mbar]$	$[°C]$	$[°C]$	$[-]$
1	6	3.5	66.5	800	119	20	No
2	6	3.6	60.1	400	86	20	No
3	6	3.5	60.2	250	67	20	No
4	1	4.2	60	950	120	20	No
5	1	4.6	52.5	950	102	20	Yes
6	1	4.6	52.5	950	114	20	Yes
7	1	4.6	52.5	950	123	20	Yes
8	1	6.5	47.8	750	105	20	Yes
9	1	6.5	47.8	750	107	20	No
10	1	6.5	47.8	600	109	20	Yes
11	1	6.5	47.8	600	109	20	No
12	1	5.9	50.2	950	109	48	Yes
13	2	6.5	53.6	950	120	20	No
14	2	5.9	52.5	950	120	20	No
15	2	5.7	54.7	2000	128	20	No

Note that the reflux is not quantified, this is because the experimental setup could not measure the actual reflux. However, zero and total reflux can be realized by adjusting the setup slightly and therefore compared to the stripper model. Furthermore, experiments with a non quantified partial reflux are performed to see the effect of a reflux, but it is hard to draw conclusions regarding the effect of this partial reflux.

To understand the significance of kinetics inside the stripping column, so called kinetic experiments are designed. These experiments investigate if for a specific hold up time, the time that a feed mixture

particle spends in a stage or the reboiler, equilibrium is reached. Note that the hold up time is a function of the feed mass flow and the hold up volume of either a stage or the reboiler. The designed kinetic experiments are listed in table 4.4.

Table 4.4: Experimental plan to investigate the role of kinetics inside the stripping column.

Experiment	# stages	CO_2	TEPA	P_{exp}	T_{reb}	T_{feed}	Hold up time
	$[-]$	$[mol/kg]$	$[wt\%]$	$[mbar]$	$[℃]$	$[℃]$	$[s]$
1	1	4.0	60	950	115	20	1366
2	1	4.0	60	950	114	20	1139
3	1	4.0	60	950	114	20	1004
4	1	4.0	60	950	113.5	20	840
5	1	4.0	60	950	116	20	4615
6	1	4.0	53	950	115	20	785
7	1	4.0	53	950	117	20	400
8	1	4.0	53	950	114	20	280
9	1	5.1	47	950	105	20	465
10	1	5.1	47	950	106	20	1094
11	1	5.1	47	950	104	20	158
12	1	6.4	50	950	113	20	1116
13	1	6.4	50	950	115	20	963
14	1	6.4	50	950	111	20	313
15	1	6.4	50	950	111	20	252

4.2.3 Methodology

All the experiments performed in this research follow a sequence which is presented in figure 4.3. It is clear that the experimental procedure exist of three different phases; experimental preparation phase, experimental phase and post-experimental phase. In the experimental preparation phase, the experiment is prepared and the system is brought into equilibrium. When the system reaches equilibrium, the experiment can start. **The mass flow is determined by measuring the amount of liquid flowing in and out of the column during the experimental phase. Note that to be able to estimate the mass flow, new rich and lean sorbent bottles are used for this phases. However, the rich sorbent bottles contain the same feed composition otherwise switching these bottles would result in disturbance of the equilibrium in the system during the experiment.** In the post-experimental phase, the system is shut down and the collected samples are analysed. The analysis methodology will be explained in the following section.

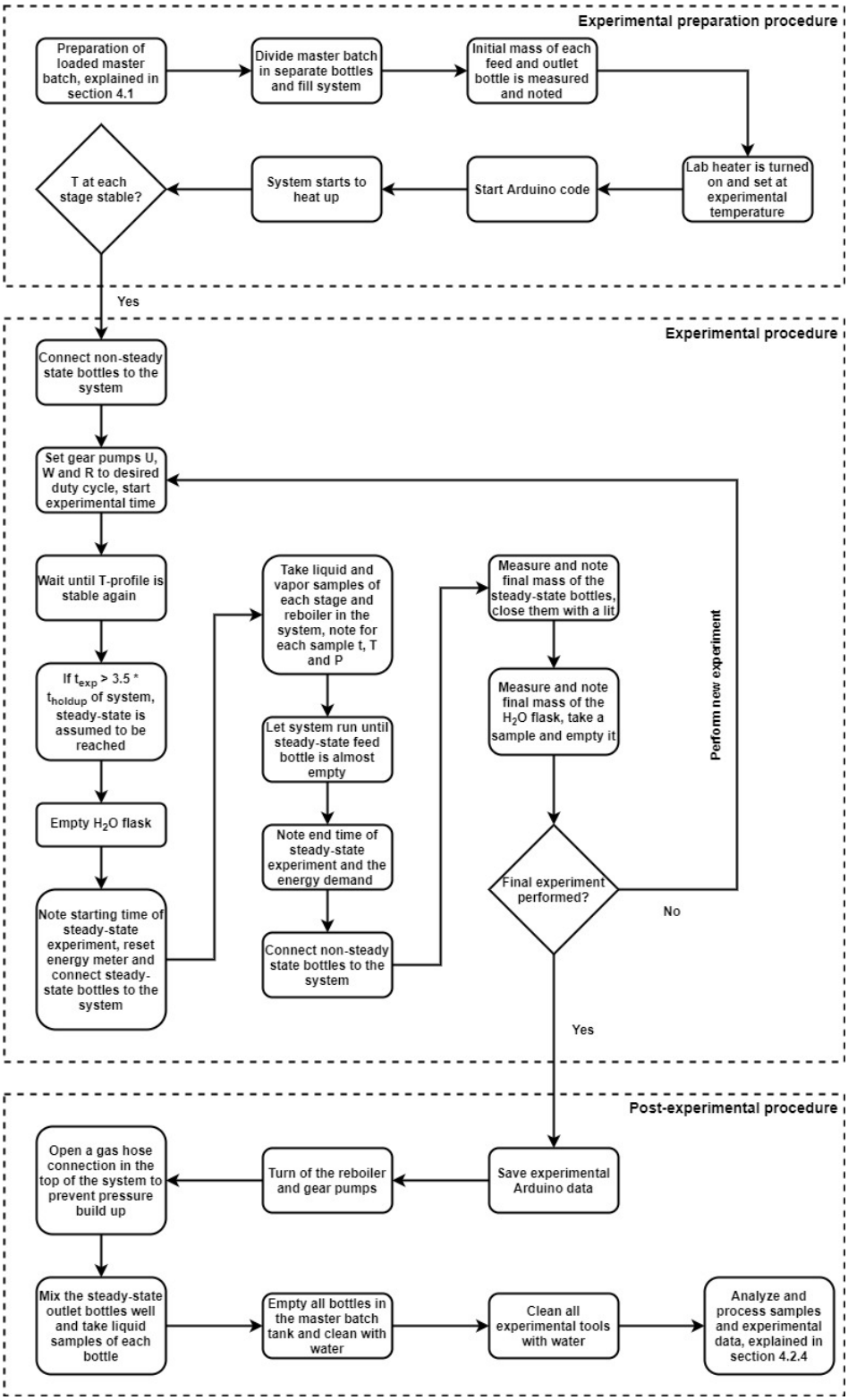

Figure 4.3: Flow chart of the experimental procedure including experimental preparation and post-experimental procedures.

4.2.4 Assumptions

In order to analyse and validate the experiments, assumptions are required. These are listed underneath:

- **The CO_2 vapor stream is assumed to be an ideal gas.** This facilitates to mass flow meter to calculate the vapor mass flow rate according to the ideal gas law, this is explained more in depth in section 4.2.5.
- The system is pressure controlled and operates within absolute pressure fluctuations of 50 $mbar$. Since the pressure determines the temperature inside the column, the temperature also fluctuates slightly during operation. **However, the temperature inside the column is assumed to be constant.** The temperature fluctuations are small, within $\pm 1 ℃$, which justifies this assumption.
- **The complete setup is assumed to be leak tight**. The setup is tested on leak tightness before the start of every experiment. Consequently, the pressure build up inside the stripping column is solely caused by desorption of H_2O and CO_2.
- **When taking gas samples from the stripping column, the gas is assumed to be an ideal gas. Also, the friction inside the syringe is negligible.**
- **The sampling methods do not influence the equilibrium conditions inside the column.** Some of the liquid and vapor is taken out for analysis but this is a small fraction compared to the volumes present in the stage. The amount of liquid and vapor taken per sample is 1 and 5 ml respectively.
- **There is no pressure drop inside the stripping column.** One can estimate the pressure drop according to:

  $$\Delta p = 2\rho_L g h_w n \tag{4.1}$$

  Where: ρ_L = density of the liquid mixture, g = gravitational constant, h_w = height of the weir and n = number of stages. For a 6 stages setup, this would mean a pressure drop of 13 $mbar$. This is small relative to the absolute operating pressure and therefore negligible.
- **A constant mass flow in and out of the system is assumed.** Due to small pressure fluctuations, the mass flow through the system is not always constant. As mentioned before, these pressure fluctuations are small and would not influence the mass flow much.
- **Each stage inside the stripping column is assumed to be in equilibrium.** This means that the concentration of the components in the liquid and vapor phase are constant throughout the experiment. This is estimated to happen for all the stages within 3.5 times the hold up time of the complete system. **To confirm this assumption, two samples were taken with a substantial amount of time in between. When the samples contain the same composition, the stage is assumed to be in equilibrium.**
- **The density of the liquid mixture is assumed to constant.** Ovaa et al. [14] found that the effect of H_2O and CO_2 concentration in the TEPA solution can be neglected.

4.2.5 Data Analysis

To measure the concentration of H_2O and CO_2 in TEPA, a Fourier-transform infrared spectroscopy (FTIR) is used. A Karl-Fischer titrator and gas chromatographer are used to quantify the purity of the

H_2O and CO_2 product streams respectively from the stripper. All the measuring setups are subsequently discussed in the following sections.

Real time experimental data

During an experiment, the Arduino code, explained in section 4.2.1, prints every second real time data of the stripping column. The data consists of; experimental time, temperatures of each stage and reboiler, pressure inside the column and mass flow meter and the moments when the solenoid valve opens. All this data is processed in Matlab and visualized in section C.1.

VLE sample analysis

To measure the concentrations of TEPA, H_2O and CO_2 in the ternary mixture, a Fourier-transform infrared spectroscopy (FTIR) is used. Infrared spectroscopy is an analysis of the interaction of light with a molecule. The molecule absorbs infrared radiation and the chemical bonds inside the molecule start to vibrate. The outcome of an infrared spectroscopy is an infrared spectrum, where the infrared intensity is plot against the wavelength of light. The position of the peaks, intensities, width and shapes inside the plot say something about the presence of specific chemical bonds inside the molecule [85] [86]. FTIR is used as an analytical method to analyse mostly organic materials. For this research, a Agilent Cary 630 FTIR is used, shown in figure 4.4.

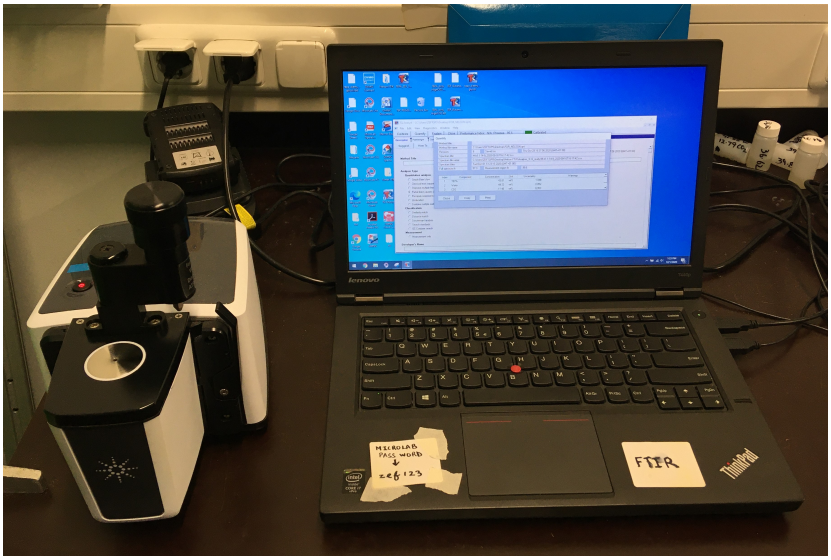

Figure 4.4: Fourier-transform infrared spectroscopy (FTIR) setup.

A typical infrared spectrum for a TEPA master batch with high H_2O and CO_2 loading is presented in figure 4.5. The peaks that represent the amount of H_2O and CO_2 correspond with a wavenumber of around 3200 and 1300 cm^{-1} respectively.

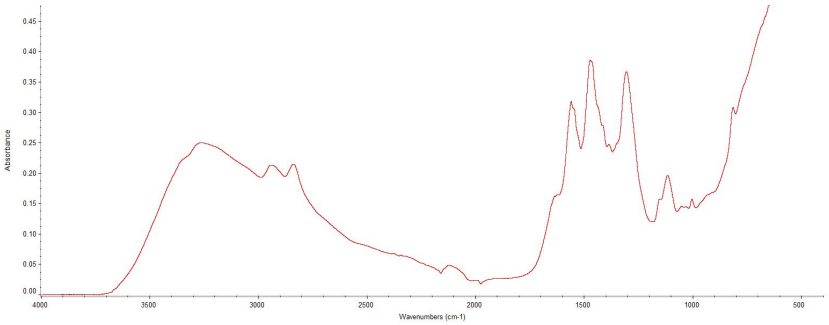

Figure 4.5: Typical infrared spectrum for a loaded TEPA master batch.

The final infrared spectrum that is produced by the FTIR is send to a computer for further analysis. This is done with TQ Analyst, a software tool that extracts qualitative and quantitative information from the spectrum. The tool can be calibrated using known sample spectra and can therefore be used as a robust quantitative analysis method. Sinha et al. [11] has provided a calibration curve for a TEPA-H_2O-CO_2 mixture. The details for the H_2O and CO_2 analysis in TEPA are presented in table 4.5.

Table 4.5: FTIR calibration curve details for a TEPA-H2O-CO2 mixture provided by [11].

Component	Concentration range $[wt\%]$	Error $[\%]$
H_2O	0 - 43	± 0.4
CO_2	0 - 18	± 1.5
TEPA	50 - 100	± 2

The FTIR is used to measure the concentrations in the rich master batch, the lean loaded TEPA that leaves the stripper at the bottom and the liquid equilibrium mixture at each stage.

A syringe is used to take gas samples from inside the stripping column when equilibrium is reached. The syringe consists of a needle, Luer Lok connection and 5 ml syringe, shown in figure 4.6. First, the syringe is preheated up to 80 $^{\circ}C$, higher temperatures would permanently deform the Luer Lok connection. Preheating the syringe prevents the water vapor from condensing while taking the sample, which would cause significant measurement errors. When equilibrium is reached, the needle is placed through the sample port and gas is sucked into the syringe until 5 ml of gas is captured. The Luer Lok connection is closed such that no gas can escape. Now the syringe is left to cool down until it has reached ambient temperature.

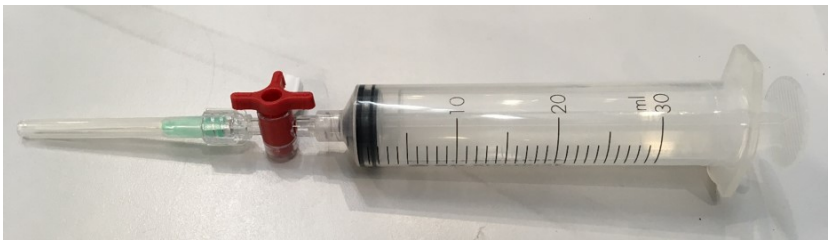

Figure 4.6: Syringe with Luer Lok connection to take a gas sample of the VLE inside the stripping column.

By making use of the ideal gas law, equation 4.2, one can estimate the P_{CO_2} and P_{H_2O} inside the column. When the gas sample has cooled down, it has shrunken in volume. This is partly due to the pressure difference between the column and ambient pressure. This volume decrease can be calculated according to the ideal gas law. The extra decrease in volume is caused by condensation of water vapor inside the syringe. The leftover volume inside the syringe is consequently pure CO_2 vapor. The V_{H_2O}:V_{CO_2} ratio inside the syringe corresponds with the P_{H_2O}:P_{CO_2} inside the column. Note that this sampling analysis only works when the stripping column is operating at pressures lower than ambient pressure. Also, assumptions are made for this analytical method which are listed in section 4.2.4.

H_2O analysis

The H_2O that is produced during a experiment is collected in a flask and is documented in the experimental sheet. To test the purity of the produced H_2O, a Mettler Toledo Karl-Fischer titrator, figure 4.7, was used to analyse these liquid samples. Methanol works as a sorbent and a small amount of the liquid sample is added and continuously mixed. The machine measures the electrical resistance of the mixture through an electrode. Due to the addition of H_2O, this resistance differs from the initial resistance. Iodine is delivered in the container of the sorbent mixture and reacts with the H_2O in the liquid sample. This continues until the initial resistance value is restored. Iodine reacts with H_2O in a 1:1 molar ratio and with the known amount of iodine added, the concentration of H_2O in the sample can be determined.

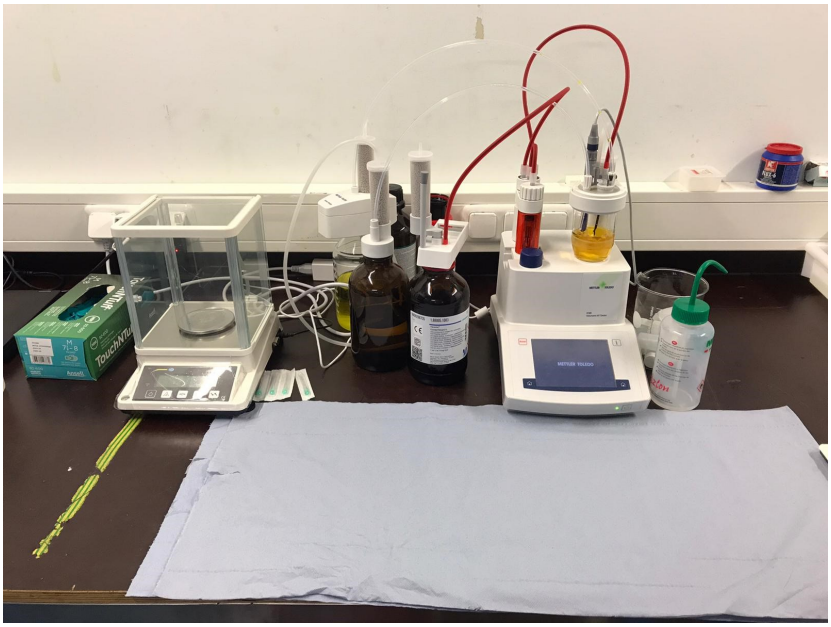

Figure 4.7: Karl-Fischer titrator setup.

CO_2 analysis

To find the purity of the produced CO_2 stream, a gas chromatographer (GC) is used. GC is a frequently used type of chromatography to analyse compounds in a complex gas sample. The system consists of two main components. The mobile phase is a carrier gas, such as helium or nitrogen. The stationary phase is a thin layer of liquid or polymer on a solid support inside a column. The compounds that are

analyzed react with the stationary phase. Each component elutes at a different moment in time which is referred to as the retention time. By comparing the retention times, the GC is able to identify the present compounds both qualitative and quantitative [87].

Mass flow meter

To measure the amount of CO_2 that is produced, a mass flow meter is implemented at the end of the CO_2 product stream. CO_2 gets pumped inside the mass flow meter when the pressure of the column exceeds the set experimental pressure. When the pressure inside the mass flow meter exceeds the release pressure, this is measured by a pressure sensor, the solenoid valve opens and CO_2 is released into the ambient air. The amount of CO_2 that is released can be calculated according to the ideal gas law, equation 4.2, where $P = P_{release} - P_{ambient}$. A release pressure of 1.5 bar corresponds with a CO_2 release volume of 110 ml when the release valve opens.

$$PV = nRT \tag{4.2}$$

Energy usage

An energy meter is used to measure the energy usage of the lab heater during the experiment in kWh. An average energy demand in W can be calculated when the experimental time is taken into account. Note that the energy demand of the lab heater is not equal to the energy demand of the reboiler due to heat transfer losses. This is explained more in depth in section 4.2.6.

4.2.6 Validation of Experiments

To validate the performed experiments, mass balances are constructed. Furthermore, energy balances are investigated by comparing the measured energy demand during the experiments with the theoretical energy demand proposed in chapter 2. These are presented and explained in the subsequent sections.

Experimental mass balances

Figure 4.8 gives an overview of the mass flows in and out of the experimental setup during the performed experiments. The concentrations of each mass flow should be known to close the mass balance and validate the experiments. These concentrations are referred to in mass fractions per component i as: z_i = mass fraction of feed concentration, $y_{s,i}$ = mass fraction of lean sorbent mixture, $y_{l,i}$ = mass fraction of liquid product and x_i = mass fraction of vapor product. Where for i: 1 = TEPA, 2 = H_2O and 3 = CO_2 mass fraction. The governing equations for the mass balance are established:

$$F = S + L + V \tag{4.3}$$

$$Fz_i = Sy_{s,i} + Ly_{l,i} + Vx_i \tag{4.4}$$

Where equation 4.3 represents the total mass balance and equation 4.4 represents the mass balances per component. An overview of the error in these mass balances for the performed experiments is given in table 4.6 and 4.7.

The mass flows are measured during the experiment according to the procedure described in section 4.2.3. The measurements of the mass flow concentrations are explained in section 4.2.5. However, for the vapor product this works differently. The vapor product concentration can not be constantly

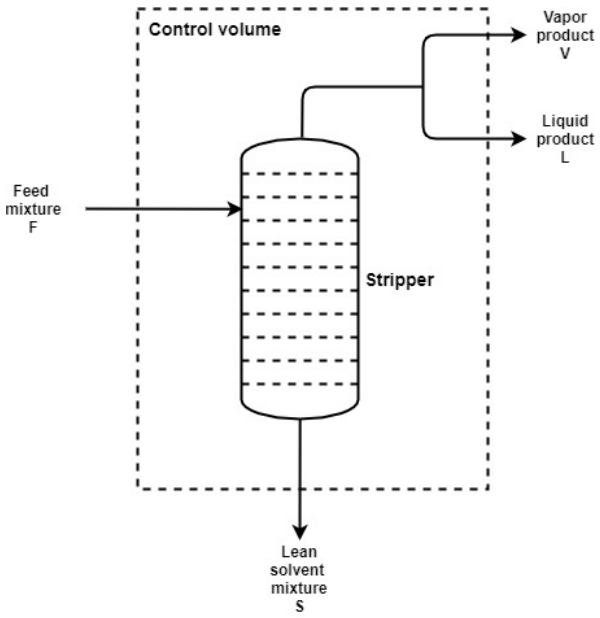

Figure 4.8: Schematic of the mass flows in and out of the experimental setup.

measured and the produced volume is too large to store in a container. Therefore a single sample is taken during the experiment as explained in section 4.2.5. To calculate the mass flow of the vapor product components, the following equation is used:

$$Vx_i = \frac{nV\rho w_i M_i}{w_i M_i + w_j M_j} \tag{4.5}$$

Where n = number of puffs, V = escaped volume per puff, ρ = density of the vapor product, w = mole fraction in vapor product, M = molar mass and i and j are the interested and remaining component. To estimate the density and mole fractions, a simple model of the top cooler and flash tank was made in COCO simulator. The COCO model is in detail explained in appendix D.1 and was verified with the single sample taken during the experiment. Also the specified assumptions are listed in appendix D.1. Table 4.6 and 4.7 present the mass balance results of the performed experiments in terms of error for equation 4.3 and 4.4. The error was calculated according to equation 4.6.

$$Error = \frac{|m_{i,in} - m_{i,out}|}{m_{i,in}} \cdot 100 \tag{4.6}$$

Where m_i is the total mass of component i.

Table 4.6: Mass balances validation experiments.

Experiment	Feed	Total error	CO_2 error	H_2O error	TEPA error
	$[g]$	$[\%]$	$[\%]$	$[\%]$	$[\%]$
1	1347	4.56	3.93	7.40	3.34
2	2543	2.25	1.94	0.09	4.67
2 (duplo)	2517	0.05	0.40	0.98	0.48
3	2810	0.48	1.32	0.10	0.72
4	806	12.96	2.6	18.38	12.55
4 (duplo)	592	4.20	8.8	16.44	8.87
4 (triplo)	393	2.60	12.1	2.03	3.19
5	282	0.59	0.95	4.14	5.19
6	236	1.05	0.72	10.86	8.43
7	203	1.53	4.26	5.14	9.63
8	337	4.66	6.08	15.07	3.71
9	336	1.87	11.47	9.99	12.39
10	248	3.04	2.38	8.33	20.54
11	362	0.94	6.51	8.24	10.46
12	203	2.36	13.76	3.92	5.08
13	452	4.13	11.47	9.14	1.96
14	462	0.82	0.40	5.17	2.81
15	972	2.39	1.39	2.47	6.67
Average		2.80	5.03	7.11	6.71

Table 4.7: Mass balances kinetic experiments.

Experiment	Feed	Total error	CO_2 error	H_2O error	TEPA error
	$[g]$	$[\%]$	$[\%]$	$[\%]$	$[\%]$
1	133	1.99	2.44	0.17	3.13
2	93	2.63	10.70	0.55	3.63
3	330	3.82	8.10	1.59	4.66
4	426	2.26	18.60	2.47	3.16
5	133	1.48	14.97	5.37	4.09
6	335	1.95	5.32	1.19	1.99
7	594	0.07	3.22	1.28	1.93
8	718	0.54	8.11	1.17	1.23
9	403	4.14	6.79	4.22	3.34
10	225	0.17	0.78	1.39	0.99
11	881	1.70	2.59	0.27	3.24
12	245	0.56	10.82	9.19	7.78
13	260	2.62	15.18	6.49	9.64
14	563	1.89	12.68	5.52	7.19
15	596	0.31	8.61	7.96	6.48
Average		1.74	8.59	3.26	4.17

When one compares the FTIR errors presented in table 4.5 to the calculated mass balance errors in table 4.6 and 4.7, it can be concluded that the mass balance errors are significantly higher than the FTIR errors. This can be explained in various ways. Firstly, accumulation of H_2O might happen in the flash tank and influences therefore the H_2O mass balance. Also, the samples taken are assumed to represent a well mixed and therefore homogeneous solution. However, the high viscosity of the solution implies that a homogeneous solution is difficult to establish. This might result in an increase in the mass balance error. A correlation between the feed mass and mass balance error can be concluded from table 4.6 and 4.7. A higher total feed mass into the system results in a smaller mass balance error. On component level, this can explain the high mass balance errors of CO_2 since there is a relatively small amount of CO_2 traveling in and out of the system.

Experimental energy balances

To analyse the experiments in terms of energy usage an energy balance is created. For this energy balance, a single stage setup with zero reflux is assumed and a schematic of the heat transfer through the system is presented in figure 4.9. **Note that this is a rather simplified schematic**, but will nevertheless shine light on the factors that cause the high energy demand of the experimental system.

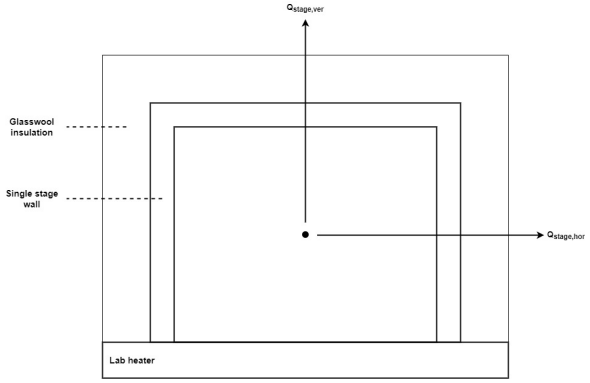

Figure 4.9: Energy transfer schematic for the experimental setup.

The energy demand during the experiment is measured by the energy meter, explained in section 4.2.5, which should be equivalent to the theoretical energy demand of the phenomena inside the system plus the heat losses that occur during the experiment. This equalization is mathematically explained by the energy balance, equation 4.7.

$$Q_{exp} = Q_{sens} + Q_{des} + Q_{vap} + Q_{loss,stage} \tag{4.7}$$

Where Q_{exp} = energy usage measured during experiment, Q_{sens} = energy required for sensible heat, Q_{des} = energy required for desorption of CO_2, Q_{vap} = energy required for vaporization of H_2O and $Q_{loss,stage}$ = energy loss from single stage into the atmosphere. Each component of the energy balance is elaborated on in appendix D.2 where also a list of assumptions is given. The results of the zero reflux experiments are listed underneath.

Table 4.8: Energy demand for performed single stage experiments with zero reflux, including the difference between the experimental and theoretical energy demand.

Experiment	Q_{exp}	Q_{sens}	Q_{des}	Q_{vap}	$Q_{loss,stage}$	Difference
	$[W]$	$[W]$	$[W]$	$[W]$	$[W]$	$[W]$
4 (tab 4.3)	296.2	24.5	5.3	0.5	19.8	246.1
9 (tab 4.3)	999.7	32.5	8.1	63.6	17.5	878
11 (tab 4.3)	886.5	21.3	7	51.2	17.9	789.1
7 (tab 4.4)	341.2	53.4	9.5	80.9	19.6	177.8
8 (tab 4.4)	377.3	72.7	6.9	101.9	18.7	177.1
9 (tab 4.4)	193.4	41.1	3.3	0.3	17	131.7
11 (tab 4.4)	232.1	118.7	0	0	16.7	96.6
14 (tab 4.4)	1195.8	62.8	12.2	95.4	18.3	1007
15 (tab 4.4)	1284.8	77.5	14.2	122.4	18.2	1052.5

Table 4.8 suggests that the high experimental energy demand does not match the theoretical energy demand of the single stage setup. Neglecting the energy loss from the lab heater to the solution inside the single stage might provide a reason for the big difference. This is elaborated on in section D.2. Additionally, it was found that the energy meter did not describe the energy usage accurately as the lab heater has a max rated power of 1000 W, which is clearly exceeded according to table 4.8. **Consequently, the experimental energy demand can not be used to analyse the performance of the stripping column.**

4.2.7 Experimental Observations

While performing the proposed experiments, general observations were done on the performance characteristics of the stripping column. A list of the main observations is given underneath.

- **A six stage setup results in continuous temperature profile for multiple stages in the top.** In other words, the top stages have the same temperature and therefore function as a single stage. This can be explained by the fact that the temperature profile is determined by the P_{H_2O} profile over the stages. When P_{H_2O} is constant for multiple stages, the temperature for the equivalent stages is also constant.
- **During the experiments, the equilibrium of the column builds up from the bottom.** This is, the reboiler stages reaches equilibrium first, where after the upper stages reach equilibrium one-by-one. This is shown in table 4.10 where it is clear that the top stage has not reached equilibrium yet.
- **It takes a long time, multiple hours, for a six stage setup to reach equilibrium in all the present stages.** This can be explained by the low feed mass flow rate chosen for the performed experiments. A typical start up time for a column to reach equilibrium is 3.5 times the time that a single particle spends inside the column.
- **It was found that the T_{reb} was determined by P_{abs} and the liquid concentration in the reboiler stage, described by the vapor curve.** For each P_{abs} and specific liquid concentration, a maximum T_{reb} could be achieved.
- **The gas sampling method, proposed in section 4.2.5, did not provide the expected data**

on the partial pressures inside the column. An example is given in table 4.9, which indicates a negative P_{CO_2} in the reboiler stage. The error is most probably caused by the large ΔT between the system and the syringe, resulting in H_2O condensing inside the syringe while taking the vapor sample. This affects the estimated volumes significantly and therefore the prediction of the partial pressures inside the column.

Table 4.9: Obtained partial pressure data for experiment 1 (table 4.3) through the gas sampling method.

Stage $[-]$	P_{abs} $[mbar]$	P_{H_2O} $[mbar]$	P_{CO_2} $[mbar]$
1	755.5	171.4	584.1
2	764.5	572.9	191.6
3	752.7	580.9	171.8
4	762.1	582.9	179.2
5	754.6	543.1	211.5
6	746.8	927.5	-180.7

- **Due to the temperature profile in the column, absorption in the upper stages can occur.** This was an effect of a relatively low rich loading and stage temperatures in the upper stages. The low temperatures shift the VLE curve up, which results in an equilibrium loading that is higher than the rich loading in the feed. Consequently, equilibrium is achieved, which means that CO_2 is being absorbed in these stages.
- **During experiment 15, table 4.3, it was found that operating the stripping column at higher pressures, the CO_2 production yield also increased significantly.** In chapter 5, this phenomenon will be investigated further and an explanation will be presented.

4.2.8 Validation of Model through Experiments

In order to characterize the stripper, the stripping model must be validated as well. This will be done according to the performed experiments, the experimental settings are used as input in the stripping model. The zero reflux experiments are equipped since they quantify the reflux ratio during the specific experiment. Examples of the validation are given in tables 4.10, 4.11, 4.12, 4.13 and 4.14. These correlations between the experiments and model outputs represent the similarity between all the performed experiments with the stripping model.

Table 4.10: Model validation through 6-stage experiment 1 from table 4.3.

Experiment 1 (table 4.3)

Parameter	Experiment	Model	Error
	Stage 1		
T	75.6 $[°C]$	101.41 $[°C]$	25.5 $[\%]$
L	3.84 $[mol/kg]$	3.88 $[mol/kg]$	1.1 $[\%]$
w_{TEPA}	65 $[wt\%]$	57 $[wt\%]$	12.2 $[\%]$
	Stage 2		
T	99.9 $[°C]$	101.44 $[°C]$	1.5 $[\%]$
L	3.89 $[mol/kg]$	3.84 $[mol/kg]$	1.2 $[\%]$
w_{TEPA}	61 $[wt\%]$	57 $[wt\%]$	6.2 $[\%]$
	Stage 3		
T	99.36 $[°C]$	101.47 $[°C]$	2.1 $[\%]$
L	3.95 $[mol/kg]$	3.79 $[mol/kg]$	4.2 $[\%]$
w_{TEPA}	60 $[wt\%]$	57 $[wt\%]$	5.4 $[\%]$
	Stage 4		
T	99.08 $[°C]$	101.5 $[°C]$	2.4 $[\%]$
L	4.59 $[mol/kg]$	3.73 $[mol/kg]$	18.8 $[\%]$
w_{TEPA}	59 $[wt\%]$	57 $[wt\%]$	4.0 $[\%]$
	Stage 5		
T	97.91 $[°C]$	101.61 $[°C]$	3.6 $[\%]$
L	4.72 $[mol/kg]$	3.66 $[mol/kg]$	22.6 $[\%]$
w_{TEPA}	59 $[wt\%]$	57 $[wt\%]$	4.2 $[\%]$
	Stage 6		
T	118.99 $[°C]$	118.99 $[°C]$	0 $[\%]$
L	2.43 $[mol/kg]$	2.28 $[mol/kg]$	6.0 $[\%]$
w_{TEPA}	75 $[wt\%]$	79 $[wt\%]$	5.9 $[\%]$

It was found that the measured loadings in stage 4 and 5 of table 4.10 were sampling measurement errors by the FTIR. The table also shows a clear temperature deviation in stage 1 between the experiment and model. This indicates that the **top stage had not yet reached equilibrium**, which also explains the large deviation in mass fraction of TEPA. The other stages seem to have been pretty accurately simulated by the model.

Table 4.11: Model validation through single stage experiment 4 from table 4.3.

Experiment 4 (table 4.3)

Parameter	Experiment	Model	Error
	Stage 1		
T	120.96 $[°C]$	120.96 $[°C]$	0 $[\%]$
L	3.16 $[mol/kg]$	2.75 $[mol/kg]$	13.0 $[\%]$
w_{TEPA}	64 $[wt\%]$	77 $[wt\%]$	17.6 $[\%]$

Table 4.12: Model validation through single stage experiment 11 from table 4.3.

Experiment 11 (table 4.3)

Parameter	Experiment	Model	Error
	Stage 1		
T	109.02 $[℃]$	109.02 $[℃]$	0 $[\%]$
L	2.91 $[mol/kg]$	2.9 $[mol/kg]$	0.3 $[\%]$
w_{TEPA}	70 $[wt\%]$	79 $[wt\%]$	11.6 $[\%]$

Table 4.11 and 4.12 show both a large deviation in the mass fraction of TEPA. It was found for all the single stage experiments that the model consistently over predicts the mass fraction of TEPA in the liquid mixture. An explanation of this error is the assumption that the effect of CO_2 on the vapor curve is negligible, stated in section 3.2. **The single stage experiments might prove that the assumption is incorrect.** More research on the effect of P_{CO_2} on the vapor curve is required, this is elaborated on in chapter 7. The loading in table 4.11 also shows inconsistency with the model. This mismatch is caused by the interpolation in the SIT model of the obtained experimental VLE data points by Dowling et al. The data points have a standard deviation of around ± 0.25 mol $CO_2/kg\, TEPA$ from the calculated VLE curve [12]. This deviation is even higher in the lower ranges of P_{CO_2} and L.

Table 4.13: Model validation through 2-stage experiment 13 from table 4.3.

Experiment 13 (table 4.3)

Parameter	Experiment	Model	Error
	Stage 1		
T	96.03 $[℃]$	101.56 $[℃]$	5.4 $[\%]$
L	5.33 $[mol/kg]$	5.31 $[mol/kg]$	0.3 $[\%]$
w_{TEPA}	48 $[wt\%]$	49 $[wt\%]$	0.4 $[\%]$
	Stage 2		
T	119.82 $[℃]$	119.82 $[℃]$	0 $[\%]$
L	2.74 $[mol/kg]$	2.72 $[mol/kg]$	0.9 $[\%]$
w_{TEPA}	77 $[wt\%]$	76 $[wt\%]$	1.7 $[\%]$

Table 4.14: Model validation through 2-stage experiment 14 from table 4.3.

Experiment 14 (table 4.3)

Parameter	Experiment	Model	Error
	Stage 1		
T	99.04 $[℃]$	101.88 $[℃]$	2.8 $[\%]$
L	5.02 $[mol/kg]$	5.11 $[mol/kg]$	1.7 $[\%]$
w_{TEPA}	46 $[wt\%]$	49 $[wt\%]$	4.6 $[\%]$
	Stage 2		
T	119.48 $[℃]$	119.48 $[℃]$	0 $[\%]$
L	2.95 $[mol/kg]$	2.67 $[mol/kg]$	9.4 $[\%]$
w_{TEPA}	73 $[wt\%]$	76 $[wt\%]$	4.2 $[\%]$

For the 2-stage experiments, it was found that the model predicts the performed experiments accurate. The top stage temperature in table 4.13 and 4.14 is slightly off. This might be caused by a small reflux of H_2O which occurred at the top of the column during the experiment. Another explanation is that the assumption of zero heat losses in the model overestimates the temperatures of the stages above the reboiler.

Chapter 5

Results and Discussion

In this chapter, the results of this thesis work are presented. First, the effect of kinetics in the stripping column is investigated, followed by an analysis of the diffusion and reaction rate relation. This relation will describe the limitations of the desorption phenomenon inside the stripping column. Subsequently, a sensitivity analysis on the input parameters is presented to understand the effect on the performance of the stripping column.

5.1 Kinetics

5.1.1 Hold Up Time

To get an understanding of the importance of reaction kinetics in an equilibrium stage, one must specify the hold up time for that specific stage. The hold up time is defined as the time that a particle of the species of interest remains in the system. In the case of a multi-stage stripper, each stage is identified as a separate system. Equation 5.1 gives the general formula that is used to calculate the hold up time.

$$t_{hold} = \frac{V_{stage}}{\dot{m}_{out}} \tag{5.1}$$

Where V_{stage} = liquid volume in the stage and $\dot{m}_{out}$ = mass flow rate out of the stage. The hold up time can be used to express the time that is required for a stage to reach VLE equilibrium. In other words, the feed mixture remains long enough in the stage to desorb the contained H_2O and CO_2 so that it coincides with the VLE curve for the specific T and P_{CO_2} of the stage. When the equilibrium is reached, the vapor and liquid composition inside the stage remains constant. So from this point on, an increase in the hold up time would not affect the composition.

Figure 5.1 shows the data points acquired through the single stage experiments for the 115℃ isotherm at P_{abs} = 950 mbar. In Matlab, the cftool application is used to create a curve fit of the presented data points.

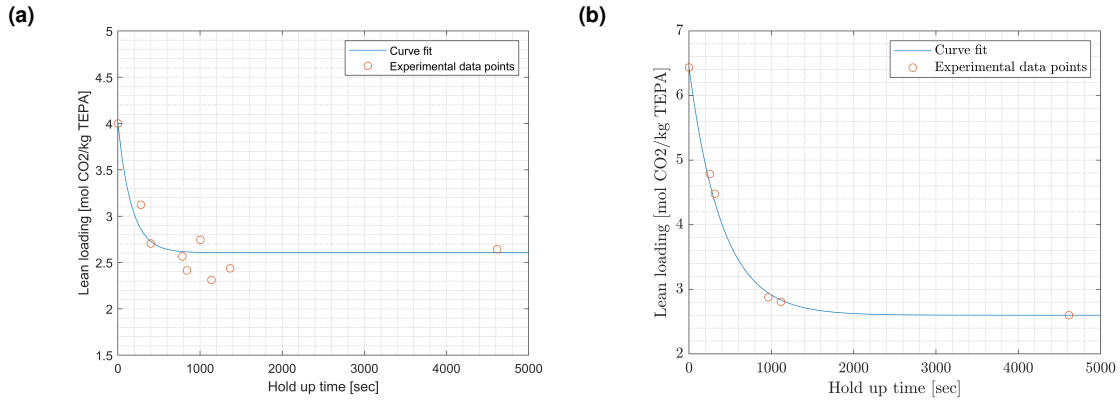

Figure 5.1: Lean loading versus hold up time for performed experiments at 115℃ and P_{abs} = 950 mbar and (a) a rich loading of 4 $mol\ CO_2/kg\ TEPA$ and (b) a rich loading of 6.5 $mol\ CO_2/kg\ TEPA$.

Before drawing conclusions, assumptions must be taken into account. The relevant assumptions are listed underneath:

- **The lean loading at t_hold is 0 s equals the rich loading in the feed mixture.** This is a theoretical starting point, in reality the lean loading will always be lower when it has spend time inside the system.
- **$\dot{m}_{in}$ and $\dot{m}_{out}$ are assumed to be equal, so also represent the average mass flow rate from stage to stage inside the column.** Accordingly, $\dot{m}_{out}$ can be used to calculate the hold up time of each stage individually.
- **Besides varying the mass flow rate of the feed, constant experimental conditions are assumed for each data point.**
- **It is assumed that the rich loading does not determine the equilibrium loading presented by the VLE.** As P and T inside the stage are constant, the lean loading is fixed and is therefore not affected by a change in rich loading. According to this assumption, the equilibrium loading at t_{hold} is 4500 s presented in figure 5.1.a is implemented as equilibrium loading point in figure 5.1.b. **This assumption will be investigated in section 5.2.**

Figure 5.1 demonstrates that, under the specified conditions, to reach VLE equilibrium, a minimum hold up time of respectively 600 and 1500 seconds is required. At these points, the curve fit is about horizontal, which indicates that the lean loading does not decrease when increasing the hold up time and thus equilibrium is reached. **It can also be concluded that a higher rich loading leads to a larger hold up time that is required to reach equilibrium.** So, as the cyclic capacity increases, the required hold up time to reach equilibrium increases too.

Note that the error between the data points and the curve fit in especially figure 5.1.a are relatively big. This can be explained by the small variations in T_{abs}, w_{H_2O} and L_{rich} between the different performed experiments. These variations were smaller in 5.1.b which can be clearly observed by the accurate correlation between the data points and the curve fit. Moreover, the FTIR analysis also contributes slightly to the presented error, which is explained in section 4.2.5.

Since the hold up time directly affects the CO_2 production yield, it is of interest to dive deeper in the phenomena that cause the specific hold up time and investigate how to minimize it. As explained in section 2.2.1, desorption of CO_2 is determined by the reaction kinetics and diffusion. The following section will shine light on the importance of both phenomena regarding the performed experiments.

5.1.2 Reaction Kinetics vs Diffusion

This discussion is purely based on assumptions, although a basic understanding can be established according to the findings presented underneath. Nevertheless, further research on this topic is required. Consequently, no concrete quantification can be drawn from this analysis. To discuss the limitations of the performed experiments in terms of reaction kinetics and diffusion, the Damköhler number, explained in section 2.2.1, is used. The Damköhler number is calculated according to equation 2.10. To do so, one must find the diffusion coefficient D at 120 $℃$. A diffusion coefficient of 10^{-15} was found at 20 $℃$ by De Matteis et al. [13]. Scaling of D can be done, since it is inversely proportional to the viscosity μ according to the Stokes-Einstein relation, equation 2.7. The viscosity at 20 $℃$ can be found in figure 2.9 and corresponds to 5 $Pa \cdot s$. The T-μ relation proposed by Sinha et al. [11] is accurate for temperatures between 20 - 40 $℃$. Extrapolating the T-μ relation results in μ

equals $10^{-7} Pa \cdot s$ at 120 $\mathcal{C}$, which is unrealistically low. An analogy with the T-μ relation for H_2O can be made according to equation 5.2. It was found that μ equals 1.15 $Pa \cdot s$ at 120 $\mathcal{C}$. Implementing the viscosity in the T-μ relation would suggest a temperature of around 40 $\mathcal{C}$. Consequently, this analogy is not used to estimate μ at 120 $\mathcal{C}$.

$$\frac{\mu_{TEPA,20\mathcal{C}}}{\mu_{TEPA,120\mathcal{C}}} = 5000 \cdot \frac{\mu_{H_2O,20\mathcal{C}}}{\mu_{H_2O,120\mathcal{C}}} \tag{5.2}$$

As the above mentioned viscosity estimate methods did not result in a realistic μ at 120 $\mathcal{C}$, experimental observations will be used to suggest a viscosity. During experiments, it was observed that the lean loaded TEPA mixture leaving the single stage at 120 $\mathcal{C}$ had a viscosity which is close to μ of H_2O at 20 $\mathcal{C}$. **For this reason, μ at 120 $\mathcal{C}$ is assumed to equal $10^{-3} Pa \cdot s$.** Consequently, D at 120℃ is calculated via equation 5.3.

$$\frac{D_{120\mathcal{C}}}{D_{20\mathcal{C}}} = \frac{\mu_{20\mathcal{C}}}{\mu_{120\mathcal{C}}} \tag{5.3}$$

Next to the viscosity assumption at 120℃, there are some other assumptions that should be stated regarding the calculation of the Damköhler number:

- **For simplicity reasons, the solution inside the single stage is assumed to be a flat liquid film. In the experimental setup, the lean solvent outlet is placed 0.01 m above the bottom surface. However, the solution is boiling which causes the diffusion length to be much lesser. A diffusion length of 0.001 m is assumed.** A sensitivity analysis on the diffusion length will be performed in section 5.1.3 to find the effect of this assumption. **Moreover, this assumption implies that the calculated Damkohler number can be compared to the Hatta numbers found in literature, section 2.2.1.** This will give insight in the limitation of the experimental system compared to liquid amine systems in industry.
- **Due to boiling, the solution inside the stage is slowly mixing, based on experimental observations, however can not be assumed as an homogeneous solution.** This backs up the diffusion length assumption as the diffusion length should have a significant length compared to the film height due to a lack of mixing. **Heavily boiling would enhance mixing and consequently lead to a shorter diffusion length.**
- **To calculate the volume of produced CO_2, the ideal gas law is used.** This is explained more in detail in section 4.2.5.

The outcome of the Stokes-Einstein scaling method and the corresponding Damköhler number is presented in table 5.1 for a generic single stage experiment.

Table 5.1: Experimental variables used to calculate Damköhler number for a generic single stage experiment.

Temperature	Diffusion coefficient	CO2 produced	Exp. time	Mass feed mixture	Concentration CO_2 in feed	Da_{II}
$[\mathcal{C}]$	$[m^2/s]$	$[g]$	$[s]$	$[g]$	$[wt\%]$	$[-]$
120	$5{\cdot}10^{-12}$	20	7200	500	10	11.1

It was found in section 2.2.1 that typical Hatta numbers for desorption of CO_2 from liquid amines are in the range of 10 to 35. **Consequently, it can be concluded that the desorption process inside the stripper corresponds to the suggested literature and is limited by diffusion.**

5.1.3 Sensitivity Analysis

In section 5.1.2, assumptions were suggested for the viscosity of the solution at 120 $℃$ and the diffusion length. To understand the effect of viscosity and diffusion length on the Damköhler number, a sensitivity analysis is performed and visually presented in figure 5.2.

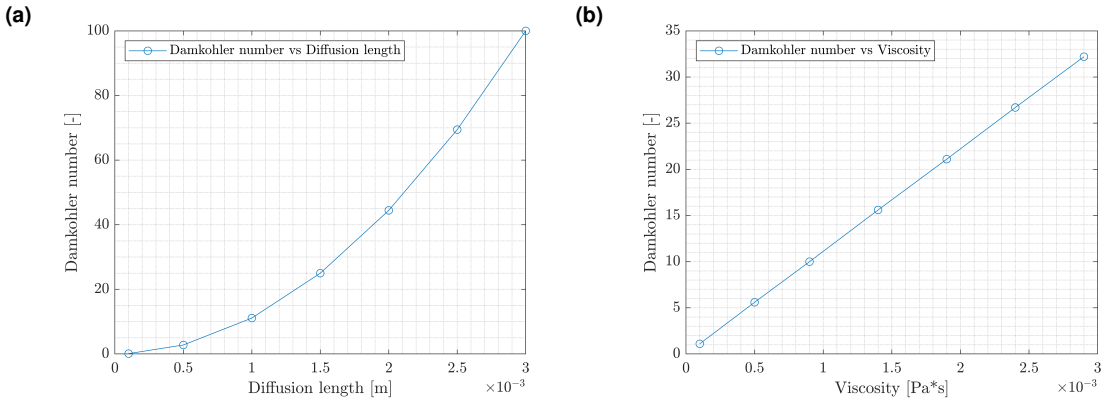

Figure 5.2: Sensitivity analysis on the Damköhler number where (a) expresses the effect of change in diffusion length and (b) the effect of change in viscosity.

One can see from the graphs that the diffusion length scales exponentially with the Damköhler number. Moreover, the viscosity of the liquid mixture scales directly proportional with Da_{II}. This means that changing the diffusion length has the largest impact on Da_{II}. **Both assumptions have a strong effect on the Damköhler number which means that it is difficult to draw concrete quantification from this analysis. More research on this subject is required which is proposed in section 7.**

5.2 Effect of Parameters

As stated in chapter 1, the stripping column is analyzed through the effect of parameters on the performance of the stripper. In order to perform the analysis, three groups of different parameters and results are distinguished. **Input parameters** are the parameters that can be set to obtain a certain performance of the stripper. **Internal results** describe the phenomena that occur inside the stripper that are a consequence of the input parameters. Note that the internal results can be stage specific or for the entire stripping column. Finally, **output results** are the results in which the performance of the stripper is measured. An overview of all these parameters and results is presented in table 5.2.

Table 5.2: Overview of parameters and results to analyse the performance of the stripping column.

Input parameters	Internal results	Output results
P_{abs}	$P_{CO_2,i}$	L_{lean}
T_{reb}	$P_{H_2O,i}$	CC
T_{feed}	T_i	E
$\dot{m}_{feed}$	L_i	R_{top}
R	$w_{H_2O,i}$	
L_{rich}	Q_{reb}	
w_{H_2O}		
N		

5.2.1 Base Case

In order to analyse the effect of input parameters on the performance of the stripping column, a base case is proposed. A list of the chosen input parameter values is given in table 5.3. P and T_{feed} are, for convenience, chosen to be at ambient conditions. L and w_{H_2O} present typical rich loaded TEPA concentrations of CO_2 and H_2O [13]. T_{reb} is chosen to be the maximum reboiler temperature determined by the before mentioned parameters in combination with the vapor curve. This will be explained in more detail in section 5.2.2. $\dot{m}_{feed}$ is chosen to be close to the experimental mass flow rates. Note that $\dot{m}_{feed}$ is depending on the amount of TEPA and H_2O $mols$ in the feed solution only, this is explained in section 2.2.1.

Table 5.3: Base case input parameters.

Parameter	Value	Units
L	4	$[mol\,CO_2/kg\,TEPA]$
w_{H_2O}	40	$[wt\%]$
P	1000	$[mbar]$
T_{reb}	120	$[℃]$
T_{feed}	20	$[℃]$
N	2	$[-]$
R	0	$[-]$
$\dot{m}_{feed}$	0.006	$[mol/s]$

An overview of the base case performance outputs is presented in table 5.4 and 5.5 per stage and for the total stripping column respectively. These values will be used in the following sensitivity analyses on the effect of parameters.

Table 5.4: Overview of outputs per stage for base case.

Parameter	Value	Units
Stage 1		
T	106.7	$[℃]$
L	4.11	$[mol\,CO_2/kg\,TEPA]$
w_{H_2O}	45	$[wt\%]$
P_{H_2O}	929.9	$[mbar]$
P_{CO_2}	70.1	$[mbar]$
Stage 2		
T	120	$[℃]$
L	2.63	$[mol\,CO_2/kg\,TEPA]$
w_{H_2O}	25	$[wt\%]$
P_{H_2O}	946.7	$[mbar]$
P_{CO_2}	53.3	$[mbar]$

Table 5.5: Overview of outputs for total stripping model for base case.

Output	Value	Units
Q_{reb}	230.6	$[W]$
E	1297.8	$[kJ/mol\,CO_2]$
R_{top}	13.3:1	$[mol\,H_2O : mol\,CO_2]$
CC	1.37	$[mol\,CO_2/kg\,TEPA]$

To analyse the internal and output results from the base case, one must take the stripping model assumptions, presented in chapter 3, into account. Table 5.4 shows that absorption is taking place in the top stage of the stripping column. Also, the concentration of H_2O is higher the top stage compared to the rich feed. In the reboiler, both the CO_2 and H_2O concentrations are lower compared to the rich feed, this implies that desorption of both components is happening here. Table 5.5 presents the energy usage of the stripping column which is relatively high compared to industrial stripper applications stated in section 2.1.2. Furthermore, the top vapor ratio is high which suggests a large amount of H_2O going over the top, resulting in a high energy demand.

5.2.2 Sensitivity Analyses

In this section, sensitivity analyses on the effect of each input parameter on the performance of the stripping column are presented. A qualitative analysis is done for each input parameter individually and expressed in terms of performance parameter alteration. A combination of these sensitivity analyses, to find the optimal stripping configuration in terms of energy usage, will be presented in chapter 6.

Rich loading

To find the effect of the rich loading on the performance parameters, it is varied between 1 and 9 $mol\,CO_2/kg\,TEPA$. The output results for this input parameter range are presented in table 5.6.

Table 5.6: Effect of rich loading L_{rich} on performance parameters.

L_{rich} $[mol\,CO_2/kg\,TEPA]$	CC $[mol\,CO_2/kg\,TEPA]$	L_{lean} $[mol\,CO_2/kg\,TEPA]$	E $[kJ/mol\,CO_2]$	R_{top} $[P_{H_2O}/P_{CO_2}]$
1	0.12	0.88	$1.33{\cdot}10^4$	143
2	0.36	1.64	4430	47.1
3	0.79	2.21	2149	22.5
4	1.37	2.63	1297	13.3
5	2.08	2.92	900	8.9
6	2.88	3.12	683	6.6
7	3.74	3.26	551	5.1
8	4.64	3.36	463	4.2
9	5.57	3.43	402	3.5

To understand the relation between the rich loading and the lean loading and consequently the cyclic capacity, these are plotted against one another in figure 5.3.

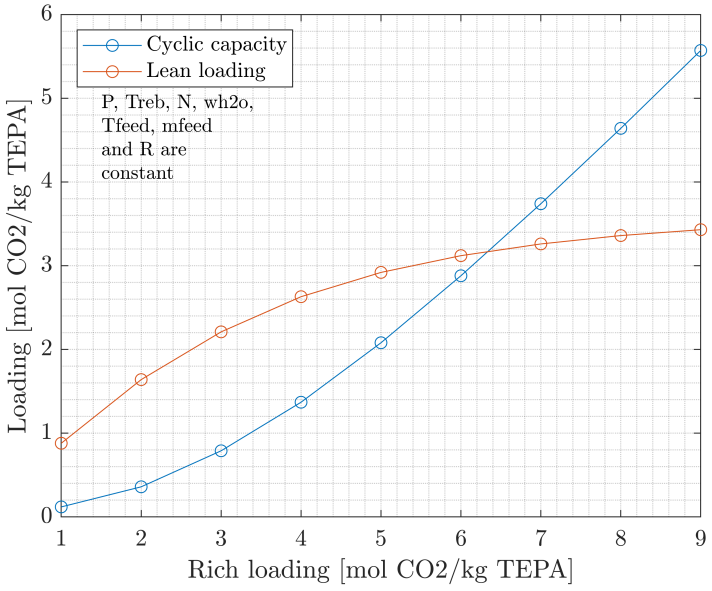

Figure 5.3: Effect of the rich loading L on the cyclic capacity and lean loading.

Figure 5.3 suggests that when increasing the rich feed loading, the lean loading increases fast at first and flattens around 5 $mol\,CO_2/kg\,TEPA$. Consequently, the cyclic capacity increases slow at first but will shift towards a linear scaling with the rich loading. This is explained by the increase of P_{CO_2} in the reboiler stage, since an increase in P_{CO_2} results in a higher equilibrium loading according to the VLE. Note that this conclusion only holds for this rich loading domain. As the VLE might behave differently outside of the analysed rich loadings, phenomena might occur that are not described here. **This suggests that the assumption regarding a constant lean loading, section 5.1, only holds for high rich loadings.**

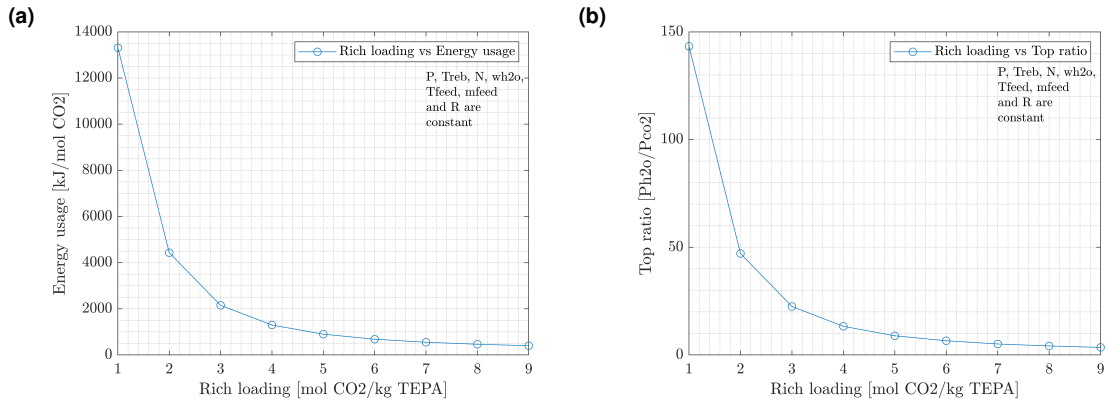

Figure 5.4: Effect of the rich loading L_{rich} on (a) the energy usage per CO_2 yield and (b) vapor ratio in the top stage.

The energy demand of the stripping column decreases when the rich loading goes up. This can be explained by a large increase in desorbed CO_2 while the energy duty of the reboiler only rises a relatively small amount. **The vapor top ratio decreases too when intensifying the rich loading.** The amount of CO_2 in the vapor phase, P_{CO_2}, rises while P_{H_2O} remains relatively constant, which implies that the vapor top ratio decreases.

Mass fraction H_2O in feed

To analyse the effect of H_2O in the feed stage on the performance of the system, a range of 25 to 70 $wt\%$ of H_2O in the feed is chosen. Note that the mass fractions relate to the binary TEPA-H_2O mixture used in the vapor curve, so CO_2 is not taken into account. The output results for this input parameter range are presented in table 5.7.

Table 5.7: Effect of the mass fraction of H_2O, w_{H_2O}, in the feed on the performance parameters.

w_{H_2O} $[wt\%]$	CC $[mol\,CO_2/kg\,TEPA]$	L_{lean} $[mol\,CO_2/kg\,TEPA]$	E $[kJ/mol\,CO_2]$	R_{top} $[P_{H_2O}/P_{CO_2}]$
25	0.26	3.74	2213	6.3
30	0.71	3.29	1274	8.5
40	1.37	2.63	1297	13.3
50	1.89	2.11	1597	19.0
60	2.37	1.63	2068	26.8
70	2.83	1.17	2834	38.6

Figure 5.5 visualizes the relation between w_{H_2O} in the rich feed to the lean loading and cyclic capacity.

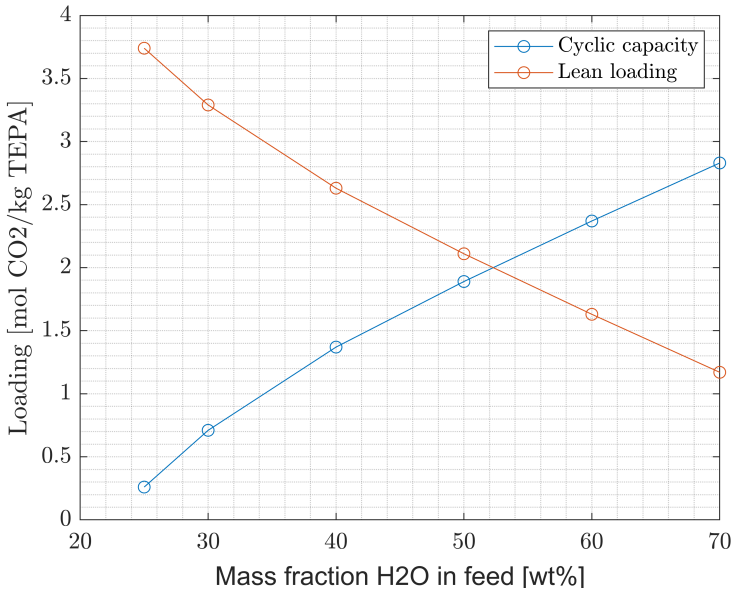

Figure 5.5: Effect of the mass fraction of H_2O, w_{H_2O}, in the feed on the cyclic capacity and lean loading.

One can see from figure 5.5 that when increasing the mass fraction of H_2O in the feed, the lean loading decreases. This induces the cyclic capacity to rise since the rich loading in the feed remains constant. An explanation for this relation is the increase of P_{H_2O} in the reboiler stage when increasing w_{H_2O}. An increase in P_{H_2O} results in a decrease in P_{CO_2} in the reboiler stage and therefore a lower lean loading and consequently higher cyclic capacity.

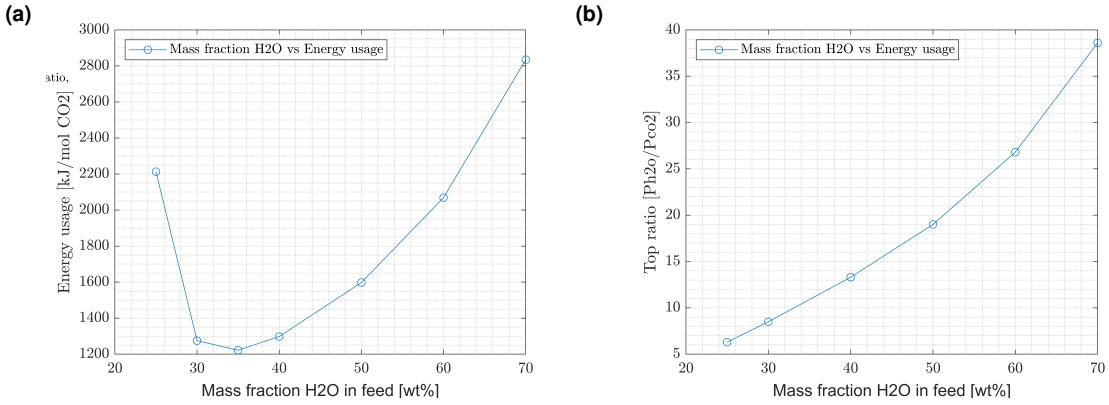

Figure 5.6: Effect of the mass fraction of H_2O, w_{H_2O}, in the feed on (a) the energy usage per CO_2 yield and (b) vapor ratio in the top stage.

Figure 5.6 suggests that there is a minimum for the energy demand around a H_2O mass fraction of 35 $wt\%$**.** Initially, with almost no H_2O in the feed, the cyclic capacity is low and rises with increasing H_2O mass fraction. When the minimum energy usage is reached, increase of sensible heat due to increasing amount of w_{H_2O} in the feed becomes dominant and therefore results in a rising energy usage. **The vapor top ratio grows with** w_{H_2O}**.** Since $w_{H_2O,top}$ increases with an increase of w_{H_2O}, P_{H_2O} increases too which leads to a larger vapor top ratio.

Absolute pressure and reboiler temperature

One of the findings during the experimental phase is that P_{abs}, T_{reb} and $w_{H_2O,reb}$ are a closely related concept. Due to the presence of H_2O in the mixture, the T_{reb} to facilitate boiling of the solution is determined by the vapor curve. Subsequently, P_{abs}, T_{reb} and $w_{H_2O,reb}$ will not be analysed as individual parameters. Therefore, P_{abs} will be varied and the corresponding T_{reb} that facilitates boiling of the solution is taken to find the output parameters. This is done for a constant $w_{H_2O,reb}$ of 30 $wt\%$. The results are presented in table 5.8.

Table 5.8: Effect of absolute pressure P_{abs} and corresponding maximum T_{reb} on performance parameters.

P_{abs} $[mbar]$	T_{reb} $[℃]$	CC $[mol\ CO_2/kg\ TEPA]$	L_{lean} $[mol\ CO_2/kg\ TEPA]$	E $[kJ/mol\ CO_2]$	R_{top} $[P_{H_2O}/P_{CO_2}]$
250	78.5	0.45	3.55	2605	29.5
500	96.0	0.68	3.32	1892	19.4
750	107.5	0.90	3.10	1556	15.2
1000	115.8	1.04	2.96	1376	12.7
1250	122.8	1.20	2.80	1245	11.1
1500	128.7	1.33	2.67	1152	9.9
2000	138.4	1.56	2.44	1027	8.5

Table 5.8 indicates that increasing P_{abs}, results in a lower lean loading and thus a larger cyclic capacity. This is visually presented in figure 5.7, 5.8 and 5.9.

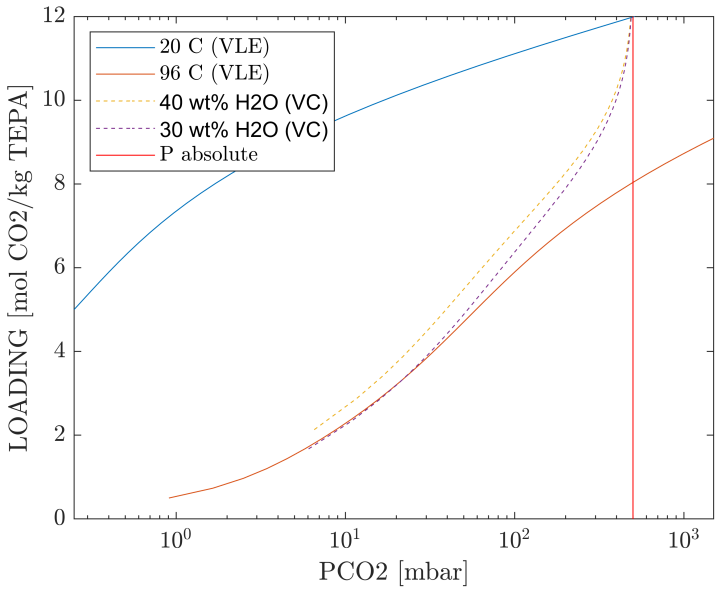

Figure 5.7: Effect of absolute pressure P_{abs} on the lean loading for P_{abs} = 500 $mbar$.

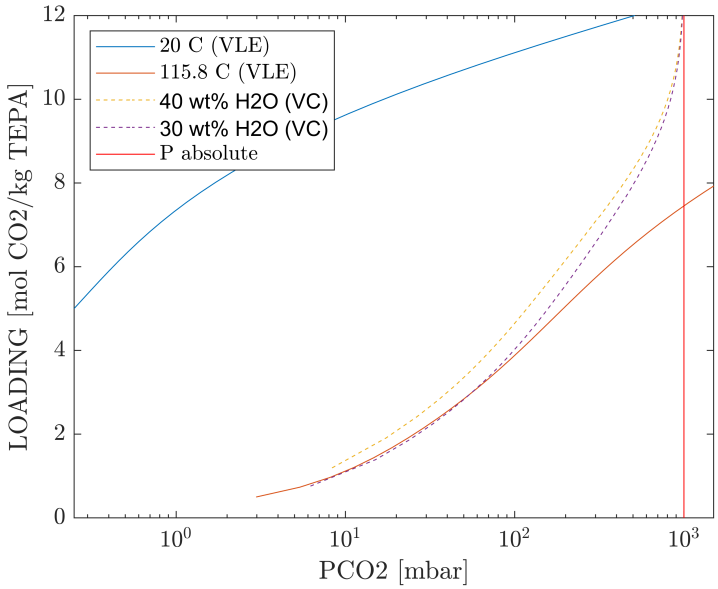

Figure 5.8: Effect of absolute pressure P_{abs} on the lean loading for P_{abs} = 1000 $mbar$.

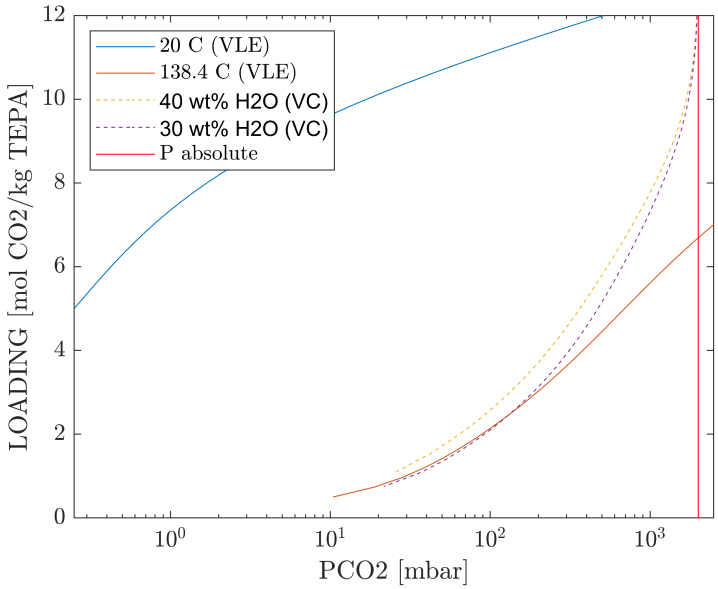

Figure 5.9: Effect of absolute pressure P_{abs} on the lean loading for P_{abs} = 2000 $mbar$.

In these figures, the T_{reb} isotherm in the VLE is plotted against the vapor curve for the $w_{H_2O,reb}$. As the T_{reb} increases with an increase in P_{abs}, the VLE is shifting down. As the vapor curve remains constant due to a constant assumed $w_{H_2O,reb}$, the intersection point of the VLE and vapor curve goes down which corresponds to a lower equilibrium loading. To conclude, **an increase in P_{abs} results in a lower lean loading and larger cyclic capacity.**

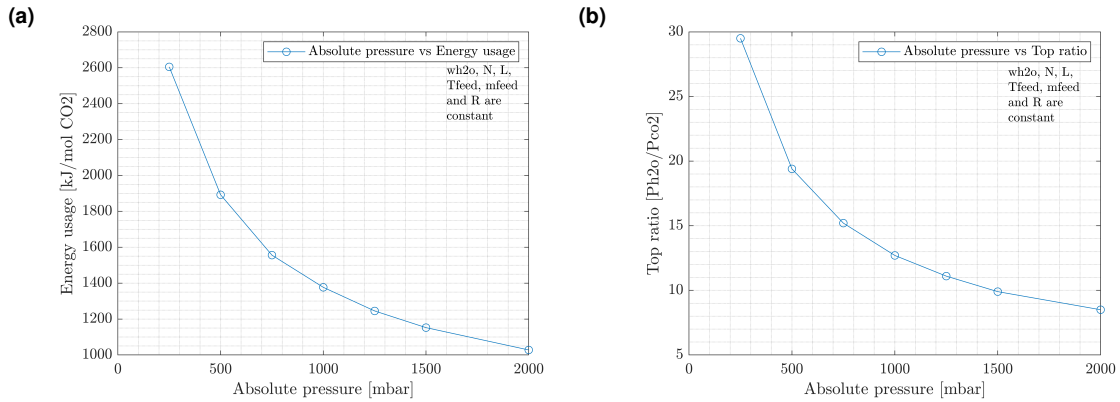

Figure 5.10: Effect of the absolute pressure P on (a) the energy usage per CO_2 yield and (b) vapor ratio in the top stage.

Figure 5.10indicates that the energy usage for an increasing absolute pressure drops. The larger temperature difference between T_{feed} and T_{reb} results in a higher reboiler duty. Moreover, the increase in amount of desorbed CO_2 also intensifies the reboiler duty. Nonetheless, the increase in desorbed CO_2 is dominant over the increase in reboiler duty, which results in a drop in energy usage for the system, figure 5.10. **The top ratio reduces while the absolute pressure increases.** P_{CO_2} rises significantly faster than P_{H_2O} in the top stage when increasing P_{abs}. This leads to a reduction of the vapor top ratio.

Number of stages

For the sensitivity analysis on the number of stages, a rich loading of 6 $mol\ CO_2/kg\ TEPA$ was chosen to emphasize the effect of the number of stages on the performance parameters. The results of this analysis are presented in table 5.9.

Table 5.9: Effect of number of stages N on performance parameters.

N $[-]$	CC $[mol\ CO_2/kg\ TEPA]$	L_{lean} $[mol\ CO_2/kg\ TEPA]$	E $[kJ/mol\ CO_2]$	R_{top} $[P_{H_2O}/P_{CO_2}]$
1	2.37	3.63	841	8.4
2	2.88	3.12	683	6.6
3	3.17	2.83	618	5.8
4	3.35	2.65	583	5.4
5	3.48	2.52	562	5.2
6	3.57	2.43	548	5.0
7	3.63	2.37	538	4.9
8	3.68	2.31	531	4.8

To explain the effect of N on the lean loading, a 1, 3 and 8 stage column are compared in table 5.10 in terms of internal results in the top and bottom stage.

Table 5.10: Effect of number of stages N on H_2O mass fraction and partial pressures at bottom and top stage, where T_{bottom} remains constant at 120℃.

N	T top	w_{H_2O} top	P_{CO_2} top	P_{H_2O} top	T bottom	w_{H_2O} bottom	P_{CO_2} bottom	P_{H_2O} bottom
$[-]$	$[℃]$	$[wt\%]$	$[mbar]$	$[mbar]$	$[℃]$	$[wt\%]$	$[mbar]$	$[mbar]$
1	120.0	23.6	106	894	120	23.6	106	894
3	104.0	45.4	147	853	120	25.0	62	938
8	103.3	45	172	828	120	25.8	42	958

It is clear that an increase in the number of stages results in a higher mass fraction of H_2O in the bottom stage. This leads to a higher P_{H_2O} and lower P_{CO_2} in the bottom stage. This is visually presented in figure 5.11 where the VLE isotherm of 120 $℃$ is plotted against the vapor curve for the different w_{H_2O} in the bottom stage.

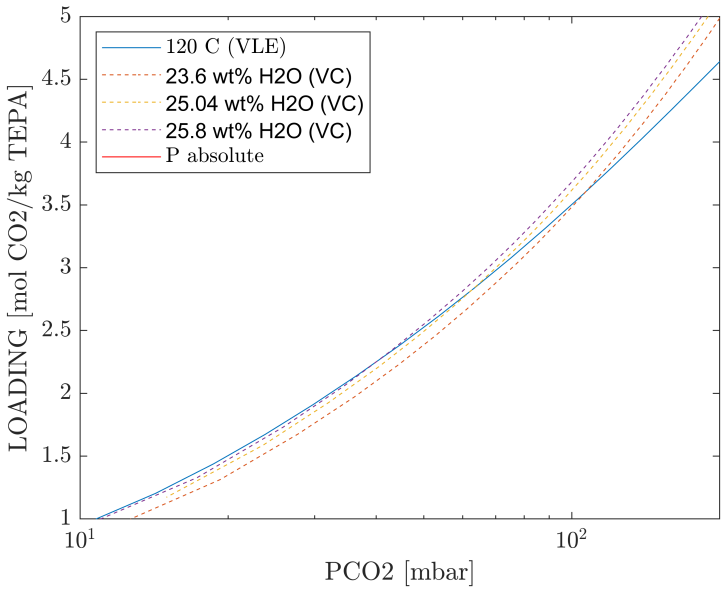

Figure 5.11: Lean loading for a 1, 3 and 8 stages stripping column.

Figure 5.11 shows that a rise in the amount of H_2O present in the bottom stage, increases $P_{H_2O,bottom}$ and decreases $P_{CO_2,bottom}$, which results in a lower lean loading and therefore larger cyclic capacity. **So, increasing the number of stages results in a lower lean loading and thus a larger cyclic capacity.**

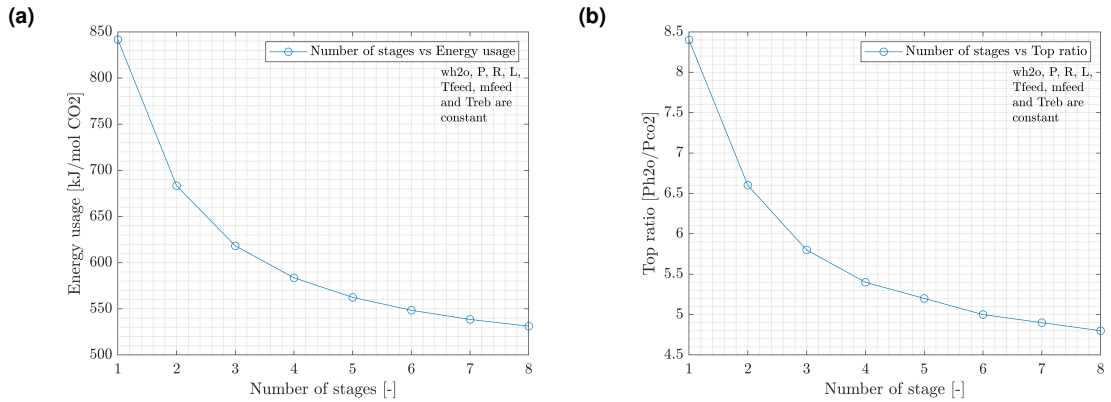

Figure 5.12: Effect of the number of stages N on (a) the energy usage per CO_2 yield and (b) vapor ratio in the top stage.

Figure 5.12 implies that E goes down when N rises. The amount of desobed CO_2 rises for increasing N, which results in a higher reboiler duty. Nevertheless, the rise in amount of desorbed CO_2 is dominant over the increase in reboiler duty, so results in a reduction in energy usage. Increasing N induces a decrease in T_{top}. This results in a lower P_{H_2O} in the top and therefore a higher P_{CO_2} implying a smaller vapor top ratio. Thus, **increasing N results in a decrease in the vapor top ratio.** Note that table 5.9 shows that w_{H_2O} finds a maximum in the chosen range of N. Due to the decrease of T_{top} when increasing N, a maximum or minimum is not found for the vapor top ratio.

Reflux ratio

For the reflux ratio, a range between 0 and 3 is investigated. The results are presented in table 5.11.

Table 5.11: Effect of reflux ratio R on performance parameters.

R $[-]$	CC $[mol\,CO_2/kg\,TEPA]$	L_{lean} $[mol\,CO_2/kg\,TEPA]$	E $[kJ/mol\,CO_2]$	R_{top} $[P_{H_2O}/P_{CO_2}]$
0	1.37	2.63	1298	13.3
0.5	1.66	2.34	1436	16.1
1	1.87	2.13	1582	18.7
1.5	2.05	1.95	1728	21.2
2	2.20	1.80	1871	23.6
3	2.43	1.57	2152	28.1

A graphical presentation of the R, lean loading and cyclic capacity relation is shown in figure 5.13.

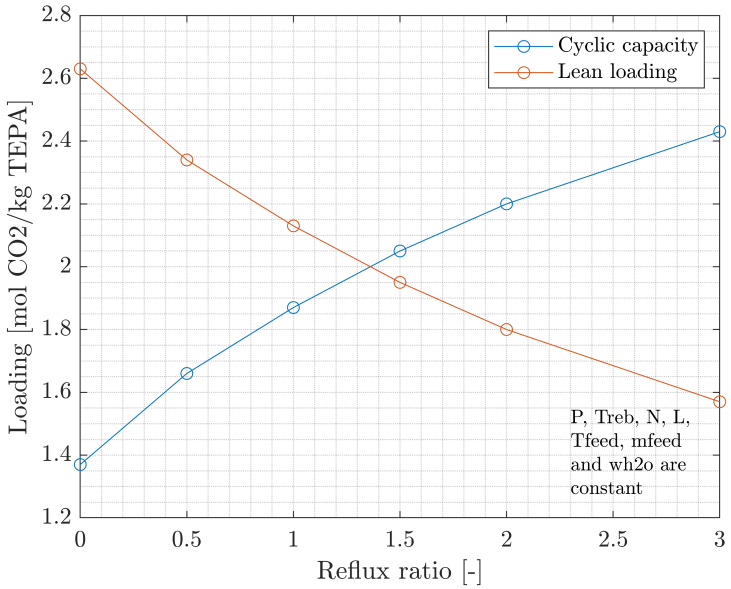

Figure 5.13: Effect of the reflux ratio R on the cyclic capacity and lean loading.

It was found that the increase of reflux leads to a decrease of the lean loading and an increase of the cyclic capacity. A higher reflux leads to a higher H_2O mass fraction in the reboiler stage, which results in a higher P_{H_2O} and therefore a lower P_{CO_2}. Consequently, the equilibrium loading in the reboiler stages is decreasing for an rising reflux ratio. As the rich loading remains constant, the cyclic capacity increases too.

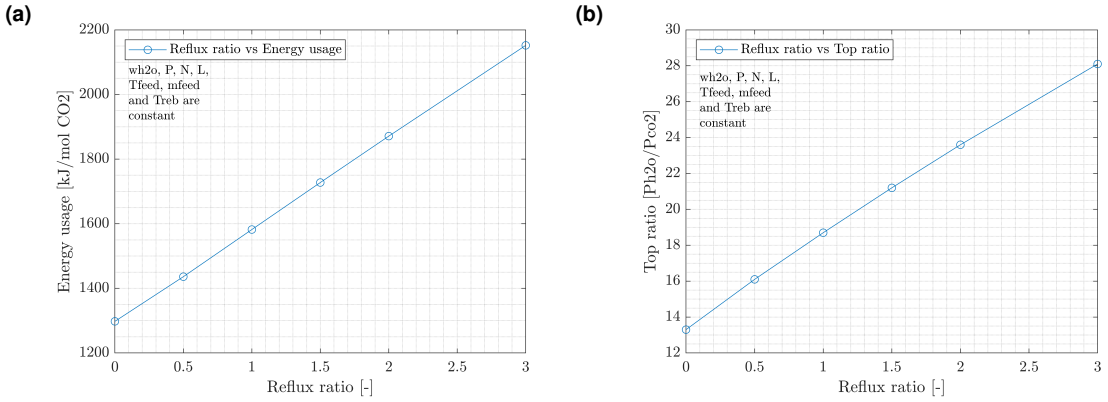

Figure 5.14: Effect of the reflux ratio R on (a) the energy usage per CO_2 yield and (b) vapor ratio in the top stage.

From figure 5.14, it can be concluded that **when the reflux ratio rises, the energy usage of the stripper rises linearly.** This is due to an increase in reboiler duty to heat and evaporate the refluxed H_2O. **The vapor top ratio grows almost linearly with the reflux ratio.** This is caused by the increase of w_{H_2O} and therefore increase of P_{H_2O} in the top stage.

Feed temperature

It was found that the effect of the feed temperature on the lean loading, cyclic capacity and vapor top ratio is relatively small and therefore assumed to be negligible. The effect on the energy usage of the stripping column is presented in figure 5.15. A T_{feed} range of 20 to 80 $℃$ is chosen, since higher feed temperatures would cause desorption to occur before the feed reaches the column. This is further investigated in chapter 6.

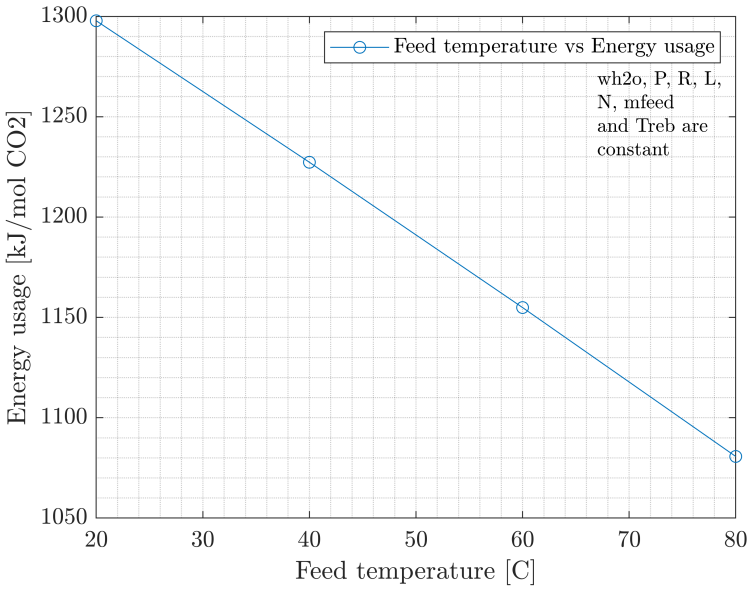

Figure 5.15: Effect of the feed temperature T_{feed} on the energy usage per CO_2 yield.

For the specific T_{feed} range, it can be concluded that **the energy usage scales inverse linearly with the feed temperature.** This means that the non-linear effects in the chosen range are relatively small. When increasing T_{feed}, the temperature difference between T_{feed} and T_{reb} becomes smaller which results in a lower reboiler duty.

Feed mass flow rate

The effect of $\dot{m}_{feed}$ on the perfromance of the stripping column is presented in table 5.12.

Table 5.12: Effect of feed mass flow rate $\dot{m}_{feed}$ on performance of the stripping column.

$\dot{m}_{feed}$ $[mol/s]$	CC $[mol\,CO_2/kg\,TEPA]$	L_{lean} $[mol\,CO_2/kg\,TEPA]$	E $[kJ/mol\,CO_2]$	R_{top} $[P_{H_2O}/P_{CO_2}]$
0.002	1.37	2.63	1298	13.3
0.016	1.37	2.63	1298	13.3
0.064	1.37	2.63	1298	13.3

As the stripping model assumes equilibrium, varying the mass flow rate does not affect the

performance of the stripping column. The reboiler duty and amount of desorbed CO_2 scale directly proportional with the feed mass flow rate. Consequently, the energy usage of the stripping column remains constant when increasing the mass flow rate.

A side effect of increasing the feed mass flow rate is the fact that equilibrium might not be achieved inside the stripping column. This influences the performance of the stripper drastically, which is explained in depth in section 5.1.

Figure 5.16 presents a visual overview of the performed sensitivity analyses, which can be used to predict the performance of the stripper in comparison to the base case.

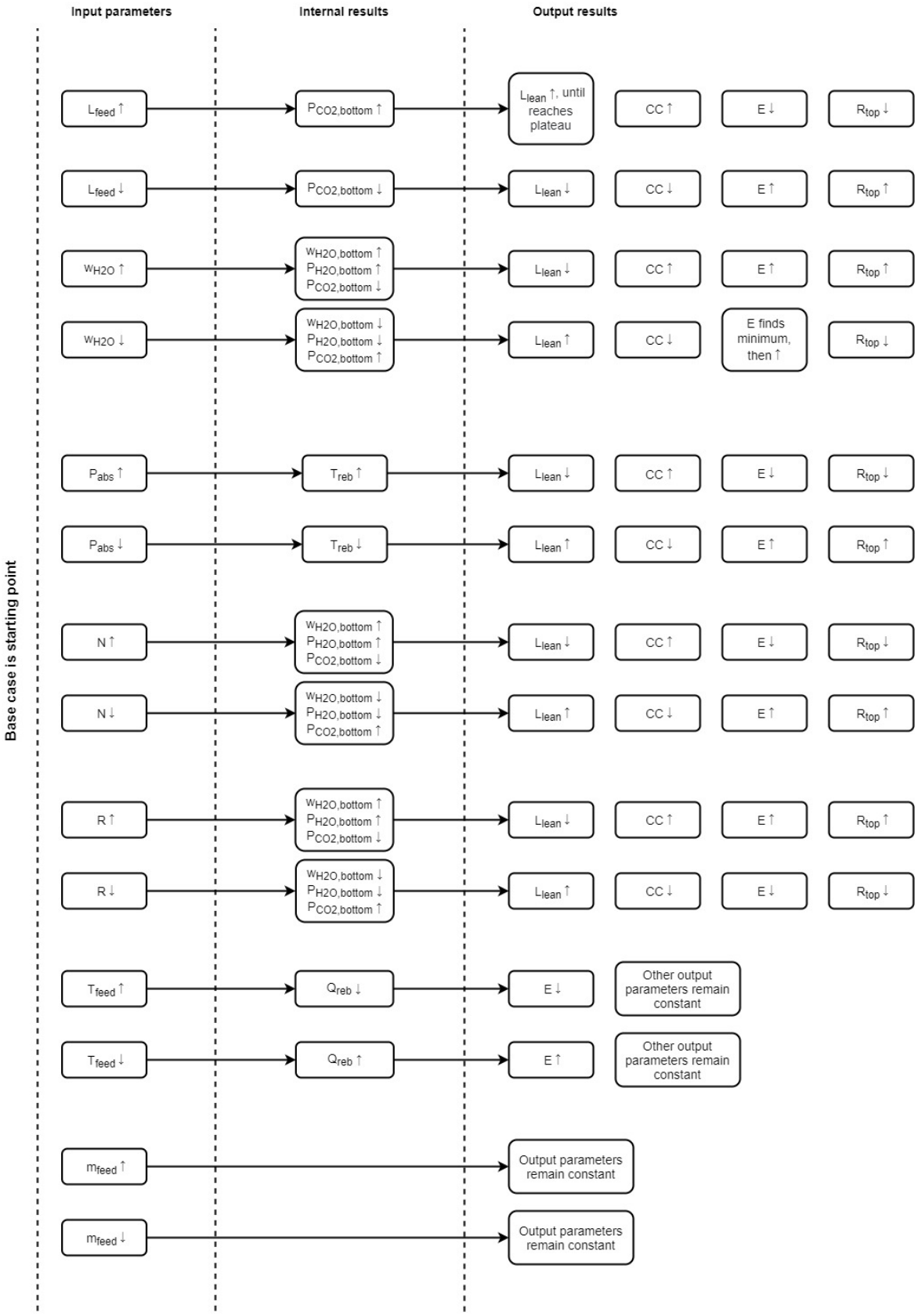

Figure 5.16: Overview of the sensitivity analysis on the effect of input parameters on the performance of the stripper.

Chapter 6

DAC System Engineering

As the final research question indicates, a new version of ZEF's stripping column to desorb CO_2 and H_2O from the ternary TEPA-H_2O-CO_2 mixture is designed and proposed in this chapter. Firstly, ZEF's operating requirements and relevant assumptions are listed. Subsequently, the most favorable operating conditions of the stripping column are found followed by a design of the stripping column. Finally, a design of the total DAC system of ZEF is proposed and compared to other CO_2 capture companies in terms of energy demand.

6.1 ZEF's Operating Requirements

ZEF has established a number of operating requirements that must be met to fulfill the methanol production target presented in section 1.2. These requirements determine the performance of the stripping column and are listed underneath:

- **ZEF is aiming at a CO_2 production of 18.75 mol per daily operational period of 8 hours.**
- **In order to produce methanol, a 3:1 molar ratio of H_2O and CO_2 product streams is required as output from the stripping column.** That is, the vapor ratio in the top stage of the stripping column must match the 3:1 ratio. This directly determines the production rate of H_2O, which is equal to 56.25 mol per day.
- **The stripping column is operating at P_{abs} equals 1000 $mbar$.** The main reason for operating at this pressure is due to simplicity of the system, the absorption and stripping column are operating at the same pressure.

6.2 Assumptions

Next to the operating requirements given by ZEF, assumptions are required to establish boundary conditions for the stripper to operate within. In designing the stripping column, the following assumptions are considered:

- **The stripping column operates at equilibrium.** This means that the stripping model can be used to predict the performance for specific operating conditions.
- According to the VLE, a higher cyclic capacity can be achieved when one increases the temperature or the rich initial loading. In varying research works, it is described that TEPA is starting to degrade at temperatures above 120 $℃$ [88] [89]. For this reason, **the T_{reb} is set at 120 $℃$.**
- The sensitivity analysis has shown that when increasing the number of stages at an absolute pressure of 1000 $mbar$, T_{top} is relatively close to 100 $℃$. Therefore, in combination with P_{CO_2} is 250 $mbar$, the equilibrium loading can be found in the VLE, presented in figure 6.1. Hence, 6.9 $mol\ CO_2/kg\ TEPA$ is the lowest rich feed loading that can be used without absorption taking place in the top stage.

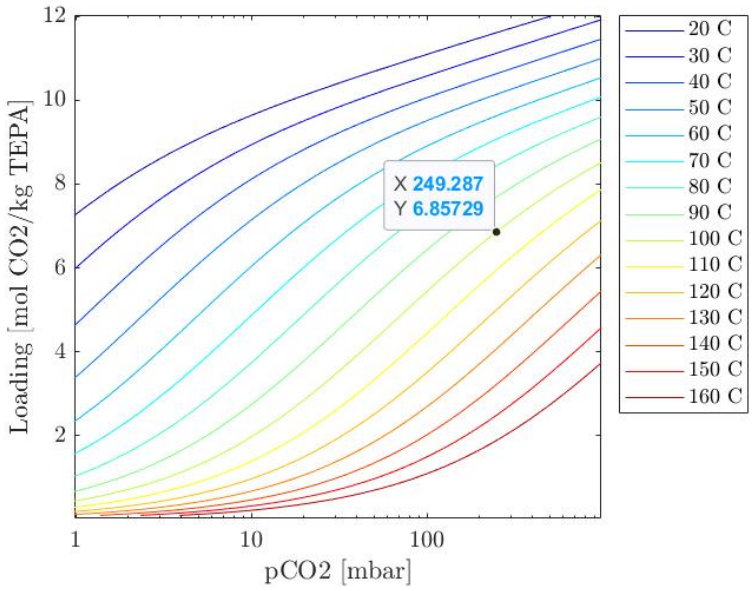

Figure 6.1: VLE where the equilibrium loading at 100 ℃ is given for a top ratio of 3:1 (P_{CO_2} = 250 $mbar$).

De Matteis et al. [13] found that the maximum loading of TEPA in ambient conditions equals 9 $mol\,CO_2/kg\,TEPA$. This presents a rich feed loading range of 6.9 - 9 $mol\,CO_2/kg\,TEPA$. Moreover, as an increase in loading results in a decrease in energy demand per produced CO_2, **6.9 $mol\,CO_2/kg\,TEPA$ is chosen as the rich feed loading to design the stripping column for.** Also, the viscosity of the feed scales quadratically with increased CO_2 loading. So, a lower feed loading will result in a lower energy demand of the feed pump, this will be elaborated on later in this chapter.

- The stripping column is designed for a warm and humid climate. As w_{H_2O} in the feed is depending on the relative humidity [90], w_{H_2O} **is chosen to equal 30 $wt\%$.** Also, since the system is operating in a warm climate, **the absorption column operating temperature T_{abs} is chosen to be 30 $℃$.**

- **Liquid mass flow in and out of a stage is assumed to be equal.** In this way, $\dot{m}_{feed}$ describes the mass flow of the solvent through the system and can be used to calculate the required hold up volume per stage.

- **The maximum T_{feed} is determined by the temperature of the top stage.** Since the column is operating at an absolute pressure of 1000 $mbar$, a T_{feed} that exceeds T_{top} results in desorption of CO_2 before the feed enters the column. Moreover, in the top stage, absorption will take place as the temperature is lower and therefore the equilibrium loading is higher than the feed loading. When absorption takes place, to fulfill the required vapor top ratio, a higher reflux ratio is required which results in a higher energy demand. This is investigated in section 6.3.

- **The hold up time of 600 s to reach equilibrium, found in chapter 5, is used to size the hold up volume of all the stages inside the stripping column.** In other words, the hold up time is not temperature dependent. It is also assumed that the concentration of the solvent mixture is not affecting the hold up time to reach equilibrium.

6.3 Stripper Design for ZEF

The presented operating boundary conditions for the stripping column are combined and visualized in figure 6.2. The red parameters represent the parameters that can be adjusted to optimize for the minimal energy demand of the system.

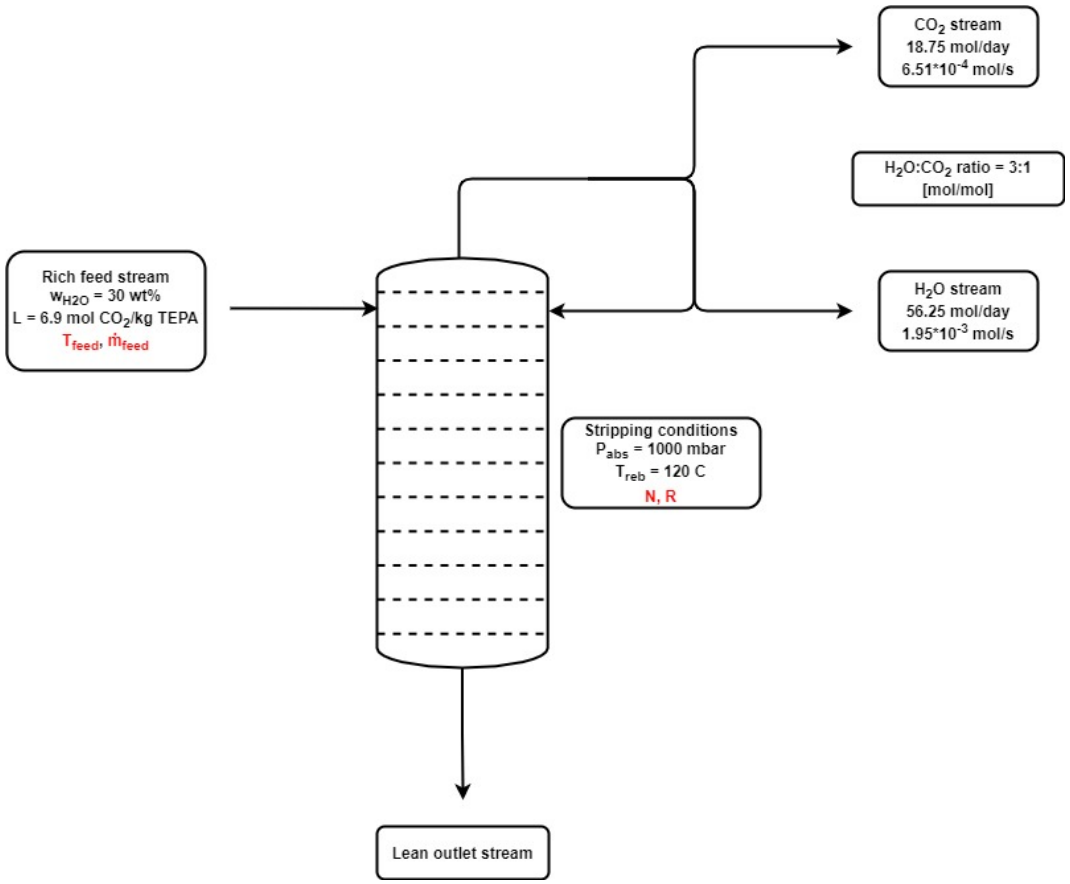

Figure 6.2: Overview of the operating boundary conditions and relevant parameters for the stripping column.

Figure 6.3 presents the procedure that is used to arrive at the final stripping column design for ZEF's DAC system. Firstly, according to the sensitivity analyses performed in chapter 5, N is found for a minimal energy demand of the stripper, followed by the optimal T_{feed} and the corresponding R while satisfying the 3:1 top vapor ratio. After which the $\dot{m}_{feed}$ is determined based on the required CO_2 and H_2O production streams. Also, the hold up volume of each stage inside the stripper is determined. Finally, the new stripper design is presented.

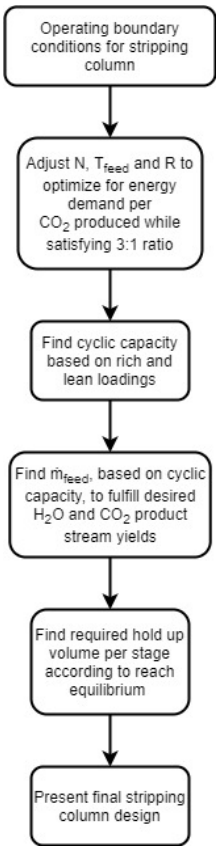

Figure 6.3: Overview of the procedure used to find the proposed stripping column design.

The sensitivity analyses presented in chapter 5 are used to find the optimum value of N for a minimal energy demand of the stripper per produced CO_2. **It was found that a 5 stage stripping setup resulted in the lowest energy demand per produced CO_2.** Increasing the number of stages even more did not result in a significantly lower energy demand.

To minimize the energy demand of the stripping column, preheating of the feed mixture is required. Ideally, the feed mixture will be preheated up to the point where it starts to desorb CO_2 and H_2O. The relation between T_{feed} and the CO_2 and H_2O concentrations is presented in figure 6.4.

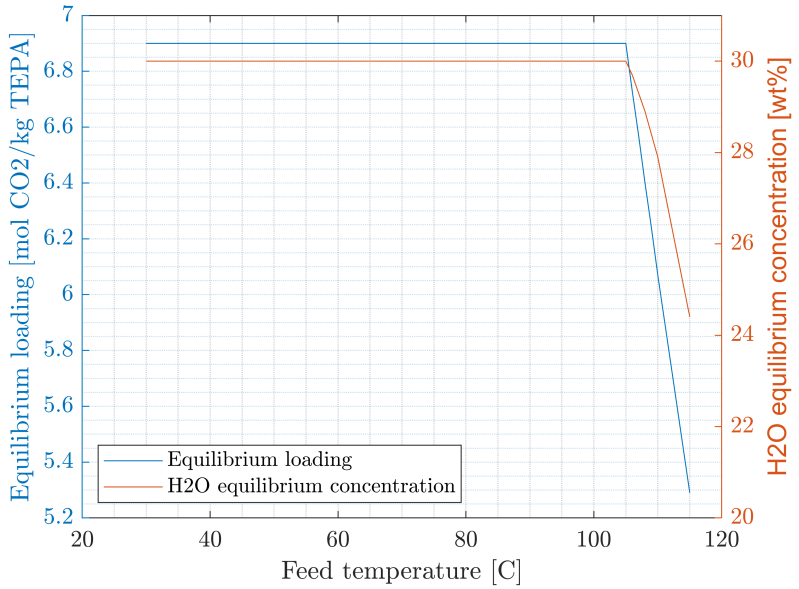

Figure 6.4: Relation between T_{feed} and the CO_2 and H_2O equilibrium concentrations in the feed mixture.

It was found that at T_{feed} equals 105 $\mathcal{C}$, CO_2 and H_2O start to desorb from the mixture at an absolute pressure of 1000 $mbar$. The relation of the feed concentrations and temperature is subsequently used as input in the 5 stage model and is optimized for the energy demand of the stripping column. A correlation between T_{feed} and the energy demand of the stripper is visually presented in figure 6.5. For each T_{feed}, a value for R was found to satisfy the 3:1 vapor ratio in the top of the column.

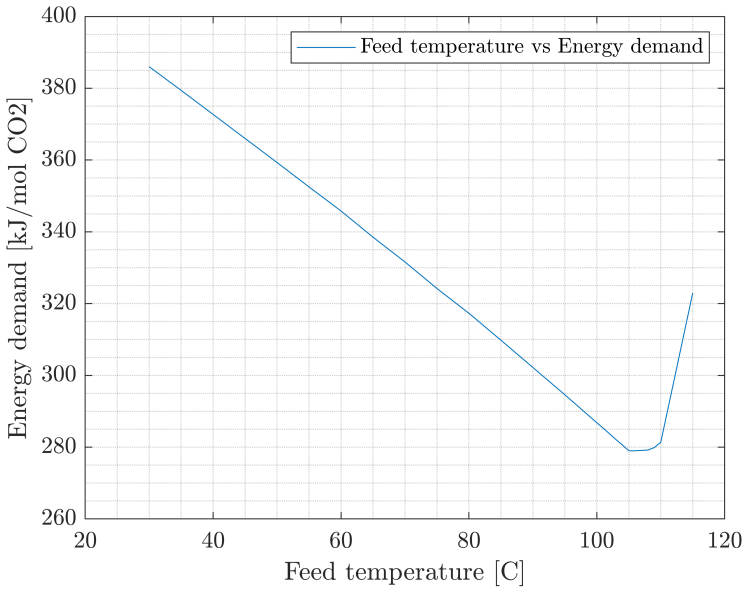

Figure 6.5: Correlation between T_{feed} and the energy demand of the stripping column.

From figure 6.5 can be concluded that the 5 stage stripping column has a minimum energy demand for a T_{feed} of 105 $\mathcal{C}$. For these conditions, a reflux ratio of 0.55 was found to satisfy the 3:1 vapor ratio in the top of the column. The minimum in the energy curve can be explained by the decrease in equilibrium concentrations of CO_2 and H_2O in the feed at temperatures higher than 105 $\mathcal{C}$. Implementing these stripper operating conditions in the stripping model produces the output results presented in table 6.1.

Table 6.1: Overview of the output results for the stripping column of ZEF where N is 5 and R equals 0.55.

Output results	Value	Units
E	279	$[kJ/mol\,CO_2]$
L_{lean}	3.6	$[mol\,CO_2/kg\,TEPA]$
CC	3.3	$[mol\,CO_2/kg\,TEPA]$
R_{top}	3	$[-]$

The main conclusion that can be drawn from these output results is regarding the feed mass flow rate. Since the cyclic capacity of the stripping column equals 3.3 $[mol\,CO_2/kg\,TEPA]$, which combined with the required CO_2 production per day and composition of the rich feed loading, **results in a feed mass flow rate of 0.31 g/s into the stripping column.** An overview of the stage specific conditions inside the stripping column is presented in table 6.2.

Table 6.2: Overview of the internal results of the proposed stripping column for the DAC system of ZEF where N is 5 and R equals 0.55.

internal result	Value	Units
Stage 1		
T	106.2	$[℃]$
L	6.3	$[mol/kg]$
w_{H_2O}	33.7	$[wt\%]$
P_{CO_2}	250	$[mbar]$
P_{H_2O}	750	$[mbar]$
Stage 2		
T	107.6	$[℃]$
L	5.9	$[mol/kg]$
w_{H_2O}	34.2	$[wt\%]$
P_{CO_2}	204	$[mbar]$
P_{H_2O}	796	$[mbar]$
Stage 3		
T	108.6	$[℃]$
L	5.4	$[mol/kg]$
w_{H_2O}	34.7	$[wt\%]$
P_{CO_2}	167	$[mbar]$
P_{H_2O}	833	$[mbar]$
Stage 4		
T	109.5	$[℃]$
L	5.0	$[mol/kg]$
w_{H_2O}	35.1	$[wt\%]$
P_{CO_2}	134	$[mbar]$
P_{H_2O}	866	$[mbar]$
Stage 5		
T	120	$[℃]$
L	3.6	$[mol/kg]$
w_{H_2O}	23.8	$[wt\%]$
P_{CO_2}	101	$[mbar]$
P_{H_2O}	899	$[mbar]$

It is clear from table 6.2 that there is no absorption of CO_2 taking place inside the stripping column. Also, desorption of H_2O only happens in the reboiler stage. All the upper stages have a higher w_{H_2O} than is present in the feed mixture.

As mentioned in the assumptions, a hold up time of 600 s is required per stage to reach equilibrium. Together with the $\dot{m}_{feed}$, the hold up volume per stage can be calculated according to equation 6.1.

$$V_{hold} = \frac{t_{hold}\dot{m}_{feed}}{\rho} = 187\,ml \tag{6.1}$$

Where V_{hold} is the hold up volume, t_{hold} is the hold up time and ρ is the density of the solvent mixture. When one assumes the weir height and the reboiler outlet height of 0.01 m, **the required radius**

of each stage is 7.7 cm**.** The estimation of the hold up volume is an optimistic one, since the hold up time is found for a rich feed loading of 4 $[mol\ CO_2/kg\ TEPA]$. A higher rich feed loading will require a larger hold up time to reach equilibrium. Moreover, the hold up time was found at 115 $^{\circ}C$, where the stages above the reboiler are all cooler. The diffusion and reaction rate both go up with an increasing temperature. As a consequence, the hold up time that is required for the upper stages to reach equilibrium is probably larger than assumed. On the other hand, the hold up time for the reboiler stage is smaller than assumed. To improve the design in terms of hold up volume, more experimental data on hold up time is required. This is proposed in chapter 7.

The hold up volume of gas per stage is assumed to be at least 10x of the liquid hold up volume. This would mean that when the liquid is boiling heavily it does not overflow into the upper stage, which would disturb equilibrium in the system. More research is required to find the optimum gas hold up volume per stage. The final design of the stripping column for ZEF's DAC system is presented in figure 6.6. Figure 6.7 shows a section view of the stripping column including general dimensions. Each stage contains 3 bubble caps, an outlet weir, a temperature sensor port and a sampling port. The number of bubble caps is the same as in the experimental setup as no research on the optimum number of bubble caps is performed. The stripper design does not contain the top condenser and flash tank. These will be discussed in section 6.4.

Figure 6.6: New design of the stripping column for ZEF's DAC system.

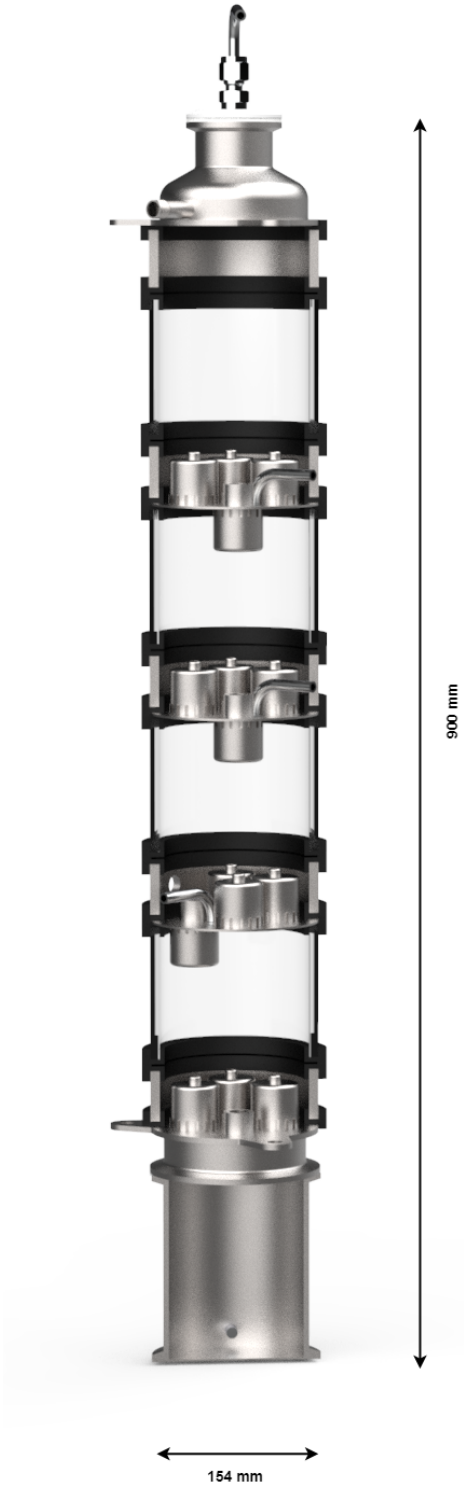

Figure 6.7: Section view of the stripping column including general dimensions.

6.4 DAC System Design for ZEF

This section combines the stripping column presented above with the absorption column to give an estimate of the total energy demand of ZEF's DAC system. In this work, no research or experiments have been done regarding the absorption column, which is therefore modelled as a black box. Only in and out stream concentrations are defined and some operating conditions are assumed:

- **Viscosity of the solvent mixture is depending on the CO_2 loading, H_2O concentration and temperature [11].** A relation between these three parameters is presented by Sinha et al. [11] and will be used to calculate the viscosity of the solvent mixture.

- **The pumping mass flow rate inside the absorption column is assumed to be 100 times larger than the $\dot{m}_{out}$ of the stripping column [13].** This leads to a mass flow rate of 2.7 $\cdot 10^{-3} m^3/s$ produced by the gear pump.

- The energy demand of the gear pump is defined by the mass flow rate and viscosity of the solvent mixture in combination with the diameter of the pipe [13]. **Based on figure 6.8 and a pipe diameter of 1 cm, an energy demand of 363 $kWh/ton\, CO_2$ was found.**

- **The temperature and pressure of the flash tank are chosen to be 40 $℃$ and 1000 $mbar$ respectively.**

- **The top condenser is assumed to be naturally cooled, in contrary to the experiments where a fan was used [5].** This means that the duty of the top condenser does not add up to the total energy demand of the DAC system. Nevertheless, the duty of the top condenser was found to be 93.4 W [5].

- As stated before, the absorption column is assumed to operate at T_{abs} equals 30 $℃$. **For this reason, the temperature of the streams between the absorption column and heat exchanger are also assumed to be 30 $℃$.**

- **The air mass flow rate is left outside the scope of this analysis.** It is assumed that enough air is sucked through the absorption column to facilitate the high rich loading required for the stripping column. **The fan that is used to blow the air through the absorption column is assumed to have a rated power of 20 W and is continuously operating at full power [13].**

An overview of the total DAC system is presented in figure 6.8. **The volume of the absorption column is typically 10 times larger than the stripping column [13].**

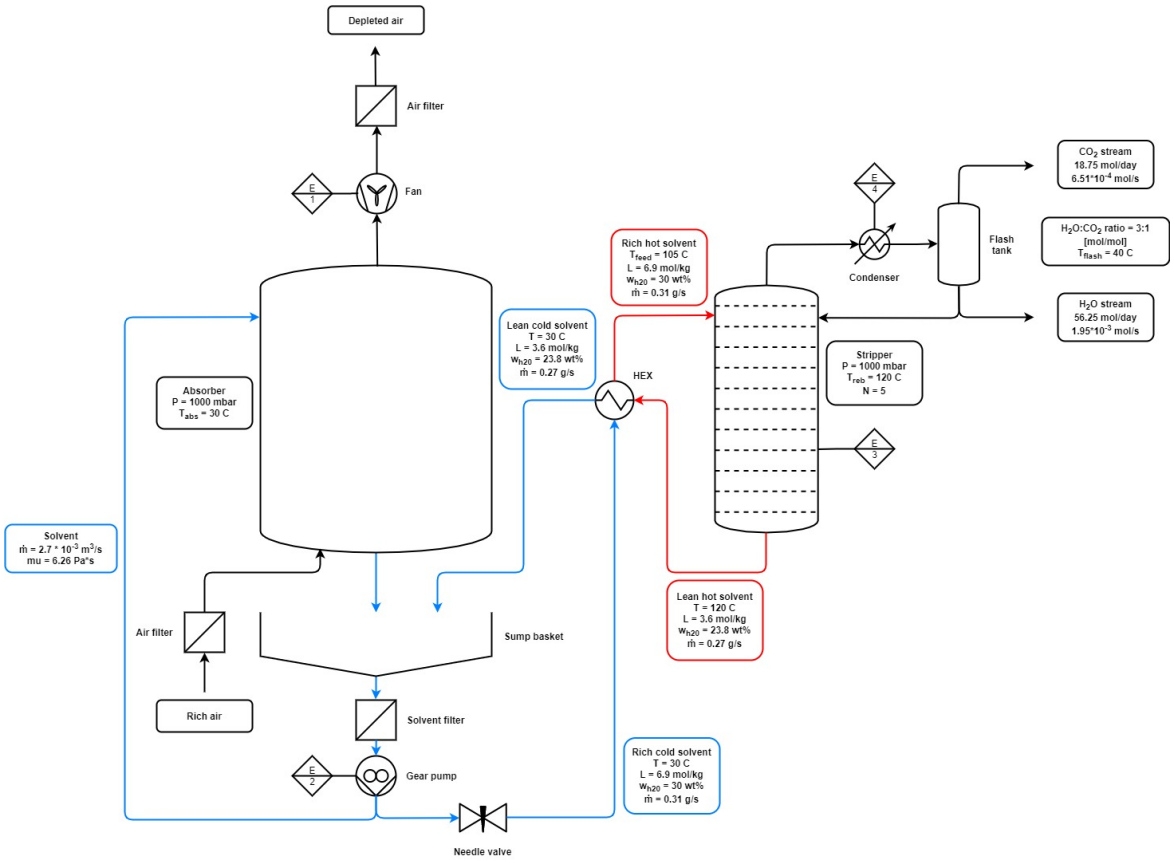

Figure 6.8: Process flow diagram of ZEF's DAC system.

Figure 6.8 shows that an heat exchanger is implemented to transfer the heat from the lean sorbent mixture leaving the stripping column to the rich sorbent mixture entering the stripping column. A sump basket is used to collect the rich sorbent mixture from the absorption column. From this basket, a gear pump pumps most of the sorbent mixture back to the top of the absorption column. The corresponding μ for the sorbent mixture pumped through the absorption column is estimated according to the viscosity relation described above. Moreover, a small part is pumped from the sump basket to the top stage of the stripping column. The mass flow rate is regulated by a needle valve.

Regarding the energy demand of the complete DAC system, an energy balance is established based on the energy demand of the reboiler in the stripping column, fan and pump in the absorption column, equation 6.2. The energy demand of the top condenser is left outside the total energy demand of the DAC system as mentioned in the assumptions.

$$E_{tot} = E_{reboiler} + E_{fan} + E_{pump} \tag{6.2}$$

An overview of the energy demand per component is presented in table 6.3.

Table 6.3: Overview of the DAC energy demand per component according to figure 6.8.

Number	Name	Value	Units
1	E_{fan}	194	$[kWh/ton\,CO_2]$
2	E_{pump}	363	$[kWh/ton\,CO_2]$
3	$E_{reboiler}$	1762	$[kWh/ton\,CO_2]$
4	$E_{condenser}$	906	$[kWh/ton\,CO_2]$

The duty of the top condenser is relatively high. This could mean that assuming the condenser to cool naturally is a somewhat optimistic assumption. More research on the top condenser during these operating conditions is required. For the heat exchanger, to operate within the assumed temperatures, mass flow rates and concentrations, an efficiency can be found according to equation 6.3 and 6.4.

$$Q_{HEX} = (C_{p,TEPA}\dot{m}_{TEPA} + C_{p,H_2O}\dot{m}_{H_2O,lean})(T_{reb} - T_{abs}) \tag{6.3}$$

$$\eta = (T_{feed} - T_{abs})\frac{(C_{p,TEPA}\dot{m}_{TEPA} + C_{p,H_2O}\dot{m}_{H_2O,rich})}{Q_{HEX}} \tag{6.4}$$

Where, Q_{HEX} is the heat released by the lean solvent, $\dot{m}_{TEPA}$ is the mass flow rate of TEPA through the system, $\dot{m}_{H2}O, lean$ is the mass flow rate of H_2O in the lean solvent, $\dot{m}_{H2}O, rich$ is the mass flow rate of H_2O in the rich solvent, T_{abs} is the temperature of the solvent inside the absorption column and η is the heat exchanger efficiency. **A required heat exchanger efficiency of 0.76 was found.** Note that the mass flow of TEPA in and out of the stripping column is equal, which is due to the assumption that TEPA does not leave the system as a vapor. The equations used to determine $T_{feed,max}$ are very simplified and give therefore an indication of the required heat exchanger efficiency. More research on the heat exchanger is necessary to provide for more in depth conclusions regarding the heat exchanger.

To conclude, a comparison of the total energy demand of ZEF's DAC system can be made with the DAC companies introduced in chapter 2. This is presented in table 6.4.

Table 6.4: Comparison of ZEF's DAC energy demand to the companies introduced in chapter 2.

Company	Electrical energy	Heat	Units
ZEF	2319	-	$[kWh/ton\,CO_2]$
Climeworks	200 - 300	1500 - 2000	$[kWh/ton\,CO_2]$
Carbon Engineering	366	1460	$[kWh/ton\,CO_2]$
Global Thermostat	150 - 160	1190 - 1400	$[kWh/ton\,CO_2]$

It can be concluded from table 6.4 that the energy demand of ZEF's DAC system is relatively close to DAC companies introduced in chapter 2. Especially, since optimizations of the DAC system can reduce the energy demand even further, competing with these companies can be seen as a realistic goal.

Chapter 7
Conclusions and Recommendations

7.1 Conclusions

What are the main parameters influencing the stripper and how do they do so?
The following conclusions can be drawn regarding the performance of the stripping column at VLE equilibrium.

- For an increasing **rich loading**, the lean loading will increase and finally find a maximum. The cyclic capacity increases first exponentially but changes to a linear increase when the lean loading has found its maximum. The vapor top ratio is reducing as well.
- An increase of the **H_2O mass fraction in the feed** leads to a lower lean loading, and thus a larger cyclic capacity. Furthermore, the vapor top ratio rises.
- When rising the **absolute pressure**, the maximum reboiler temperature rises too. This results in a drop in lean loading and therefore a rise in cyclic capacity. The vapor top ratio reduces when increasing the absolute pressure.
- When one expands the **number of stages**, the lean loading reduces where consequently the cyclic capacity enlarges. Also, the vapor top ratio drops.
- A rise in **reflux ratio** introduces a decrease in lean loading so an increase in cyclic capacity. The vapor top ratio goes up as a consequence.
- An increase in the **feed temperature** and **feed mass flow rate** does not affect the performance of the stripping column. However, when continuously increasing the feed temperature, the feed mixture will start to desorb before it enters the stripper which results in a lower cyclic capacity.

Which role plays kinetics during desorption inside the stripper?
It was found that a typical hold up time for the performed experiments to achieve equilibrium equals 600 s. Furthermore, the Damköhler number for these experiments is around 11.1 where it was found that industrial applications are within the range of 10 - 35. This means that the performed experiments are diffusion limited. Moreover, the effect of both diffusion length and viscosity on the Damköhler number was significant, which could be used to optimize the desorption process.

How can the energy demand of the stripper be minimized? What factors influence it? The following conclusions can be drawn regarding the energy demand of the stripping column at VLE equilibrium.

- The energy demand of the stripping column decreases for an increase in **rich loading**.
- An increase of the **H_2O mass fraction in the feed** will find a minimum in the energy demand of the stripping column.
- The energy demand of the stripping column reduces when rising the **absolute pressure**.
- When increasing the **number of stages**, the energy demand of the stripping column drops.

- The energy demand of the stripping column increases when one increases the **reflux ratio**.
- An increase in the **feed temperature** induces the energy demand of the stripper to drop.
- Varying the **feed mass flow rate** does not affect the energy demand of the stripping column.

Which stripper design meets ZEF's requirements best?
A 5 stage stripping column was designed to fulfill ZEF's operating conditions. It operates with a reboiler temperature of 120 $℃$, absolute pressure of 1000 $mbar$ and reflux ratio of 0.55. The feed is preheated up to 105 $℃$, contains 30 $wt\%$ H_2O, is loaded with 6.9 $mol\ CO_2/kg\ TEPA$ and has a mass flow rate of 0.31 g/s. Each stage has an hold up volume of 187 ml. A vapor top ratio of 3.0 and a cyclic capacity of 3.3 $mol CO_2/kg TEPA$ are achieved, resulting in an energy demand of 279 $kJ/mol CO_2$ which equals 1762 $kWh/ton\ CO_2$.

7.2 Research Recommendations

Based on this work, different topics for further research are distinguished:

- **It is recommended to perform experiments with controlled reflux to validate the reflux in the stripping model.** For now, only experiments with zero and total reflux could be quantified and used to validate the model as no measuring technique for the reflux was present.
- **Transient behaviour of the stripping column requires more investigation.** As the stripping column only operates 8 hours per day, insights in the start up and shut down procedure of the stripper are necessary. This means that experiments should be designed that target these procedures to gain understanding and facilitate optimization of the operational conditions of the stripping column.
- **More research on the Damköhler number is required to understand the limitations of the desorption process inside the proposed stripping column design.** The calculated Damköhler number in chapter 5 is based on assumptions that can not be validated. To present a quantitative conclusion regarding the Damköhler number, more experiments should be performed. Nonetheless, suggestions can be given in order to optimize the process for each type of limitation. If the Damköhler number is larger than 1, diffusion limited, one might reduce the viscosity of the solvent mixture. Moreover, reducing the diffusion length increases the diffusion term. This can be achieved by reducing the height of the weir outlet or reboiler outlet. Furthermore, increasing the temperature enhances mixing and the formation of bubbles which both results in a decrease in diffusion length. When the Damköhler number is smaller than 1, reaction kinetics limited, the addition of a catalyst can be considered. In a study performed by Zhang et al. [91], it was shown that adding a catalyst to a CO_2 loaded aqueous amine solution enhances reaction kinetics in the desorption process.
- **More research is required to reduce the viscosity of the sorbent mixture.** As concluded in chapter 5, reducing the viscosity of the sorbent mixture boosts the diffusion rate during desorption in the stripping column. Consequently, the Damköhler shifts towards 1 which means that the desorption process is becoming less limited by diffusion. Moreover, it was found that the viscosity has a large effect on the energy demand of the gear pump [13]. This is visually presented in figure 7.1 for the viscosity and mass flow rate found in chapter 6.

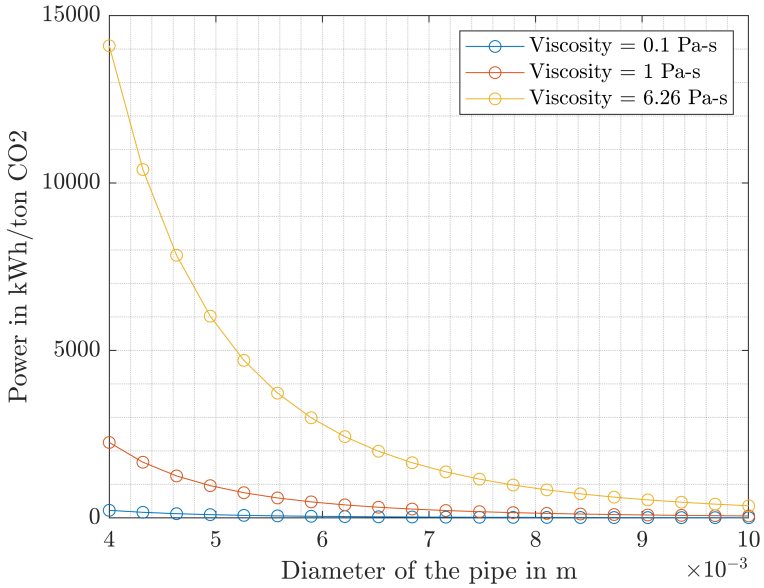

Figure 7.1: Correlation between the power of the gear pump in the absorber, viscosity and diameter of the pipe [13].

Reducing the viscosity of the sorbent mixture can be achieved by choosing another sorbent with a lower viscosity or adding a dilute to the existing ternary TEPA-H_2O-CO_2 mixture.

- **The effect of dilutes on the performance of the stripping column should be investigated.** Since dilutes could potentially reduce the viscosity of the sorbent mixture, it is of interest to understand the effect of dilutes on the performance of the stripping column. During this research, an experiment with 15 $wt\%$ PEG-200 as dilute was performed. The outcome of the experiment is compared to the stripping model where only TEPA is considered for similar operating conditions and presented in table 7.1.

Table 7.1: Effect of PEG-200 on the desorption process inside the stripping column.

	PEG-200 exp.	TEPA model	Units
T_{reb}	120.9	120.9	$[°C]$
P_{abs}	950	950	$[mbar]$
$w_{H_2O,feed}$	29.1	29.1	$[wt\%]$
L_{rich}	2.8	2.8	$[mol\ CO_2/kg\ TEPA]$
$w_{H_2O,lean}$	22.9	23	$[wt\%]$
L_{lean}	1.39	2.46	$[mol\ CO_2/kg\ TEPA]$
CC	1.41	0.34	$[mol\ CO_2/kg\ TEPA]$

It was found that adding PEG-200 as dilute has a positive effect on the net cyclic capacity. However, a VLE of the quaternary TEPA-PEG-200-H_2O-CO_2 mixture is required to explain the larger net cyclic capacity.

- **Investigate the effect of degradation on different sorbents and sorbent-dilute combinations.** The sensitivity analysis presented in chapter 5 concluded that higher reboiler tempera-

tures would lead to a larger cyclic capacity and therefore a lower energy demand of the stripping column. Since TEPA is starting to degrade around 120 $^{\circ}C$, it might be interesting to perform research on sorbents or sorbent-dilute combinations that can go to higher temperatures.

- In chapter 4, it was concluded that the heat loss during the experiments were significant. **For this reason, it is recommended to investigate the heating process of the sorbent mixture inside the reboiler stage.** For example, immersion heaters might have a higher heating efficiency which means lesser heat losses.

7.3 Stripping Model Recommendations

A number of recommendations for the stripping model are listed underneath:

- **Include the evaporation of TEPA during the desorption process.** A very small amount of TEPA evaporates during the desorption process inside the stripping column. In the stripping model, this amount is assumed to be negligible. To prevent evaporated TEPA from leaving the system in the top product streams, one can **include a water wash stage in the model.** Ideally, a water wash stage is implemented in the top of the stripping column to purify the product streams.
- **Integrate the VLE and vapor curve that describe the ternary TEPA-H_2O-CO_2 mixture.** The stripping model is build on two correlations that describe the partial pressure of H_2O and CO_2 separately. These are then combined to predict the total pressure of the H_2O-CO_2 system. Integrating these correlations would decrease the error of the stripping model as the VLE becomes a better representation of the ternary mixture. For instance, the effect of CO_2 absorption on the phase behaviour of H_2O would be taken into account as it is now neglected [12]. The data to create a certain ternary mixture VLE model could be generated by a VLE setup including a gas phase sensor that measures simultaneously the amount of H_2O and CO_2 in the vapor phase.
- **The temperature and concentration dependency of the specific heat and heat of desorption are currently assumed to have a minor effect in the stripping model.** Nonetheless, adding these relations would provide for a more realistic and complete stripping model.
- **Adjust the stripping model so that it can predict the performance of the stripper while using different sorbents.** This means that the VLE and vapor curve input should be flexible. That is, the VLE and vapor curve of a sorbent, in combination with H_2O and CO_2, can be inserted into the stripping model as input.
- **Connect the stripping model to the absorption column model proposed by De Matteis et al. [13], to facilitate the performance prediction of the complete DAC system for specific operating conditions and for different sorbents.**

7.4 DAC Design Recommendations

Based on the findings in chapter 6, multiple recommendations can be formulated regarding the DAC system of ZEF:

- **A more detailed design of the stripping column is required.** Based on a more in depth hold up time analysis, the specific hold up volume per stage can be estimated. The dimensions of

each stage should then be based on the Damköhler number and corresponding diffusion length that is required to optimize the desorption process.

- The efficiency of the heat exchanger was found to be 76 %, however this number is based on relatively simple calculations. **It is recommended to do more research on the heat exchanger.** This includes the type of heat exchanger, required efficiency for specific operating conditions and the feasibility of the DAC operating assumptions proposed in chapter 6.
- **A more in depth analysis on the cooling duty of the top condenser is required.** It was found that the cooling duty of the top condenser is relatively large. To facilitate the condenser to cool naturally, more research must be done on the condenser. This could be done in terms of condenser length, type of fins and optimal T_{flash} related to the cooling duty and purity of the CO_2 product stream.
- **Understand the effects of relative humidity and temperature on the performance of the complete DAC system.** Relative humidity and temperature play an important role in the absorption process of H_2O and CO_2 [13]. This means that different locations might require different DAC configurations to operate in a cost efficient manner. Further research on this subject is recommended.

Bibliography

[1] H. Ritchie and M. Roser, "Energy Production & Changing Energy Sources," 2018. [Online]. Available: https://ourworldindata.org/energy-production-and-changing-energy-sources

[2] D. Lüthi, M. Le Floch, B. Bereiter, T. Blunier, J. M. Barnola, U. Siegenthaler, D. Raynaud, J. Jouzel, H. Fischer, K. Kawamura, and T. F. Stocker, "High-resolution carbon dioxide concentration record 650,000-800,000 years before present," *Nature*, vol. 453, no. 7193, pp. 379–382, 2008.

[3] P. Tans and R. Keeling, "Trends in Atmospheric Carbon Dioxide." [Online]. Available: https://www.esrl.noaa.gov/gmd/ccgg/trends/global.html

[4] C. P. Morice, J. J. Kennedy, N. A. Rayner, and P. D. Jones, "Quantifying uncertainties in global and regional temperature change using an ensemble of observational estimates: The HadCRUT4 data set," *Journal of Geophysical Research: Atmospheres*, vol. 117, no. D8, 4 2012. [Online]. Available: http://doi.wiley.com/10.1029/2011JD017187

[5] P. S. M. Vroegindeweij, "Design and implementation of the ZEF 6 continuous direct air capture system," Tech. Rep., 2020.

[6] B. Metz, O. Davidson, H. De Coninck, M. Loos, and L. Meyer, "CARBON DIOXIDE CAPTURE AND STORAGE," Cambridge University Press, Cambridge, Tech. Rep., 2005.

[7] M. Bui, C. S. Adjiman, A. Bardow, E. J. Anthony, A. Boston, S. Brown, P. S. Fennel, S. Fuss, A. Galindo, and L. A. Hackett, "Carbon capture and storage (CCS): the way forward," *Energy & Environmental Science*, no. 5, 2018.

[8] M. Fasihi, O. Efimova, and C. Breyer, "Techno-economic assessment of CO 2 direct air capture plants," *Journal of Cleaner Production*, vol. 224, pp. 957–980, 7 2019.

[9] D. W. Keith, G. Holmes, D. St. Angelo, and K. Heidel, "A Process for Capturing CO2 from the Atmosphere," *Joule*, vol. 2, no. 8, pp. 1573–1594, 8 2018. [Online]. Available: https://linkinghub.elsevier.com/retrieve/pii/S2542435118302253

[10] *Negative Emissions Technologies and Reliable Sequestration*. Washington, D.C.: National Academies Press, 3 2019. [Online]. Available: https://www.nap.edu/catalog/25259

[11] M. Sinha, "Direct Air Capture Characterization and design of a novel absorption process," Tech. Rep., 2019. [Online]. Available: http://repository.tudelft.nl/.

[12] R. A. Dowling, "An experimental and computational study of CO 2 absorption in aqueous solutions of tetraethylenepentamine," Tech. Rep., 2020. [Online]. Available: http://repository.tudelft.nl/.

[13] A. De Matteis, "Continuous Direct Air Capture, understanding mass transfer in reactive absorption of carbon dioxide," Ph.D. dissertation, 2020.

[14] B. Ovaa, "Direct Air Capture: An experimental approach on the desorption of CO 2 and H 2 O from PEI and TEPA," Tech. Rep., 2019. [Online]. Available: http://repository.tudelft.nl/.

[15] National Institue of Standards and Technology, *Tetraethylenepentamine*.

[16] Engineering toolbox, “Water - specific heat,” 2004. [Online]. Available: https://www.engineeringtoolbox.com/specific-heat-capacity-water-d_660.html

[17] ——, “Carbon Dioxide Gas - specific heat,” 2005. [Online]. Available: https://www.engineeringtoolbox.com/carbon-dioxide-d_974.html

[18] A. Goeppert, M. Czaun, G. K. Surya Prakash, and G. A. Olah, “Air as the renewable carbon source of the future: an overview of CO2 capture from the atmosphere,” *Energy & Environmental Science*, vol. 5, no. 7, p. 7833, 2012. [Online]. Available: http://xlink.rsc.org/?DOI=c2ee21586a

[19] R. K. Pachauri and L. A. Meyer, “Climate Change 2014: Synthesis Report. Contribution of Working Groups I, II and III to the Fifth Assessment Report of the Intergovernmental Panel on Climate Change.” IPCC, Tech. Rep., 2014.

[20] V. Masson-Delmotte, P. Zhai, H.-O. Pörtner, D. Roberts, J. Skea, P. R. Shukla, A. Pirani, W. Moufouma-Okia, C. Péan, R. Pidcock, S. Connors, J. B. R. Matthews, Y. Chen, X. Zhou, M. I. Gomis, E. Lonnoy, T. Maycock, M. Tignor, and T. Waterfield, “Global warming of 1.5°C An IPCC Special Report on the impacts of global warming of 1.5°C above pre-industrial levels and related global greenhouse gas emission pathways, in the context of strengthening the global response to the threat of climate change, sustainable development, and efforts to eradicate poverty Edited by Science Officer Science Assistant Graphics Officer Working Group I Technical Support Unit,” Tech. Rep., 2019. [Online]. Available: www.environmentalgraphiti.org

[21] S. A. Rackley, *Carbon Capture and Storage*. Butterworth-Heinemann, 2017.

[22] F. Dalena, A. Senatore, A. Marino, A. Gordano, M. Basile, and A. Basile, *Methanol Production and Applications: An Overview*. Elsevier B.V., 2018. [Online]. Available: http://dx.doi.org/10.1016/B978-0-444-63903-5.00001-7

[23] P. Muchan, J. Narku-Tetteh, C. Saiwan, R. Idem, and T. Supap, “Effect of number of amine groups in aqueous polyamine solution on carbon dioxide (CO 2) capture activities,” *Separation and Purification Technology*, vol. 184, pp. 128–134, 8 2017. [Online]. Available: https://linkinghub.elsevier.com/retrieve/pii/S1383586617305397

[24] B. Dutcher, M. Fan, and A. G. Russell, “Amine-Based CO 2 Capture Technology Development from the Beginning of 2013—A Review,” *ACS Applied Materials & Interfaces*, vol. 7, no. 4, pp. 2137–2148, 2 2015. [Online]. Available: https://pubs.acs.org/doi/10.1021/am507465f

[25] E. I. Koytsoumpa, C. Bergins, and E. Kakaras, “The CO 2 economy: Review of CO 2 capture and reuse technologies,” *The Journal of Supercritical Fluids*, vol. 132, pp. 3–16, 2 2018. [Online]. Available: https://linkinghub.elsevier.com/retrieve/pii/S0896844617300694

[26] C. Madeddu, M. Errico, and R. Baratti, *CO2 Capture by Reactive Absorption-Stripping*. Cham: Springer International Publishing, 2019.

[27] S.-i. Nakao, K. Yogo, K. Goto, T. Kai, and H. Yamada, *Advanced CO2 Capture Technologies*. Cham: Springer International Publishing, 2019.

[28] A. Kumar, D. G. Madden, M. Lusi, K.-J. Chen, E. A. Daniels, T. Curtin, J. J. Perry, and M. J. Zaworotko, “Direct Air Capture of CO 2 by Physisorbent Materials,” *Angewandte Chemie International Edition*, vol. 54, no. 48, pp. 14 372–14 377, 11 2015. [Online]. Available: http://doi.wiley.com/10.1002/anie.201506952

[29] E. S. Sanz-Pérez, C. R. Murdock, S. A. Didas, and C. W. Jones, “Direct Capture of CO2 from Ambient Air,” vol. 116, no. 19, pp. 11 840–11 876, 2016.

[30] A. Goeppert, H. Zhang, M. Czaun, R. B. May, G. K. S. Prakash, G. A. Olah, and S. R. Narayanan, “Easily Regenerable Solid Adsorbents Based on Polyamines for Carbon Dioxide Capture from the Air,” *ChemSusChem*, vol. 7, no. 5, pp. 1386–1397, 5 2014. [Online]. Available: http://doi.wiley.com/10.1002/cssc.201301114

[31] K. S. Lackner, “The thermodynamics of direct air capture of carbon dioxide,” *Energy*, vol. 50, pp. 38–46, 2013.

[32] M. Broehm, J. Strefler, and N. Bauer, “Techno-Economic Review of Direct Air Capture Systems for Large Scale Mitigation of Atmospheric CO2,” *SSRN Electronic Journal*, 2015. [Online]. Available: http://www.ssrn.com/abstract=2665702

[33] G. Holmes and D. W. Keith, “An air–liquid contactor for large-scale capture of CO 2 from air,” *Philosophical Transactions of the Royal Society A: Mathematical, Physical and Engineering Sciences*, vol. 370, no. 1974, pp. 4380–4403, 9 2012. [Online]. Available: https://royalsocietypublishing.org/doi/10.1098/rsta.2012.0137

[34] F. Bougie and M. C. Iliuta, “Sterically Hindered Amine-Based Absorbents for the Removal of CO 2 from Gas Streams,” *Journal of Chemical & Engineering Data*, vol. 57, no. 3, pp. 635–669, 3 2012. [Online]. Available: https://pubs.acs.org/doi/10.1021/je200731v

[35] R. P. Lively and M. J. Realff, “On thermodynamic separation efficiency: Adsorption processes,” *AIChE Journal*, vol. 62, no. 10, pp. 3699–3705, 10 2016. [Online]. Available: http://doi.wiley.com/10.1002/aic.15269

[36] “Capturing CO2 from Air.” [Online]. Available: http://www.climeworks.com/co2-removal/

[37] E. Ping, M. Sakwa-Nowak, and P. Eisenberger, “Global Thermostat low cost direct air capture technology,” in *International Conference on Negative CO2 Emissions*, Gothenburg, 2018.

[38] K. S. Lackner, “Capture of carbon dioxide from ambient air,” *The European Physical Journal Special Topics*, vol. 176, no. 1, pp. 93–106, 9 2009. [Online]. Available: http://link.springer.com/10.1140/epjst/e2009-01150-3

[39] S. Voskian and T. A. Hatton, “Faradaic electro-swing reactive adsorption for CO 2 capture,” *Energy & Environmental Science*, 2019. [Online]. Available: http://xlink.rsc.org/?DOI=C9EE02412C

[40] P. D. Vaidya and E. Y. Kenig, “CO2-Alkanolamine Reaction Kinetics: A Review of Recent Studies,” *Chemical Engineering & Technology*, vol. 30, no. 11, pp. 1467–1474, 11 2007. [Online]. Available: http://doi.wiley.com/10.1002/ceat.200700268

[41] I. Kim, K. A. Hoff, and T. Mejdell, “Heat of Absorption of CO2 with Aqueous Solutions of MEA: New Experimental Data,” *Energy Procedia*, vol. 63, pp. 1446–1455, 2014. [Online]. Available: https://linkinghub.elsevier.com/retrieve/pii/S1876610214019699

[42] Q. Ye, L. Zhu, X. Wang, and Y. Lu, “On the mechanisms of CO 2 absorption and desorption with phase transitional solvents,” *International Journal of Greenhouse Gas Control*, vol. 56, pp. 278–288, 1 2017. [Online]. Available: https://linkinghub.elsevier.com/retrieve/pii/S1750583616307964

[43] G. Puxty and M. Maeder, “The fundamentals of post-combustion capture,” in *Absorption-Based Post-combustion Capture of Carbon Dioxide*. Elsevier, 2016, pp. 13–33. [Online]. Available: https://linkinghub.elsevier.com/retrieve/pii/B9780081005149000020

[44] N. El Hadri, D. V. Quang, E. L. Goetheer, and M. R. Abu Zahra, “Aqueous amine solution characterization for post-combustion CO2 capture process,” *Applied Energy*, vol. 185, pp. 1433–1449, 1 2017. [Online]. Available: https://linkinghub.elsevier.com/retrieve/pii/S0306261916303609

[45] R. J. Littel, G. F. Versteeg, and W. P. M. van Swaaij, “Kinetics of COS with primary and secondary amines in aqueous solutions,” *AIChE Journal*, vol. 38, no. 2, pp. 244–250, 2 1992. [Online]. Available: http://doi.wiley.com/10.1002/aic.690380210

[46] F. A. Chowdhury, H. Yamada, T. Higashii, K. Goto, and M. Onoda, “CO2 Capture by Tertiary Amine Absorbents: A Performance Comparison Study,” *Industrial & Engineering Chemistry Research*, vol. 52, no. 24, 6 2013.

[47] J. Brillo, A. I. Pommrich, and A. Meyer, “Relation between Self-Diffusion and Viscosity in Dense Liquids: New Experimental Results from Electrostatic Levitation,” *Physical Review Letters*, vol. 107, no. 16, p. 165902, 10 2011. [Online]. Available: https://link.aps.org/doi/10.1103/PhysRevLett.107.165902

[48] R. B. Bird, W. E. Stewart, and E. N. Lightfood, *Transport Phenomena*, 2002, vol. Second edition.

[49] H. Kierzkowska-Pawlak and A. Chacuk, “Carbon dioxide removal from flue gases by absorption/desorption in aqueous diethanolamine solutions,” *Journal of the Air and Waste Management Association*, vol. 60, no. 8, pp. 925–931, 2010.

[50] M. R. M. Abu Zahra, “Carbon Dioxide Capture from Flue Gas,” Ph.D. dissertation, TU Delft, 2009.

[51] A. Tunnat, P. Behr, and K. Görner, “Desorption Kinetics of CO2 from Water and Aqueous Amine Solutions,” *Energy Procedia*, vol. 51, pp. 197–206, 2014. [Online]. Available: https://linkinghub.elsevier.com/retrieve/pii/S1876610214008856

[52] A. C. Dimian and C. S. Bildea, “Chapter C3 - Component inventory control in recycle systems,” in *The Integration of Process Design and Control*, ser. Computer Aided Chemical Engineering, P. Seferlis and M. C. Georgiadis, Eds. Elsevier, 2004, vol. 17, pp. 401 – 429. [Online]. Available: http://www.sciencedirect.com/science/article/pii/S1570794604800683

[53] Nouryon, “Technical Data Sheet TETRAETHYLENEPENTAMINE (TEPA),” 2019. [Online]. Available: https://ethyleneamines.nouryon.com/SiteAssets/tds-tepa-2019-07-en.pdf

[54] Huntsman, “Technical Bulletin TETRAETHYLENEPENTAMINE (TEPA),” 2008. [Online]. Available: https://www.huntsman.com/performance_products/MediaLibrary/a_MC348531CFA3EA9A2E040EBCD2B6B7B06/Products_MC348531D0B9FA9A2E040EBCD2B6B7B06/Amines_MC348531D0BECA9A2E040EBCD2B6B7B06/Ethyleneamines_MC348531D0CD3A9A2E040EBCD2B6B7B06/files/tetraethylenepentami

[55] M. Sinha, “Experimental study of absorption and desorption in a continuous direct air capture system to build a concept model,” TU Delft, Tech. Rep., 2019.

[56] X. Zhang, R. Zhang, H. Liu, H. Gao, and Z. Liang, “Evaluating CO2 desorption performance in CO2-loaded aqueous tri-solvent blend amines with and without solid

acid catalysts," *Applied Energy*, vol. 218, pp. 417–429, 5 2018. [Online]. Available: https://linkinghub.elsevier.com/retrieve/pii/S0306261918302125

[57] D. H. Van Wagener and G. T. Rochelle, "Stripper configurations for CO2 capture by aqueous monoethanolamine," *Chemical Engineering Research and Design*, vol. 89, no. 9, pp. 1639–1646, 9 2011. [Online]. Available: https://linkinghub.elsevier.com/retrieve/pii/S0263876210003527

[58] E. Seader, J. D. & Henley, *Separation process principles*, 1999, vol. 36, no. 09.

[59] D. H. Van Wagener and G. T. Rochelle, "Stripper configurations for CO2 capture by aqueous monoethanolamine and piperazine," *Energy Procedia*, vol. 4, 2011.

[60] B. A. Oyenekan and G. T. Rochelle, "Alternative stripper configurations for CO2 capture by aqueous amines," *AIChE Journal*, vol. 53, no. 12, 12 2007.

[61] A. Cousins, L. T. Wardhaugh, and P. H. Feron, "Analysis of combined process flow sheet modifications for energy efficient CO2 capture from flue gases using chemical absorption," *Energy Procedia*, vol. 4, 2011.

[62] J. Calvert and K. MacKenzie, "Start-up and Shut-down times of power CCUS facilities," Department for Business, Energy & Industrial Strategy, Bristol, Tech. Rep., 2020.

[63] P. Feron, W. Conway, G. Puxty, L. Wardhaugh, P. Green, D. Maher, D. Fernandes, A. Cousins, G. Shiwang, L. Lianbo, N. Hongwei, and S. Hang, "Amine Based Post-combustion Capture Technology Advancement for Application in Chinese Coal Fired Power Stations," *Energy Procedia*, vol. 63, 2014.

[64] E. Lemaire, P. A. Bouillon, and K. Lettat, "Development of HiCapt Process for CO2 Capture from Lab to Industrial Pilot Plant," *Oil & Gas Science and Technology – Revue d'IFP Energies nouvelles*, vol. 69, no. 6, 1 2014.

[65] H. Shi, R. Idem, A. Naami, D. Gelowitz, and P. Tontiwachwuthikul, "Catalytic Solvent Regeneration Using Hot Water During Amine Based CO2 Capture Process," *Energy Procedia*, vol. 63, 2014.

[66] P. Broutin, P. Briot, S. Ehlers, and A. Kather, "Benchmarking of the DMXTM CO2 Capture Process," *Energy Procedia*, vol. 114, 7 2017.

[67] M. J. Moran and H. N. Shapiro, *Fundamentals of Engineering Thermodynamics*.

[68] Jonassen, I. Kim, and H. F. Svendsen, "Heat of absorption of carbon dioxide (CO2) into aqueous Nmethyldiethanolamine (MDEA) and N,Ndimethylmonoethanolamine (DMMEA)," in *Energy Procedia*, vol. 63. Elsevier Ltd, 2014, pp. 1890–1902.

[69] A. Abdulkadir, A. V. Rayer, D. V. Quang, N. E. Hadri, A. Dindi, P. H. M. Feron, and M. R. M. Abu-Zahra, "Heat of Absorption and Specific Heat of Carbon Dioxide in Aqueous Solutions of Monoethanolamine,3-piperidinemethanol and Their Blends," *Energy Procedia*, vol. 63, pp. 2070–2081, 2014. [Online]. Available: https://linkinghub.elsevier.com/retrieve/pii/S1876610214020384

[70] M. E. Boot-Handford, J. C. Abanades, E. J. Anthony, M. J. Blunt, S. Brandani, N. Mac Dowell, J. R. Fernández, M. C. Ferrari, R. Gross, J. P. Hallett, R. S. Haszeldine, P. Heptonstall, A. Lyngfelt, Z. Makuch, E. Mangano, R. T. Porter, M. Pourkashanian, G. T. Rochelle, N. Shah, J. G. Yao, and P. S. Fennell, "Carbon capture and storage update," pp. 130–189, 2014.

[71] P. Datt, “Latent Heat of Vaporization/Condensation,” 2011, p. 703. [Online]. Available: http://link.springer.com/10.1007/978-90-481-2642-2_327

[72] B. E. Poling, J. M. Prausnitz, and J. P. O’Connell, *Properties of Gases and Liquids*, 2001.

[73] R. Hołyst and A. Poniewierski, *Thermodynamics for Chemists, Physicists and Engineers*.

[74] “Separation Processes King, C Judson.”

[75] E. A. Guggenheim and J. C. Turgeon, “SPECIFIC INTERACTION OF IONS,” Tech. Rep.

[76] G. Scatchard, “CONCENTRATED SOLUTIONS OF STRONG ELECTROLYTES1,” Tech. Rep., 2020. [Online]. Available: https://pubs.acs.org/sharingguidelines

[77] W. K. Lewis and G. L. Matheson, “Studies in Distillation,” *Industrial & Engineering Chemistry*, vol. 24, no. 5, pp. 494–498, 1932. [Online]. Available: https://doi.org/10.1021/ie50269a005

[78] E. W. Thiele and R. L. Geddes, “Computation of Distillation Apparatus for Hydrocarbon Mixtures,” *Industrial & Engineering Chemistry*, vol. 25, no. 3, pp. 289–295, 1933. [Online]. Available: https://doi.org/10.1021/ie50279a011

[79] D. Burningham and F. Otto, “Which computer design for absorbers,” in *Hydrocarbon Process*, 1967, vol. 46, pp. 163–170.

[80] L. Naphtali and D. P. Sandholm, “Multicomponent separation calculations by linearization,” *Aiche Journal*, vol. 17, pp. 148–153, 1971.

[81] J. F. Boston and S. L. Sullivan, “A new class of solution methods for multicomponent, multistage separation processes,” *The Canadian Journal of Chemical Engineering*, vol. 52, no. 1, 2 1974.

[82] W. Yan and E. H. Stenby, “On solving the Rachford-Rice equation with higher order methods,” *Fluid Phase Equilibria*, vol. 363, 2 2014.

[83] E. H. Fernández-Martínez and E. López-López, “Some theoretical results on Rachford-Rice equation for flash calculations: Multi-component systems,” *Computers & Chemical Engineering*, vol. 140, 9 2020.

[84] R. L. Burden and J. D. Faires, “Numerical Analysis,” Tech. Rep., 2010.

[85] J. Coates, “Interpretation of Infrared Spectra, A Practical Approach,” in *Encyclopedia of Analytical Chemistry*. Chichester, UK: John Wiley & Sons, Ltd, 9 2006. [Online]. Available: http://doi.wiley.com/10.1002/9780470027318.a5606

[86] W. D. Perkins, “Fourier Transform-Infrared Spectroscopy,” *Topics in chemical instrumentations*, vol. 63, no. 1, 1986. [Online]. Available: http://web.ist.utl.pt/berberan/PQF/JCEPerkins1986.pdf

[87] D. Berger, “Organic Laboratory Techniques, 3rd Edition (Fessenden, Ralph J.; Fessenden, Joan S.; Feist, Patty),” *Journal of Chemical Education*, vol. 78, no. 10, 10 2001.

[88] A. K. Gowda, “Study of amine degradation in direct air capture,” Ph.D. dissertation, TU Delft, 2020.

[89] Mulder G, “Characterization and optimization of the sorbent system for the DAC unit at ZEF,” Tech. Rep., 2021.

[90] N. Serrano Barthe, “Absorption of CO2 from the air using polyamines: Experiments, modelling and design,” Ph.D. dissertation, Delft University of Technology, 2019. [Online]. Available: http://resolver.tudelft.nl/uuid:895913fc-987b-4f20-837e-28b369fe2fb3

[91] X. Zhang, H. Liu, Z. Liang, R. Idem, P. Tontiwachwuthikul, M. Jaber Al-Marri, and A. Benamor, “Reducing energy consumption of CO2 desorption in CO2-loaded aqueous amine solution using Al2O3/HZSM-5 bifunctional catalysts,” *Applied Energy*, vol. 229, 11 2018.

Appendix A

Vapor Liquid Equilibrium and Vapor Curve

A.1 Vapor-Liquid Equilibrium

When component i exists in a mixture, the thermodynamic equilibrium condition, also called iso-fugacity condition, is defined as:

$$f_i^V = f_i^L \tag{A.1}$$

where f_i = fugacity, V = vapor and L = liquid [72]. These fugacities are to be related to the corresponding mixture compositions. In the vapor phase, the fugacity coefficient for a component i is given by:

$$\phi_i^V = \frac{f_i^V}{y_i P} = \frac{f_i^V}{p_i} \tag{A.2}$$

where ϕ_i = fugacity coefficient, y_i = vapor phase mole fraction and p_i = partial pressure. The fugacity coefficient is by definition normalized and can therefore be interpreted as a measure of deviation from the ideal gas behaviour, for ideal gases $\phi_i^V = 1$ [72]. For components in the liquid phase, the fugacity coefficient can be calculated via the activity coefficient approach. The activity coefficient relates the fugacity of component i to the its mole fraction in the liquid phase:

$$\gamma_i = \frac{a_i}{x_i} = \frac{f_i}{x_i f_i^0} \tag{A.3}$$

where γ_i = activity coefficient, a_i = activity of component i, x_i = liquid phase mole fraction and f_i^0 = standard-state fugacity, which corresponds to the fugacity of component i at the temperature and pressure of the system, chosen purely for convenience [72]. The fugacity of pure liquid i at temperature T and pressure P can be calculated via:

$$f_i^0(T, P, x_i = 1) = P_{\text{vpi}}(T)\phi_i^s(T)\text{exp}\int_{P_{\text{vpi}}}^{P} \frac{V_i^L(T,P)}{RT} dP \tag{A.4}$$

where P_{vpi} is the saturation vapor pressure and ϕ_i^s is the fugacity coefficient of the pure component i. The exponential term, which is called the Poynting factor, can be usually neglected since the liquid is close to incompressible [72]. To arrive at the VLE relation for each component, the above mentioned formulas are put together into the iso-fugacity condition. This results in:

$$y_i P = \gamma_i x_i P_{\text{vpi}} \frac{\phi_i^s}{\phi_i} \text{exp}\int_{P_{\text{vpi}}}^{P} \frac{V_i^L dP}{RT} = \gamma_i x_i P_{\text{vpi}} F \tag{A.5}$$

The correction factor F is for low and moderate pressures often near unity. This simplification is called the modified Raoult's law:

$$y_i P = \gamma_i x_i P_{\text{vpi}} \tag{A.6}$$

If next to the correction factor F, the activity coefficient γ_i is also set to unity, equation A.6 reduces to Raoult's law:

$$y_i P = x_i P_{\text{vpi}} \tag{A.7}$$

This is justified since, unless the pressure is large, the effect of pressure on γ_i is normally small [72].

A.2 Vapor Curve

Dowling et al. performed experiments to measure the equilibrium of a binary TEPA-H_2O mixture for different concentrations and temperatures. The chosen concentrations and temperatures are shown in table A.1.

Table A.1: Investigated concentrations and temperatures for vapor curve measurements [12].

Concentration	**Temperature**
wt% TEPA	K
30	298.15 - 393.15
70	298.15 - 393.15
80	298.15 - 393.15

According to the experimental data, a binary model was created based on the modified Raoult's law, Clausius-Clapeyron equation and Wilson's equation. The modified Raoult's law is used to account for liquid phase non-idealities where the regular Raoult's law would not hold [72].

$$y_i P_{\text{tot}} = x_i \gamma_i P_i^{\text{sat}} \tag{A.8}$$

Then, the Clausius-Clapeyron equation is used to calculate the pure component vapor pressure. For this, one needs the heat of vaporization and a known vapor pressure (P_{ref}) at a known temperature (T_{ref}). For convenience, the reference temperature is set as TEPA's boiling point such that the vapor pressure equals atmospheric pressure [72].

$$\ln\left(\frac{P_{\text{TEPA}}^{\text{sat}}(T)}{P_{\text{ref}}}\right) = \frac{\Delta H_{\text{vap}}}{R}\left(\frac{1}{T} - \frac{1}{T_{\text{ref}}}\right) \tag{A.9}$$

The required heat of vaporization and boiling point are taken from the National Institute of Standards and Technology and are respectively 71.3 Kj/mole and 613.15 K [15]. The Wilson's equation is used to calculate the activity coefficients.

$$\ln\gamma_1 = -\ln(x_1 + \Lambda_{12}x_2) + x_2\left[\frac{\Lambda_{12}}{x_1 + \Lambda_{12}x_2} - \frac{\Lambda_{21}}{x_2 + \Lambda_{21}x_1}\right] \tag{A.10}$$

$$\ln\gamma_2 = -\ln(x_2 + \Lambda_{21}x_1) - x_1\left[\frac{\Lambda_{12}}{x_1 + \Lambda_{12}x_2} - \frac{\Lambda_{21}}{x_2 + \Lambda_{21}x_1}\right] \tag{A.11}$$

where Λ_{12} and Λ_{21} are the Wilson parameters, which are defined as:

$$\Lambda_{12} = \frac{v_2^L}{v_1^L} e^{-(\lambda_{12}-\lambda_{11})/RT} \tag{A.12}$$

$$\Lambda_{21} = \frac{v_2^L}{v_1^L} e^{-(\lambda_{12}-\lambda_{22})/RT} \tag{A.13}$$

where λ_{12} is the interaction energy between molecules of H_2O and TEPA, λ_{11} of 2 molecules of H_2O an λ_{22} of 2 molecules of TEPA. v_1^L and v_2^L are the molar liquid volumes of pure H_2O and TEPA,

respectively [72]. Table A.2 shows the fitted parameters for the Wilson equation to predict the VLE behaviour of the binary mixture of TEPA and H_2O.

Table A.2: Fitted parameters for the Wilson equation to describe the VLE of the binary mixture of TEPA and H_2O [12].

Fitted parameter	**Value**	**Units**
$(\lambda_{12} - \lambda_{11})$	-156.03	J/mol
$(\lambda_{12} - \lambda_{22})$	220.94	J/mol

The outcomes of the Clausius-Clapeyron and Wilson's equation are inserted into the modified Raoult's law to calculate the total pressure neglecting vapor phase non-idealities.

$$P_{\text{tot}}(T, x) = x_1 \gamma_1 P_1^{\text{sat}}(T) + x_2 \gamma_2 P_2^{\text{sat}}(T) \tag{A.14}$$

Finally, the experimental data from the vapor curve experiments are used to fit the Wilson parameters.

Appendix B

Experimental Setup Design

B.1 Detailed description of experimental setup design

The components of the experimental stripping setup used in this thesis are presented in detail in this appendix chapter. Figure B.1 shows a complete overview of the experimental setup used for zero reflux experiments. The main parts are emphasized in the figure. The experimental setup is split into the following segments: stripping column, flash tank with reflux and mass flow meter. For each segment, the assembly of all the parts is visualized and briefly elaborated on.

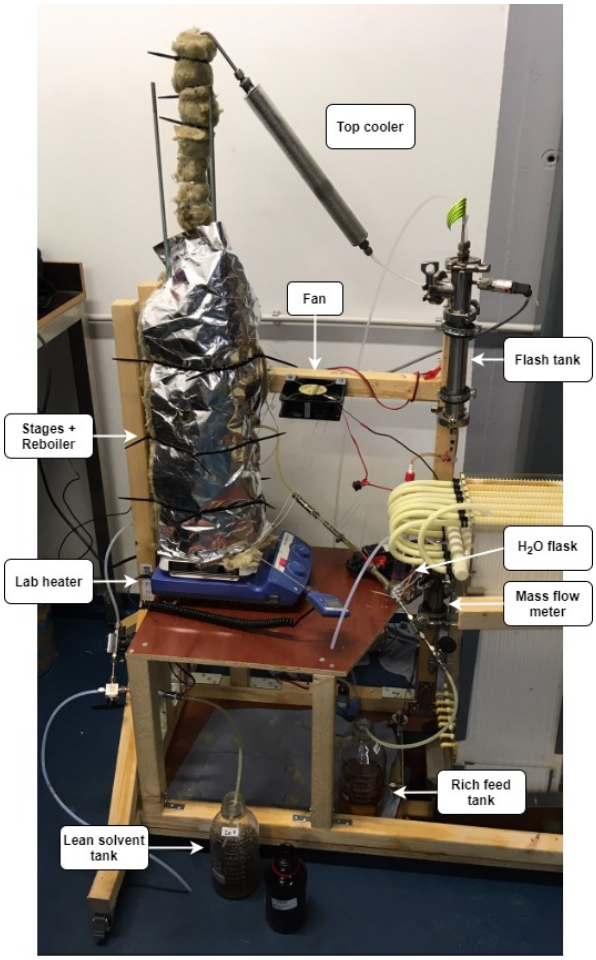

Figure B.1: Assembly of the complete stripping setup for zero reflux experiments.

B.1.1 Stripping column

The stripping column consists of a various number of stages and a reboiler, figure B.2. The feed mixture inlet is situated in the top stage and gear pump U pumps the feed mixture in the column. A check valve makes sure that no vapor escapes through the feed hose and a NTC sensor measures the feed temperature. The lean solvent mixture leaves the stripping column via the reboiler and passes the bottom cooler where it is passively cooled. The outflow of the lean solvent is controlled by gear pump W which is connected to a check valve. The lean solvent is finally collected in a tank. The vapor product leaves the stripper at the top of the stage where it passes the top cooler which actively cools the top product. The reboiler is in contact with the lab heater which provides the heat that is required for the system to operate. The complete stripping column is insulated with 2 cm glass wool and a thin aluminum sheet as shown in figure B.1.

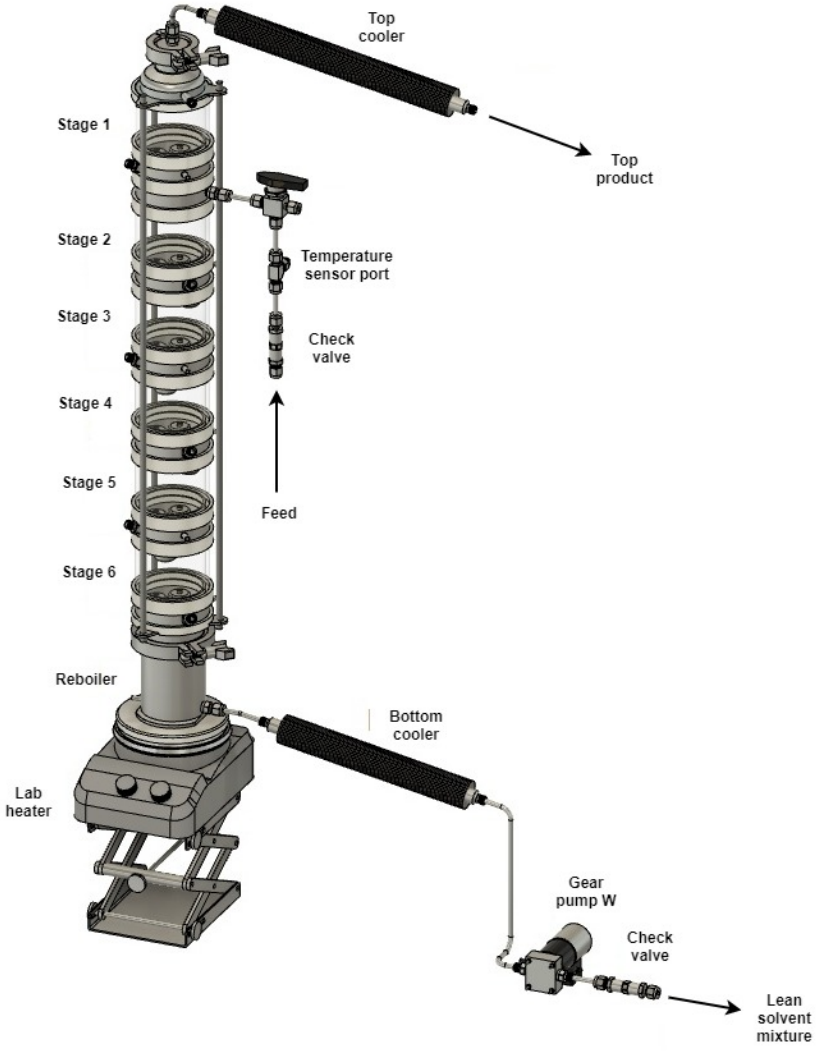

Figure B.2: Stripper column design including six stages and a reboiler [5].

Each stage, figure B.3.a, is equipped with a sample port from where liquid and vapor samples are taken with a syringe. The temperature sensor port holds inside a NTC sensor to measure the temperature of the liquid mixture. Inside the stage, a outlet weir enables the liquid mixture to flow to the stage underneath. Three bubble caps facilitate vapor from the underlying stage to bubble through the liquid mixture. The hold up volume of the stage is 30.4 ml, the outlet weir starts to overflow when a surplus of liquid mixture is present. The reboiler, figure B.3.b, is just like the stages equipped with a sample and temperature sensor port. The lean solvent mixture leaves the reboiler via the outlet port which is placed 10 mm above the flat bottom surface. For a multiple-stage setup, the reboiler has a radius of 36.3 mm, which equals a hold up volume of 49.4 ml. For a single-stage setup, the radius is 48.5 mm which is equivalent to a hold up volume of 78 ml.

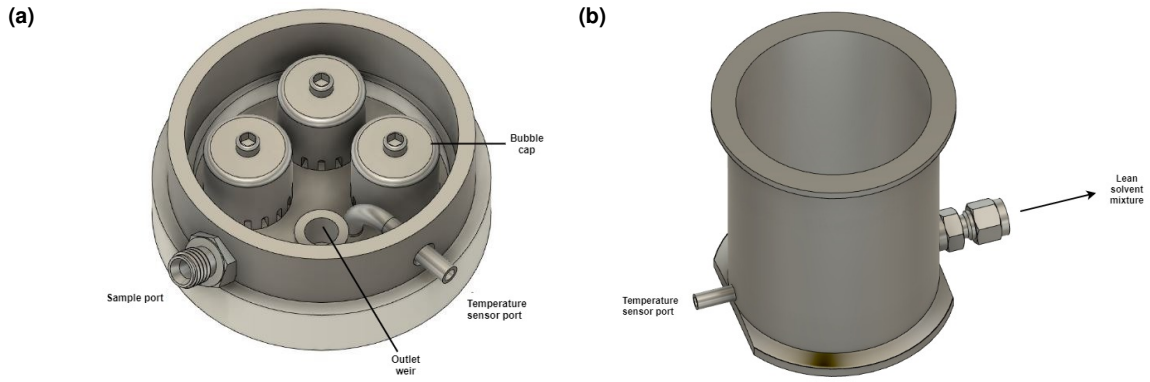

Figure B.3: Design of the stripping column components with (a) design of a general stage inside the column and (b) design of the reboiler stage at the bottom of the column [5].

B.1.2 Flash tank with reflux

The flash tank, figure B.4, is a vertically oriented tank where the top product arrives and the vapor and liquid are separated. The flash tank holds a pressure sensor which measures the pressure of the complete system. The vapor leaves the flash tank at the top whereas the liquid remains in the tank and is partially fed back into the top of the column by gear pump R.

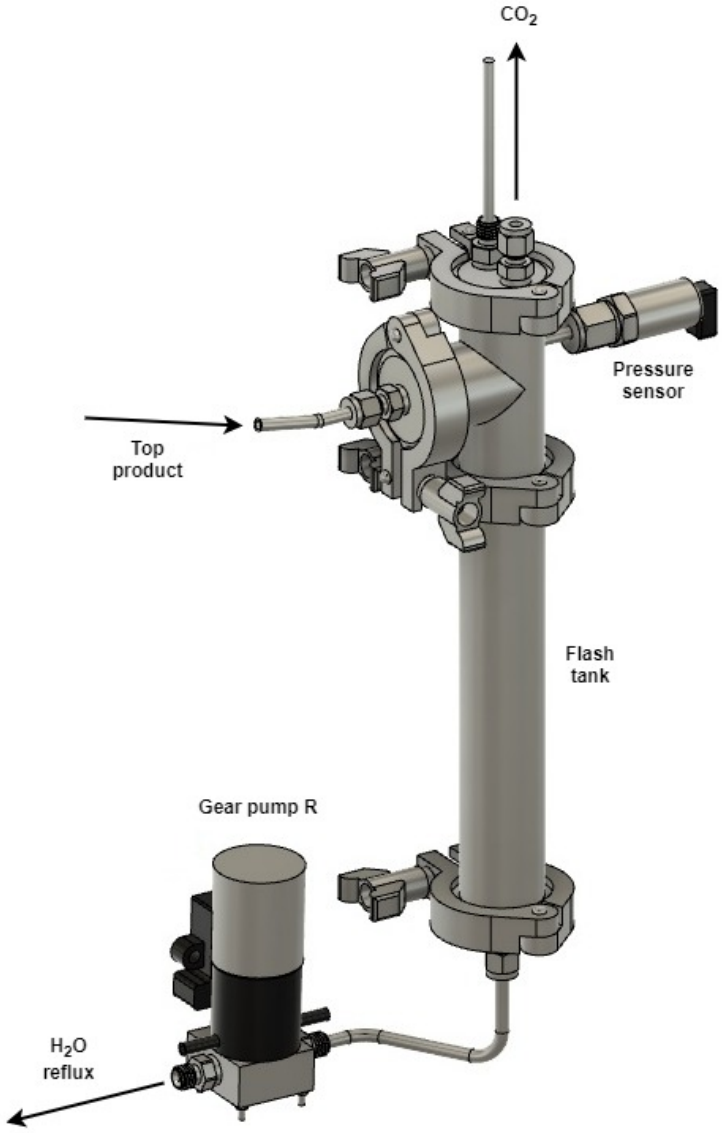

Figure B.4: Flash tank with reflux design [5].

B.1.3 Mass flow meter

The vapor from the flash tank is sucked by vacuum pump V into the mass flow meter, figure B.5. The mass flow meter is a horizontally oriented tank with a volume of 232.6 ml. It holds a pressure sensor and a solenoid valve. The solenoid valve opens when the pressure inside the meter exceeds 1.5 bars so that the surplus of vapor escapes from the system.

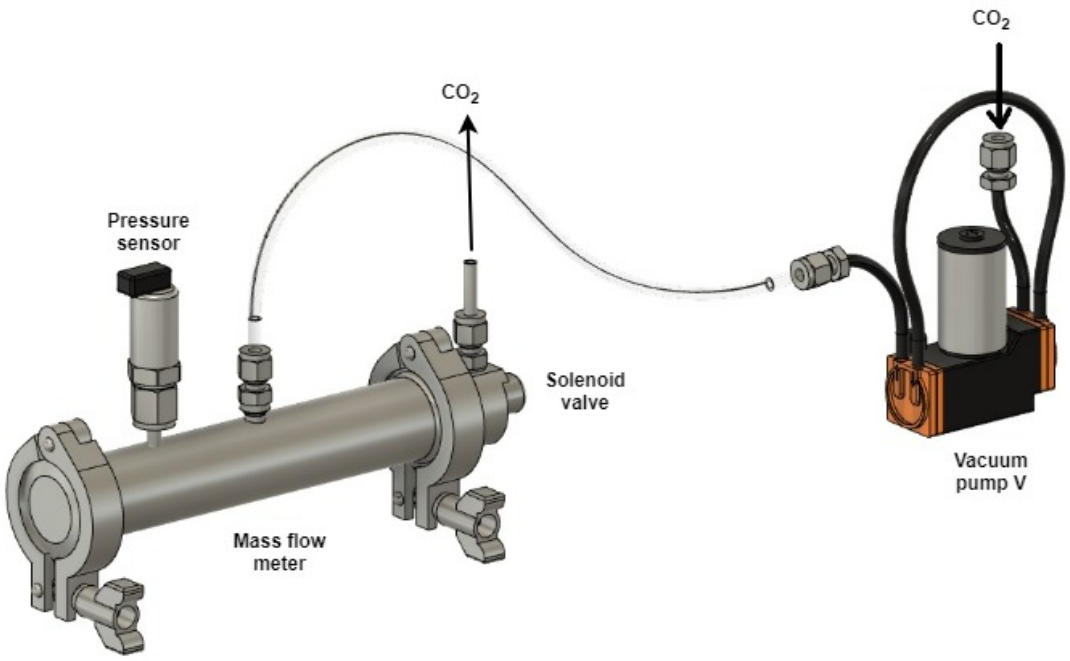

Figure B.5: Mass flow meter design [5].

Appendix C

Experimental Data Analysis

C.1 Experimental data processing

The real time experimental data that is obtained via the Arduino is visualized and presented in figure C.1 and C.2. Both figures represent a 2 stage experiment that started at t = 5670 sec. The fluctuations of temperature and pressure are a good representation of all the experiments performed in this work.

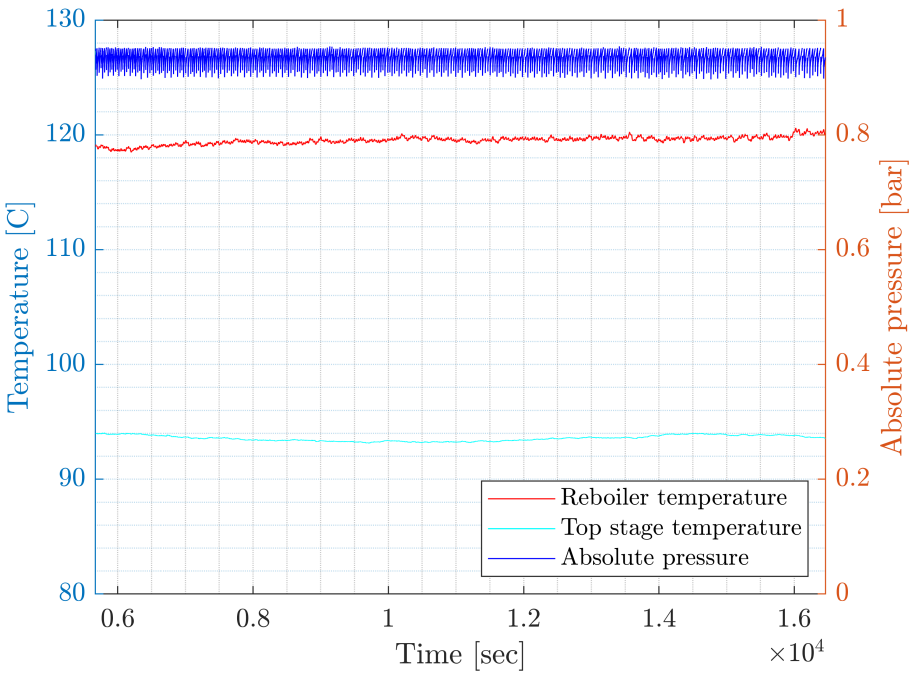

Figure C.1: Stage temperatures and absolute pressure during a general 2 stage experiment.

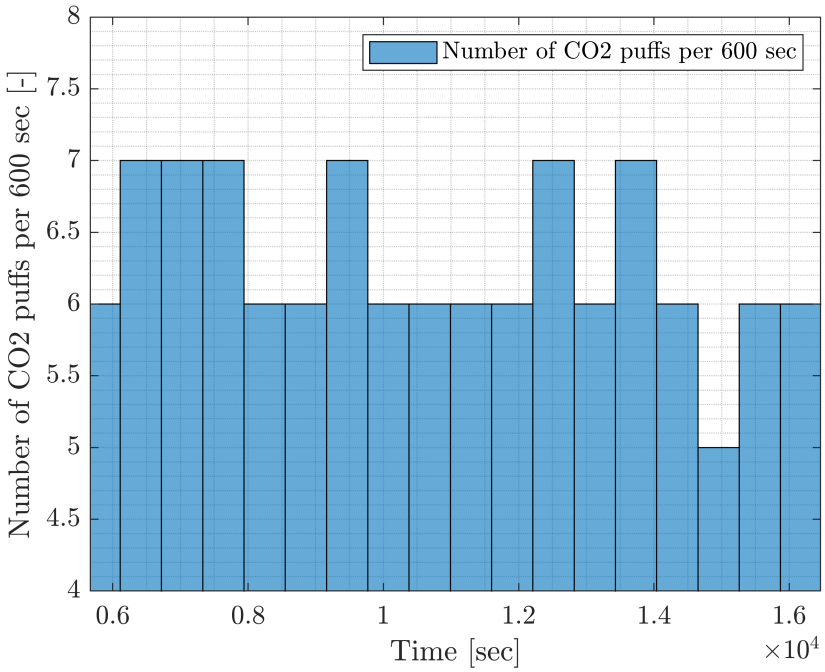

Figure C.2: Puffs of CO_2 per 600 s during a general 2 stage experiment. Each puff corresponds with a CO_2 volume of 110 ml.

Appendix D

Experimental Mass and Energy Balances

D.1 Experimental mass balance

D.1.1 Assumptions

For the mass balance given in chapter 4.2.6 a number of assumptions must be taken into account:

- The density of TEPA is not depending on loading of CO_2 and H_2O or temperature. In fact, the density of TEPA is assumed to be constant throughout the performed experiments.
- The amount of TEPA that evaporates during an experiment is negligible. This is build on the high boiling temperature of TEPA and the relatively low operating temperature of the stripping column.
- H_2O from the flash tank collected in the flask is pure H_2O. This has been analysed for the first experiments and would give a constant result of pure H_2O.
- The liquid in the stages and reboiler is well mixed and therefore a homogeneous liquid. This makes sure that the collected liquid samples are an accurate representation of the liquid compositions inside the stripper.

D.1.2 COCO model

A COCO model was made to validate the vapor sample analysis of the CO_2 vapor product stream by the GC. The model is visually presented in figure D.1. The vapor product stream arrives at the top cooler where it is partially condensed. When arriving in the flash tank, the vapor and liquid are separated. The vapor leaves the flash tank at the top. The liquid leaves the flash tank at the bottom for storage or reflux. The experimental conditions can be simulated in the model to estimate the concentrations of CO_2 and H_2O in the vapor stream leaving the flash tank.

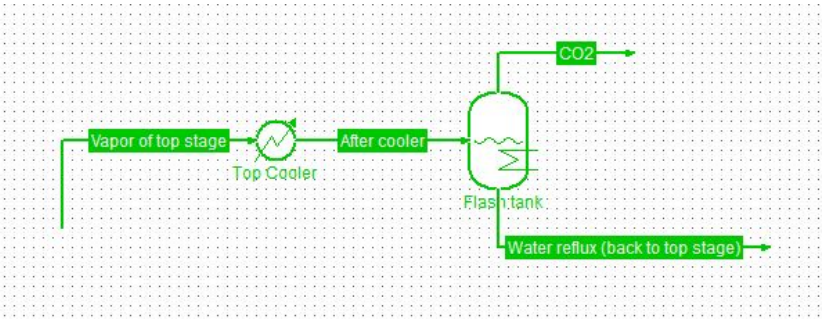

Figure D.1: COCO model to predict the concentrations of CO_2 and H_2O in the CO_2 vapor product stream.

D.2 Experimental energy balance

D.2.1 Assumptions

For the energy balance shown in chapter 4.2.6, one must take the following assumptions into account:

- There is no heat loss between the liquid and vapor inside the single stage. This results in an equal temperature of the liquid and vapor present inside the single stage.
- All heat from the lab heater travels through the bottom of single stage into the system; no heat loss from the lab heater through glass wool insulation. Since the glass wool covers the remaining surface area of the lab heater, there is no direct contact with ambient air. Also, the low thermal conductivity of glass wool compared to stainless steel substantiate the assumption.
- The walls and lit of single stage are in contact with the vapor inside the system. There is no liquid-stainless steel interface through which heat travels to the ambient environment.
- The walls and lit of the single stage have equal thickness and are completely smooth.
- Specific heat capacity of the liquid mixture is an average based on the mass fractions of the present components in the rich feed. The specific heat capacity is taken constant throughout an experiment.

D.2.2 Energy balance components

Figure D.2 shows a schematic of the heat transport through the single stage stripping column. Also, the relevant dimensions are presented to calculate the heat losses, equation D.4 and D.5. Each energy balance component is presented in the following section and the corresponding equations are given.

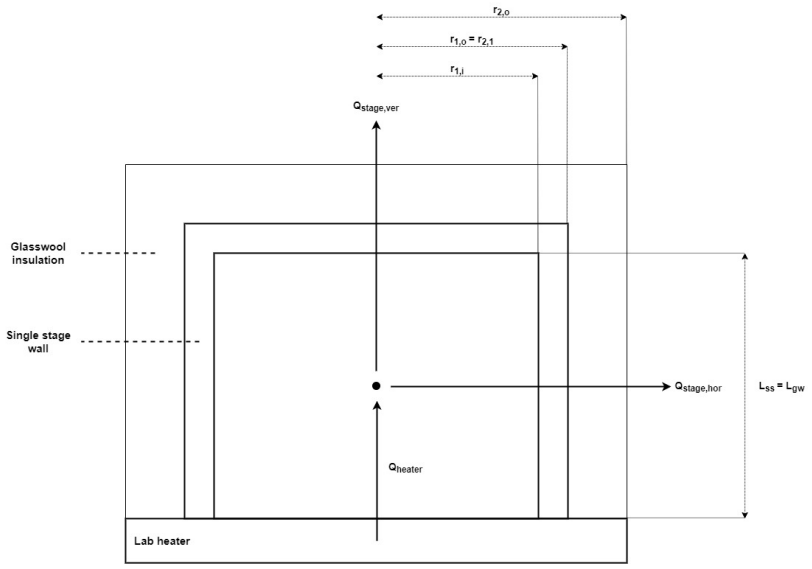

Figure D.2: Energy balance schematic for the experimental setup with dimensions.

Sensible heat

Equation D.1 describes the energy demand due to sensible heat:

$$Q_{sens} = \dot{m} C_{p_{avg}} (T_{in} - T_{amb}) \tag{D.1}$$

Where: $\dot{m}$ = feed mass flow, Cp_{avg} = average specific heat capacity of the liquid mixture based on mass fractions of the components, T_{in} = temperature of the liquid and vapor inside the system and T_{amb} = ambient temperature.

Heat of desorption CO_2

Equation D.2 describes the energy demand due to desorption of CO_2:

$$Q_{des} = \frac{m_{CO_2} H_{CO_2} \cdot 1000}{M_{CO_2} t} \tag{D.2}$$

Where: m_{CO_2} = total produced CO_2, M_{CO_2} = molar mass of CO_2, H_{CO_2} = heat of desorption of CO_2 and t = duration of the experiment.

Heat of vaporization H_2O

The energy demand based on the heat of vaporization of H_2O is estimated by combining the amount of liquid H_2O in the flash tank and the concentration of H_2O vapor in the CO_2 vapor product stream. Equation D.3 describes the energy demand due to vaporization of H_2O:

$$Q_{vap} = \frac{m_{H_2O} H_{H_2O} \cdot 1000}{M_{H_2O} t} \tag{D.3}$$

Where: m_{H_2O} = total produced H_2O, M_{H_2O} = molar mass of H_2O and H_{H_2O} = heat of vaporization of H_2O.

Heat loss single stage

As figure D.2 shows, the heat transfer from the single stage to the environment occurs in a horizontal and vertical direction. The heat losses are estimated for both directions according to the following equations:

$$Q_{loss,hor} = \frac{T_{in} - T_{amb}}{\frac{1}{2\pi L_{ss} r_{1,i} h_i} + \frac{\log \frac{r_{1,o}}{r_{1,i}}}{2\pi k_{ss} L_{ss}} + \frac{\log \frac{r_{2,o}}{r_{2,i}}}{2\pi k_{gw} L_{gw}} + \frac{1}{2\pi L_{gw} r_{2,o} h_o}} \tag{D.4}$$

$$Q_{loss,ver} = \frac{T_{in} - T_{amb}}{\frac{1}{h_i \pi r_{1,i}^2} + \frac{r_{1,o} - r_{1,i}}{k_{ss} \pi r_{1,i}^2} + \frac{r_{2,o} - r_{2,i}}{k_{gw} \pi r_{1,i}^2} + \frac{1}{h_o \pi r_{1,i}^2}} \tag{D.5}$$

$$Q_{loss,stage} = Q_{loss,hor} + Q_{loss,ver} \tag{D.6}$$

Where: k_{ss} = thermal conductivity of stainless steel, k_{gw} = thermal conductivity of glass wool, h_i = heat transfer coefficient inside single stage and h_o = heat transfer coefficient outside single stage.

Heat loss lab heater

The lab heater works by means of pulsing heat through the top plate. This results in a fluctuating heating temperature which makes it impossible to calculate the heat loss from the lab heater individually. For this reason, the energy balance, equation 4.7, is used to calculate the heat loss from the lab heater to the liquid mixture inside the stage:

$$Q_{loss,heater} = Q_{exp} - Q_{sens} - Q_{des} - Q_{vap} - Q_{loss,stage} \tag{D.7}$$

It was found and discussed in chapter 4 that calculating the energy loss from the heater to the liquid in this way could not be validated. Therefore, the calculated $Q_{loss,heater}$ is not considered in this work.


TU Delft


Z E F